

**EUSKAL HERRIKO UNIBERTSITATEA / UNIVERSIDAD DEL PAÍS VASCO**  
**BILBOKO INGENIARITZA ESKOLA**  
**ESCUELA DE INGENIERÍA DE BILBAO**

**Advanced heterogeneous catalytic systems for  
biofuels production derived from HMF**

*A dissertation submitted to the University of the Basque Country  
In partial fulfilment on the requirements for the degree of PhD from UPV/EHU*

*By*

**Ms. Nerea Viar Antuñano**

Thesis Advisors:

**Dr. Jesus Maria Requies Martinez**

**Dr. Ion Agirre Arisketa**

Bilbao, 2021



*Eman didazun indarragatik, aitite*



*“Me enseñaron que el camino del progreso no era ni rápido ni fácil”*

*Marie Curie*



*Ezer baino lehen, tesi hau burutzen lagundu didaten guztiei eskerrak ematea gustatuko litzaidake. Nire tesi-zuzendariei, Jesus Requies eta Ion Agirreri, bide luze honetan baldintza gabe eskainitako laguntzagatik eta nigan jarritako konfiantzagatik. Halaber, eskerrak eman nahi dizkiet Euskal Herriko Unibertsitateko Kimika eta Ingurumen Ingeniaritza Saileko kide guztiei, bereziki Supren ikerkuntza taldeko taldekideei. Ezin ahaztu bekadunen gelan aurkitutako lagunak.*

*Eskerrak eman nahi nizkieke Il Dipartimento di Chimica Industriale "Toso Montanari" departamentuan ezagututako ikertzaile guztiei, Italian igarotako denbora errazteagatik. Bereziki, Professor Fabrizio Cavaniri, zure ardua eta adeitasunagatik.*

*Era berean, Euskal Herriko Unibertsitatea, Eusko Jaurlaritza eta espainar estatuko Ekonomia eta Lehiakortasun Ministerioa aipatu nahiko nituzke, doktore-tesi hau egiteko jasotako diru laguntzagatik.*

*Azkenik, nire bizitzako hiru emakume eta hiru gizonei nire eskerrik beroenak eman nahi nizkieke, bihotzez. Eta ez nuke kuadrila ahaztu nahi, bai betikoa baita etorri berria ere.*

*Eskerrik asko guztiagatik.*





## Table of contents

Laburpena .....	3
Resumen.....	7
Summary.....	13
List of tables and figures.....	17
List of acronyms.....	23
CHAPTER 1. Introduction .....	27
CHAPTER 2. State of art.....	55
CHAPTER 3. Objectives and scope of the thesis.....	97
CHAPTER 4. Experimental.....	103
CHAPTER 5. Cu/ZrO <sub>2</sub> based heterogeneous catalysts screening.....	119
CHAPTER 6. The role of Ni and Cu interaction on the bimetallic Ni-Cu/ZrO <sub>2</sub> catalytic system.....	149
CHAPTER 7. Biomass-derived carbon as catalyst support in bimetallic Ni-Cu catalysts .....	179
CHAPTER 8. Conclusions.....	205
Appendix: Curriculum vitae.....	211



## **Laburpena**

Doktorego-tesi hau 2017ko martxoan hasi zen, Espainiako Gobernuaren laguntzarekin, Ekonomia eta Lehiakortasun Ministerioaren plan nazionalen REBICAT (Hondakin Biomasiakoak Bioerregai eta Produktu Berriztagarrietan Eraldatzeko Teknologia Katalitiko Aurreratuak) proiektuaren esparruan eta Bilboko Ingeniaritzako Eskolako (Euskal Herriko Unibertsitatea, UPV/EHU) Ingeniaritza Kimikoaren eta Ingurumenaren Ingeniaritza Saileko Prozesu Iraunkorren Ingeniaritzako ikerketa-taldearen (Supren) esparruan. Lan hau Jesús M. Requies Martínez doktoreak eta Ion Agirre Arisketa doktoreak gainbegiratu dute. Gainera, doktorego-tesi honetan sei hilabeteko ikerketa-egonaldia egin zen Bolognako Unibertsitateko (Italia) "Toso Montanari" Dipartimento di Chimica Industrialean, Fabrizio Cavani katedradunaren gainbegiradapean eta Tommaso Tabanelli eta Giulia Balestraren laguntza adeitsuarekin.

Urte hauetan zehar, doktorego-tesi honetan egindako lanari esker, biomasatik eratorritako 5-hidroximetilfurfural (HMF) konposatutik bioerregaiak ekoizteko sistema katalitiko aurreratuak garatu ahal izan dira. Gainera, doktorego-tesi honek lehenengo laurdenean (Q1) dauden aldizkarietan 4 artikulua eta 2. laurdenean (Q2) kokaturik dagoen aldizkari batean beste artikulua bat argitaratzeko aukera eman du. Halaber, nazioarteko zazpi kongresuetan eta kongresu nazional batean gauzatutako lana aurkezteko bidea eman du. Doktorego-tesia hainbat kapitulutuan egituratuta dago, eta hurrengo paragrafoetan laburbilduko dira.

**1. kapituluak** erregai fosil konbentzionalen erabilera ordezkatzeko beharra nabarmentzen du. Alde horretatik, biomasa da produktu petrokimikoak ordezka ditzakeen energia-iturri berriztagarri bakarra. Beraz, biomasa lignozelulosikoa balio erantsiko produktu kimiko eta bioerregaietan bihurtzeko ikertzearen garrantzia nabarmentzen da. Biomasa lignozelulosikoaren konplexutasuna dela eta, ibilbide katalitiko gehienek lehenengo berriztagarri hori hainbat molekula plataformatan bihurtzea dakarte, hala nola HMF. HMF-a produktu kimikoak eta bioerregaiak lortzeko bitarteko aldakor bat da. Kapitulu honetan, HMF-tik eratorritako bi bioerregaien propietateak eta etorkizun handiko aplikazioak deskribatzen dira, 2,5 dimetilfuranoa (DMF) eta 2,5 dimetiltetrahidrofuranoa (DMTHF) hain zuzen ere

**2. kapituluak**, DMF eta DMTHF-ren ekoizpenaren ikerketen berrikuspen sakona azaltzen da. Lehenik eta behin, biomasa eta azukreetatik abiatuta, DMF-ren ekoizpen katalitiko zuzena zehazten da. Hainbat lehengai (arto-uztondoa, agarra, glukosa, fruktosa, etab.) DMF-n eraldatze prozesua deskribatzen da. Ondoren, DMF-ren ekoizpena deskribatzen da HMF-tik abiatuta. Ildo horretan, erreazio-bide nagusiak eta sistema katalitikoak sakonki deskribatzen dira. Azkenik, DMTHF-ren ekoizpenean egin berri diren ikerketak deskribatzen dira.

**3. kapituluak** doktorego-tesi honen helburu nagusia definitzen da. Helburu nagusi hori betetzeko, zenbait helburu partzial ere deskribatzen dira. Horien artean, katalizatzaileen metal aktiboen eta euskarri ezberdinen erabilera azaltzen da.

**4. kapituluak**, doktorego-tesi hau garatzeko erabilitako prozedura experimental eta analitikoak deskribatzen dira. Ildo horretan, katalizatzailea prestatzeko metodoak, erreazio-sistema, analisi-metodoak eta karakterizazio-teknikak zehatz-mehatz deskribatzen dira.

**5. kapituluak** lan honen lehen emaitza experimentalak jasotzen ditu. Kapitulu honetan, Cu/ZrO<sub>2</sub>-n oinarritutako katalizatzaileak egokitu egiten dira sistemaren jarduera katalitikoa hobetzeko. Horretarako, lehenik eta behin, Cu-ren hainbat eduki metaliko gehitu zitzaizkion ZrO<sub>2</sub>-ren euskarriari. Gainera, ZrO<sub>2</sub>-ren euskarria eraldatu egin zen CeO<sub>2</sub>-rekin. Era berean, metal nobleak (Ru) eta ez-nobleak (Ni) gehitu zitzaizkion fase aktiboari. Katalizatzaileak HMF-ren hidrogenolisirako erabili ziren, DMF eta DMTHF ekoitziz. Screening katalitiko honen katalizatzailearik aktiboena NiCu/ZrO<sub>2</sub> izan zen. Katalizatzaile honen aktibitate handia, Ni eta Cu-ren arteko interakzioari egotzi zitzaion.

Aurreko kapituluak lortutako emaitzak ikusita, **6. kapituluak** NiCu/ZrO<sub>2</sub> sistema katalitikoaren ulermen sakona du ardatz. Ondorioz, metal kargaren eragina eta inpregnazio metodoa aztertuta ziren. Ni eta Cu metalak elkarrekin inpregnatuak izan ziren edo sekuentzialki inpregnatuak (lehenik metal bat inpregnatzen da eta gero bigarrena). Oro har, katalizatzaile bimetalikoek beren homologo monometalikoek baino errendimendu eta egonkortasun hobea aurkeztu zuten. Hau, ziur aski, Ni-Cu interakzioaren presentziaren ondorio da. Gainera, metalen inpregnazio sekuentzialak Ni-Cu interakzio handiagoa, partikula tamaina txikiagoa eta azidotetasun txikiagoa ezarri

zituen. Azkenik, katalizatzailearen gainazaleko Ni metalikoa izan zen DMTHF-ren ekoizpenaren arduraduna.

**7. kapitulu**an, ikatz komertzialaren eta biomasatik eratorritako ikatzaren erabilera aztertzen da, Ni eta Cu monometalikoek eta Ni-Cu bimetalikoek katalizatzaileetarako euskarri katalitiko gisa. Horretarako, lau euskarri prestatu ziren: ikatz komertziala, biomasatik eratorritako ikatza, tratatutako ikatz komertziala eta tratatutako biomasatik eratorritako ikatza. Azken bi euskarri hauen tratamendua ikatzak azidoarekin ( $\text{HNO}_3$ ) aurretratatzean eta ondoren NaOH-rekin neutralizatzean datza. Oro har, katalizatzaile bimetalikoek, erabilitako euskarria edozein dela eta, zentro azidoen eta zentro metalikoen balantze hobea erakutsi zuten (Ni-Cu fase aktiboa), horrek jarduera egonkorra eskainiz.

Azkenik, **8. kapitulu**ak lan esperimentaletik ateratako ondorio garrantzitsuenak laburbiltzen ditu. Ni-Cu sistema bimetaliko katalitikoak DMF eta DMTHF ekoizteko sistema aktibo eta egonkor gisa aurkezten dira ohande finkoko erreaktore katalitiko batean. Gainera, ikerketarako mesedegarria izan daitekeen etorkizuneko lana ere deskribatzen da.



## **Resumen**

La presente tesis doctoral se inició en marzo de 2017 con el apoyo del Gobierno de España en el marco del proyecto REBICAT (Tecnologías Catalíticas Avanzadas para la Transformación de Residuos Biomásicos en Biocombustibles y Productos Renovables) de los Planes Nacionales del Ministerio de Economía y Competitividad y el grupo de investigación de Ingeniería de Procesos Sostenibles (Supren), integrado en el Departamento de Ingeniería Química y del Medio Ambiente de la Escuela de Ingeniería de Bilbao (Universidad del País Vasco, UPV/EHU). Este trabajo se ha realizado bajo la supervisión del Dr. Jesús M. Requies Martínez y el Dr. Ion Agirre Arisketa. Además, durante esta tesis doctoral se llevó a cabo una estancia de investigación de seis meses en el Dipartimento di Chimica Industriale “Toso Montari” de la Universidad de Bolonia (Italia) bajo la supervisión del profesor Fabrizio Cavani y con el amable apoyo del Dr. Tommaso Tabanelli y la estudiante de doctorado Giulia Balestra.

A lo largo de estos años, el trabajo realizado en esta tesis doctoral ha permitido el desarrollo de sistemas catalíticos avanzados para producir biocombustibles a partir del compuesto 5-hidroximetilfurfural (HMF). Este compuesto es una molécula plataforma derivada de la biomasa, la cual puede ser transformada en diferentes productos químicos de valor añadido y biocombustibles.

Por otro lado, esta tesis doctoral ha posibilitado la publicación de diversos artículos científicos en diferentes revistas indexadas. Concretamente, se han publicado 4 artículos en revistas indexadas Q1 y un artículo en una revista indexada Q2. Además, ha permitido la defensa de diferentes publicaciones en siete congresos internacionales y un congreso nacional.

La tesis doctoral está estructurada en diferentes capítulos, que se resumirán brevemente en los siguientes párrafos.

El **Capítulo 1** destaca la necesidad de reemplazar el uso de combustibles fósiles convencionales. En este sentido, la biomasa es la única fuente de energía renovable que puede sustituir a los productos de tipo petroquímico. Por tanto, se destaca la importancia de investigar la conversión de la biomasa lignocelulósica en productos

químicos de valor añadido y biocombustibles. Debido a la complejidad de la biomasa lignocelulósica, la mayoría de las rutas catalíticas implican la conversión de esta materia prima renovable en varias moléculas plataforma, como el HMF, un intermedio versátil para la obtención de productos químicos y biocombustibles. En este capítulo se describen las propiedades y aplicaciones prometedoras de dos biocombustibles derivados de HMF, el 2,5-dimetilfurano (DMF) y el 2,5-dimetiltetrahidrofurano (DMTHF).

En el **Capítulo 2** se expone una revisión exhaustiva del estado del arte de la producción de DMF y DMTHF. En primer lugar, se detalla la producción catalítica directa de DMF a partir de la biomasa y azúcares. Se describe la transformación directa de DMF partiendo de diversas materias primas (rastrajo de maíz, agar, glucosa, fructosa, etc.). Posteriormente, se describe la producción de DMF a partir de HMF. En este sentido, se describen ampliamente las principales rutas de reacción y los sistemas catalíticos más novedosos. Por último, se describen las recientes investigaciones en la producción de DMTHF. La obtención de este compuesto ha cobrado importancia en los últimos años, por lo que el número de investigaciones llevadas a cabo en la transformación de HMF a DMTHF es moderado.

En el **Capítulo 3** se define el objetivo principal de esta tesis doctoral: desarrollo de tecnologías catalíticas avanzadas para la producción de biocombustibles a partir de la hidrogenólisis selectiva de la molécula de plataforma derivada de la biomasa (HMF) empleando un reactor de lecho fijo. Para cumplir con este objetivo principal, se describen algunos propósitos parciales basados en la utilización de diferentes metales activos y soportes del catalizador.

El **Capítulo 4** describe los procedimientos experimentales y analíticos empleados para el desarrollo de la presente tesis doctoral. En este sentido, se describen con exactitud los métodos de preparación de los catalizadores y las técnicas de caracterización empleadas para el estudio físico-químico de las propiedades de los catalizadores sintetizados. Además, se detalla el sistema de reacción empleado, basado en un reactor de lecho fijo al que se alimenta el HMF diluido en 1-butanol y se evapora para llevar a cabo la reacción en fase gas, mezclando a continuación una corriente de H<sub>2</sub>

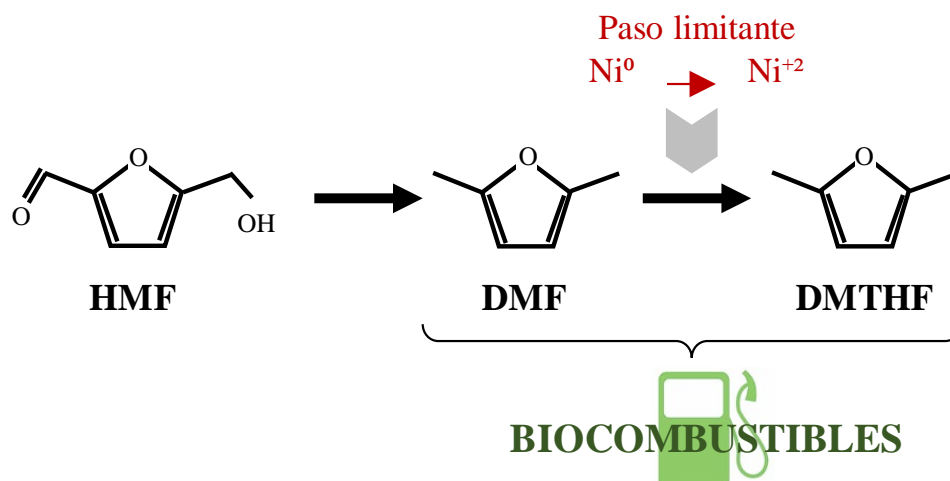


justo antes de alimentar la mezcla total al reactor. Después de la reacción, el H<sub>2</sub> se separa de la corriente mediante un condensador (célula peltier), la cual permite recoger los productos en fase líquida. Por último, se describen los sistemas de análisis con los respectivos métodos empleados para el análisis de los productos obtenidos. Se utilizan tanto un cromatógrafo de líquidos (HPLC) para la cuantificación del HMF como un cromatógrafo de gases para la cuantificación de los productos de reacción (DMF, DMTHF, productos intermedios, etc.). Por último, los posibles productos desconocidos son analizados en un cromatógrafo de gases conectado a un detector de masas (GC-MS), el cual nos permite definir qué compuestos son aquellos que desconocemos.

El **Capítulo 5** contiene los primeros resultados experimentales de este trabajo. La reacción de hidrogenólisis de HMF para la producción de DMF y DMTHF se lleva a cabo a 15 bar de H<sub>2</sub> y 275 ° C. En este capítulo, los catalizadores basados en Cu/ZrO<sub>2</sub> se modifican para mejorar la actividad catalítica del sistema. Para ello, en primer lugar, se añadieron diferentes contenidos metálicos de Cu al soporte de ZrO<sub>2</sub>. Después de estudiar la cantidad óptima de Cu (15 wt%), el soporte de ZrO<sub>2</sub> se modificó con CeO<sub>2</sub> para mejorar sus propiedades. El efecto esperado de la ceria no mejoró la actividad del catalizador. Por último, se añadieron metales nobles (Ru) y no nobles (Ni) a la fase activa. La adición de Ru mejoró levemente la actividad durante las primeras horas de reacción, pero manifestó la desactivación del catalizador. El catalizador más activo de este *screening* catalítico fue NiCu/ZrO<sub>2</sub>, obteniendo un máximo rendimiento a los productos de interés del 50 %. La elevada actividad de este catalizador se atribuyó a la interacción entre el Ni y el Cu.

En vista de los resultados obtenidos en el capítulo anterior, el **Capítulo 6** se centra en la comprensión profunda del sistema catalítico NiCu/ZrO<sub>2</sub>. En consecuencia, se estudió el efecto de la carga metálica (diferentes contenidos metálicos de Ni y de Cu) y el método de impregnación. Los metales de Ni y de Cu fueron co-impregnados (ambos metales impregnados en el mismo paso) o impregnados secuencialmente (primero se impregna un metal y en una segunda etapa el otro metal). En general, los catalizadores bimetálicos registraron un mejor rendimiento y una mayor estabilidad que sus homólogos monometálicos. Probablemente esto se deba a la presencia de la interacción Ni-Cu. Además, la impregnación secuencial de los metales estableció una

mayor interacción Ni-Cu, un menor tamaño de partícula y una menor acidez. Estas características mejoraron la actividad de dichos catalizadores. Finalmente, el Ni metálico depositado sobre la superficie del catalizador fue probablemente el responsable de la producción de DMTHF. Es decir, el Ni metálico en superficie posiblemente hidrogena el doble enlace del anillo furánico, obteniendo DMTHF a partir de DMF. El Ni es oxidado durante la reacción, reduciendo la capacidad hidrogenante del níquel. Por ello, la producción de DMTHF disminuye, aumentando la producción de DMF. Es decir, al oxidarse el Ni, pierde la capacidad de hidrogenar el anillo furánico.



El **Capítulo 7** examina el uso de carbón comercial y carbón derivado de la biomasa como soportes catalíticos para catalizadores de Ni y Cu monometálicos y Ni-Cu bimetálicos. Para ello, se prepararon cuatro soportes diferentes: carbón comercial, carbón derivado de la biomasa, carbón comercial tratado y carbón derivado de la biomasa tratado. Estos últimos se pretrataron con ácido (HNO<sub>3</sub>) y se neutralizaron con NaOH. A todos los carbones se les añadió caolín para aumentar la resistencia mecánica del catalizador. En general, los catalizadores bimetálicos, independientemente del soporte, mostraron un mejor balance de los centros ácidos y los centros metálicos (fase activa Ni-Cu), lo cual conlleva una actividad estable. En cambio, los catalizadores monometálicos mostraron altos rendimientos de los productos de interés al comienzo de la reacción. Sin embargo, sufrieron la desactivación del catalizador, probablemente

debido a la sinterización de los centros activos. Al igual que en el capítulo anterior, se observó una relación entre el contenido de Ni metálico en la superficie del catalizador y la cantidad de DMTHF producido.

Finalmente, el **Capítulo 8** resume las conclusiones más relevantes obtenidas del trabajo experimental de acuerdo con los objetivos establecidos en el Capítulo 3. Los prometedores sistemas bimetálicos catalíticos de Ni-Cu se presentan como activos y selectivos para la producción de DMF y DMTHF en un reactor catalítico de lecho fijo. Además, son estables durante 25 horas de reacción. Por último, se describe el trabajo futuro que puede ser favorable para la investigación.



## Summary

The present PhD thesis started in March 2017 with the support of the Spanish Government under the REBICAT project (Advanced Catalytic Technologies for the Transformation of Biomass Waste into Biofuels and Renewable Products) on the National Plans of the Ministry of Economy and Competitiveness and the research group Sustainable Process Engineering (Supren) integrated in the Department of Chemical and Environmental Engineering of the School of Engineering of Bilbao (University of the Basque Country, UPV/EHU). This work has been carried out under the supervision of Dr. Jesus M. Requies Martínez and Dr. Ion Agirre Arisketa. Moreover, during this PhD thesis a six month research stay in the *Dipartimento di Chimica Industriale "Toso Montari"* from the University of Bologna (Italy) was carried out under the supervision of Professor Fabrizio Cavani, and with the kind support of Dr. Tommaso Tabanelli and Giulia Balestra.

Along these years, this work permitted to progress in the development of advanced catalytic systems to produce biofuels from biomass-derived 5-hydroxymethylfurfural (HMF). Furthermore, this PhD thesis allowed the publication of five scientific papers in Q1 indexed journals and one more paper in a Q2 indexed journal. Moreover, this PhD thesis permitted the publication in seven international conferences and one national conference. The PhD thesis is structured in different chapters, which will be briefly summarized in the following paragraphs.

**Chapter 1** emphasises the need of replacing the use of conventional fossil fuels. In this sense, biomass is the only renewable energy source that can replace petrochemical-type products. Therefore, the importance of investigating the conversion of lignocellulosic biomass into value-added chemicals and biofuels is outlined. Due to the complexity of the lignocellulosic biomass, most catalytic routes involve the conversion of this renewable feedstock into several platform molecules, such as HMF, a versatile intermediate for the production of chemicals and biofuels. In this chapter, the promising properties and applications of two biofuels derived from HMF, 2,5-dimethylfuran (DMF) and 2,5-dimethyltetrahydrofuran (DMTHF), are outlined.

Consequently, in **Chapter 2** an exhaustive review of the state of art is described. Firstly, the direct catalytic production of DMF from biomass and sugars is reported. The transformation of diverse feedstock (corn stover, agar, glucose, fructose, etc.) into DMF is outlined. Subsequently, the production of DMF from HMF is described. In this sense, the main reaction pathways and catalytic systems are extensively reported. Lastly, the recent investigations in the production of DMTHF are described.

In **Chapter 3** the main objective of this PhD thesis is defined. To fulfil this main objective, some partial goals are described based on different active metals and catalyst support materials.

**Chapter 4** describes the experimental and analytical procedures employed for the development of the present PhD thesis. In this sense, the catalyst preparation methods, the reaction system, the analysis methods and the characterization techniques are precisely described.

**Chapter 5** contains the first experimental results of this work. In this chapter, Cu/ZrO<sub>2</sub> based catalysts are modified to enhance the catalytic activity of the system. For this purpose, firstly, different Cu metallic content were loaded to ZrO<sub>2</sub> support. Additionally, ZrO<sub>2</sub> support was modified with CeO<sub>2</sub>. Moreover, noble (Ru) and non-noble (Ni) metals were loaded to the active phase. The catalysts were used for the hydrogenolysis of HMF for the production of DMF and DMTHF at 15 bar of H<sub>2</sub> and 275 °C. The most active catalyst of this catalytic screening was NiCu/ZrO<sub>2</sub>. The good performance of this catalyst was attributed to the interaction between Ni and Cu.

In view of the obtained results in the previous chapter, **Chapter 6** focuses on the deep understanding of NiCuZr catalytic system. Accordingly, the effect of the metal loading and the impregnation method was studied. The Ni and Cu metals were co-impregnated (both metals impregnated in the same step) or sequentially impregnated (first one metal is impregnated and later the second metal). In general, bimetallic catalysts recorded a better performance and stability than their monometallic counterparts. This is probably due to the presence of the Ni-Cu interaction. Moreover, the sequential impregnation of the metals implied higher Ni-Cu interaction, smaller particle size and lower acidity.

Finally, metallic Ni deposited onto the surface of the catalyst was responsible for DMTHF production.

**Chapter 7** examines the use of commercial carbon and biomass-derived carbon as catalytic support for monometallic Ni and Cu and bimetallic Ni-Cu catalysts. For this purpose, four different supports were prepared: commercial carbon, biomass-derived carbon, treated commercial carbon and treated biomass-derived carbon. These last two carbons were pretreated with acid ( $\text{HNO}_3$ ) and the neutralized with NaOH. In general, the bimetallic catalysts, regardless the support, showed a better balance of the acid sites and metallic sites (Ni-Cu active phase) to end with stable operation.

Finally, **Chapter 8** summarizes the most relevant conclusions achieved from the experimental work. The promising Ni-Cu bimetallic catalytic systems are presented as active and stable for the production of DMF and DMTHF in a continuous flow reactor. Moreover, the possible future work is outlined.





## **List of tables and figures**

### **CHAPTER 1: Introduction.**

Table 1.1. Properties of conventional gasoline and different biofuels.

Figure 1.1. Global CO<sub>2</sub> emissions since 1990 and future perspective.

Figure 1.2. Total energy supply by source and change in final energy consumption by sector (2000-2018).

Figure 1.3. Global price of Brent crude and WTI crude.

Figure 1.4. Biomass global energy supply.

Figure 1.5. Lignocellulose composition: cellulose, hemicellulose and lignin.

Figure 1.6. Platform molecules obtained from lignocellulosic biomass.

Figure 1.7. Formation steps of HMF from cellulose.

Figure 1.8. HMF derived products (furan-based derivatives and ring-opening products).

Figure 1.9. Reaction pathway of HMF hydrogenolysis and hydrogenation.

### **CHAPTER 2: State of art.**

Table 2.1. DMF direct production from biomass.

Table 2.2. Activity results of monometallic noble metal catalysts.

Table 2.3. Activity results of monometallic non-noble metal catalysts.

Table 2.4. Activity results of bimetallic catalysts.

- Table 2.5. Catalytic activity of DMTHF production.
- Figure 2.1. Schematic diagram for the conversion of fructose to DMF.
- Figure 2.2. One-pot process to generate DMF from fructose.
- Figure 2.3. Main reaction pathway for the hydrogenolysis of HMF to DMF.
- Figure 2.4. Reaction pathway of HMF to DMF and DMTHF with 5-MF as intermediate.
- Figure 2.5. HMF hydrogenolysis and etherification pathway to DMF.
- Figure 2.6. Phase observation over different pressures and main product of each division.
- Figure 2.7. Difference on product distribution depending on the reaction temperature.

#### **CHAPTER 4: Experimental.**

- Figure 4.1. Catalyst preparation scheme.
- Figure 4.2. Continuous reaction system: pilote plant and scheme.
- Figure 4.3. Chromatographs employed in the analysis: HPLC and GC-FID.

#### **CHAPTER 5: Cu/ZrO<sub>2</sub> based heterogeneous catalysts screening**

- Table 5.1. Activity results after 6 hours-on-stream at different operating conditions at WHSV = 0.15 h<sup>-1</sup>.
- Table 5.2. Textural, chemical and acidic properties for the CuZr catalysts.
- Table 5.3. XPS results for the CuZr catalysts.
- Table 5.4. Textural, chemical and acidic properties for the CuCeZr catalysts.

- Table 5.5. XPS results for the CuCeZr catalysts.
- Table 5.6. Textural, chemical and acidic properties for the RuCuZr catalysts.
- Table 5.7. XPS results for the RuCuZr catalysts.
- Table 5.8. Textural, chemical and acidic properties for the NiCuZr catalysts.
- Table 5.9. XPS results for the NiCuZr catalysts.
- Figure 5.1. H<sub>2</sub>-TPR profiles for the CuZr catalysts.
- Figure 5.2. XRD patterns for the CuZr catalysts.
- Figure 5.3. Activity results for the CuZr based catalysts.
- Figure 5.4. H<sub>2</sub>-TPR profiles for the CuCeZr catalysts.
- Figure 5.5. XRD patterns for the CuCeZr catalysts.
- Figure 5.6. Activity results for the CuCeZr catalysts.
- Figure 5.7. H<sub>2</sub>-TPR profiles for the RuCuZr catalysts.
- Figure 5.8. Activity results for the RuCuZr catalysts.
- Figure 5.9. H<sub>2</sub>-TPR profiles for the NiCuZr catalysts.
- Figure 5.10. XRD patterns for the NiCuZr catalysts.
- Figure 5.11. Activity results for the NiCuZr catalysts.

**CHAPTER 6: The role of Ni and Cu interaction on the bimetallic Ni-Cu/ZrO<sub>2</sub> catalytic system.**

- Table 6.1. Chemical and textural properties for the calcined support and catalysts.
- Table 6.2. Deconvolution of H<sub>2</sub>-TPR profiles (maximum temperature of the reduction peaks and contribution in area %).

- Table 6.3. Amount of NH<sub>3</sub> desorbed in NH<sub>3</sub>-TPD.
- Table 6.4. Crystallite size of different catalysts.
- Table 6.5. Mean particle size for the bimetallic catalysts.
- Table 6.6. XPS results for the monometallic and bimetallic catalysts.
- Table 6.7. XRD results for the 15Cu-30NiZr catalyst tested at different reaction times.
- Table 6.8. XPS results for the 15Cu-30NiZr catalyst tested at different reaction times.
- Figure 6.1. H<sub>2</sub>-TPR profiles for the monometallic catalysts.
- Figure 6.2. H<sub>2</sub>-TPR profiles for the bimetallic catalysts.
- Figure 6.3. XRD patterns for the monometallic catalysts.
- Figure 6.4. XRD patterns for the bimetallic catalysts.
- Figure 6.5. XRD enlarged graph ( $2\theta = 42.0 - 46.0$ ) for the monometallic and bimetallic catalysts.
- Figure 6.6. STEM images for the bimetallic catalysts: a) 15Ni15CuZr; b) 30Ni15CuZr; c) 15Cu-15NiZr; d) 15Ni-15CuZr; e) 15Cu-30NiZr; f) 30Ni-15CuZr.
- Figure 6.7. Conversion and yield for the monometallic catalysts.
- Figure 6.8. Conversion and yield for the bimetallic catalysts impregnated in one step.
- Figure 6.9. Conversion and yield for the bimetallic catalysts impregnated in two steps.
- Figure 6.10. Relation between % Ni-Cu and maximum yield.

**CHAPTER 7: Biomass-derived carbon as catalyst support in bimetallic Ni-Cu catalysts.**

- Table 7.1. Elemental analysis for the carbon supports determined by CHN analyses.
- Table 7.2. Textural properties for the thermally treated supports (obtained from N<sub>2</sub>-physysorption).
- Table 7.3. Chemical and textural properties for the monometallic and bimetallic catalysts.
- Table 7.4. Crystallite size (nm) for the monometallic and bimetallic catalysts.
- Table 7.5. Dispersion and metallic particle size for the most relevant fresh reduced and used catalysts.
- Table 7.6. Oxidation state of Ni and Cu for the monometallic and bimetallic catalysts.
- Table 7.6. Elemental composition for the monometallic and bimetallic catalysts.
- Figure 7.1. Amount of NH<sub>3</sub> desorbed in NH<sub>3</sub>-TPD for the different thermally treated supports and catalysts.
- Figure 7.2. XRD patterns for the monometallic catalysts.
- Figure 7.3. XRD patterns for the bimetallic catalysts.
- Figure 7.4. XRD patterns for the fresh reduced bimetallic catalysts (enlarged graph).
- Figure 7.5. Particle size distribution (histograms) and cumulative frequency for the fresh reduced and used catalysts.
- Figure 7.6. Conversion and yield for the monometallic catalysts.
- Figure 7.7. Conversion and yield for the bimetallic catalysts.

Figure 7.8. Relation between DMTHF production at the beginning of the reaction and the metallic Ni content on the catalyst surface.

Figure 7.9. Relation between DMF and DMTHF mean production at the first stage of the reaction and the metallic content on the catalyst surface.

### **List of acronyms**

BC: Biomass-derived carbon.

BET: Brunauer, Emmet and Teller method.

BHMF: 2,5-bis(hydroxymethyl)furan.

BHMTFH: 2,5-bis(hydroxymethyltetrahydro)furan.

BJH: Barret, Joyner and Halenda method.

BMIMCl: 1-butyl-3-methylimidazolium chloride.

BN: Boron nitride.

CC: Commercial carbon.

CHN: Elemental analysis (carbon, hydrogen, nitrogen).

CNT: Carbon nanotube.

CSU: Coordinated unsaturated sites.

CPME: Cyclopentyl methyl ether.

DFF: 2,5-diformylfuran.

DMA: N,N-dimethylacetamide.

DMDF: Dimethyl disulphide.

DMF: 2,5-dimethylfuran.

DMSO: Dimethyl sulfoxide.

DMTHF: 2,5-dimethyltetrahydrofuran.

DOE: US Department of Energy.

EISA: Evaporation-induced self-assembly.

EMIMCl: 1-ethyl-3-methylimidazolium chloride.

FA: Formic acid.

FDCA: Furan-2,5-dicarboxylic acid.

FID: Flame ionization detector.

FMF: 5-(formyloxymethyl) furfural.

GC: Gas chromatograph.

HAADF: High-angle annular dark-field.

HCS: Hollow carbon nanospheres.

HD: 2,5-hexanedione.

HDO: 1,6-hexanediol.

HI: hydroiodic acid.

HMF: 5-hydroxymethylfurfural.

HPLC: High performance liquid chromatograph.

HT: Hydrotalcite.

HTO: 1,2,6-hexanetriol.

H<sub>2</sub>-TPR: Temperature programmed reduction with hydrogen.

ICP-OES: Inductively coupled plasma optical emission spectroscopy.

IL: Ionic liquid.

LA: Levulinic acid.



MFA: 5-methyl furfuryl alcohol.

MFOs: Metal-organic frameworks.

MS: Mass detector.

MTHFA: 5-methyl tetrahydrofurfuryl alcohol.

MW: Microwave.

NGr: N-graphene.

NH<sub>3</sub>-TPD: Temperature programmed desorption with ammonia.

NP: Nanoparticles.

NrC: Nitrogen-rich carbon.

NREL: National Renewable Energy Laboratory.

PMHS: Poly(methylhydrosiloxane).

PMO: Porous metal oxide.

rGO: Reduced graphene oxides.

RID: Refractive index detector.

S-CNT: Sulphur modified carbon nanotubes.

scCO<sub>2</sub>: Supercritical carbon dioxide.

SGO: Sulfonated graphene oxide.

SiC: Silicon carbide.

STEM: Scanning transmission electron microscopy.

TBC: Treated biomass-derived carbon.

TCC: Treated commercial carbon.

TCD: Thermal conductivity detector.

TEM: Transmission electron microscopy.

THF: Tetrahydrofuran.

WHSV: Weight hour space velocity.

WI: Wetness impregnation

WTI: West Texas Intermediate.

XPS: X-ray photoelectron spectroscopy.

XRD: X-ray diffraction.

12-MPA: 12-molybdophosphoric acid.

2-MF: 2-methylfuran.

2-MTHF: 2-methyltetrahydrofuran.

5-MF: 5-methylfurfural.

## **CHAPTER 1: Introduction**

---



## Table of contents

1.1 WORLD ENERGY OUTLOOK: CURRENT SITUATION .....	31
1.2 BIOMASS, A RENEWABLE FEEDSTOCK FOR THE ENERGETIC TRANSITION.....	33
1.3 THE BIOREFINERY CONCEPT .....	35
1.4 TOP PLATFORM MOLECULES DERIVED FROM LIGNOCELLULOSIC BIOMASS CARBOHYDRATES .....	39
1.5 DMF AND DMTHF PROPERTIES AND APPLICATIONS.....	44
1.6 BIOFUELS PRODUCTION FROM HYDROGENOLYSIS OF HMF.....	46



## 1.1 World energy Outlook: current situation

“Immediate and decisive climate action is essential”. The noticeable urgency to protect our planet is stated in the communication “*A Clean Planet for all*” of the European Commission in 2018. There is a need of limiting the increase of global temperature in 1.5 °C. For that purpose, the net-zero CO<sub>2</sub> emissions should be achieved by 2050 [1].

There is an increase in the world energy demand due to the economic growth and development, mainly relying on fossil fuels. This increment in the energy demand is closely related to the rise of the global CO<sub>2</sub> emissions. The combustion of these fossil fuels (coal, oil and gas) emitted over 33.3 Gt of CO<sub>2</sub> in 2019 (see Figure 1.1). In the last years, two-third of these emissions were produced mainly by two sectors: power and transport [2]. It is important to remark the growth of the transport sector over the last decades, which primary source is oil [2].

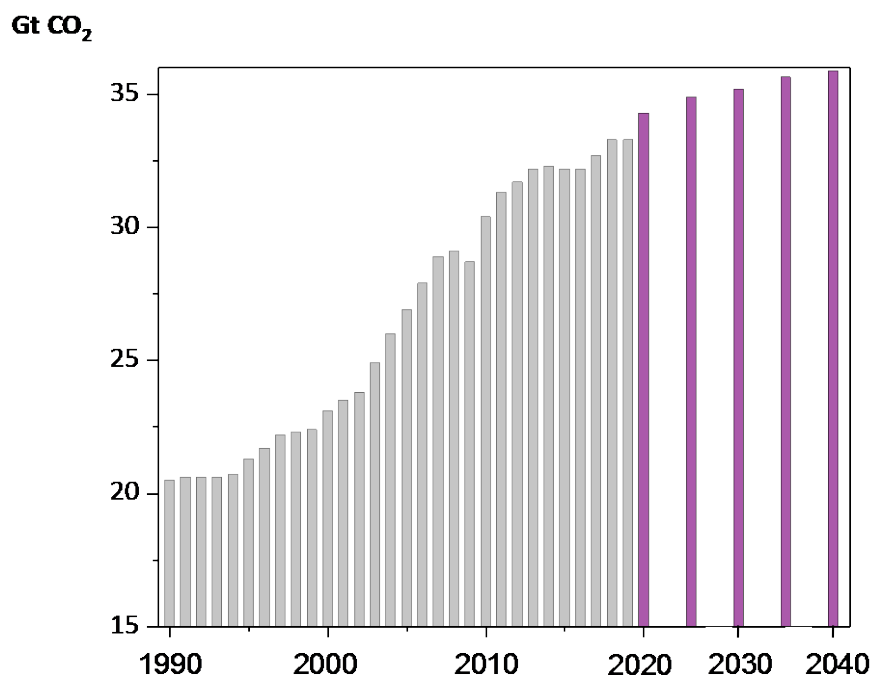


**Figure 1.1.** Global CO<sub>2</sub> emissions since 1990 (data from [3]) and future prespective [4].

The BP energy outlook estimated that the CO<sub>2</sub> emissions will exceed 35 Gt of CO<sub>2</sub> by 2040 [5]. New fuel switch policies, energy efficiency and renewable energy sources are key points in minimizing the emissions. However, still exists a strong reliance on fossil

fuels in the world energy supply. Oil, coal and natural gas were responsible for the 80 % in 2019. Oil was the leading fuel, being responsible of 31 %, followed by coal (26 %) and natural gas (23 %) (see Figure 1.2). The total final energy supply has increased by 65 % in the las three decades (see Figure 1.2), caused by the raising prosperity in fast-growing developing economies and population growth, which will continue increasing by around 1.7 billion to reach 9.2 billion people in 2040 [5].

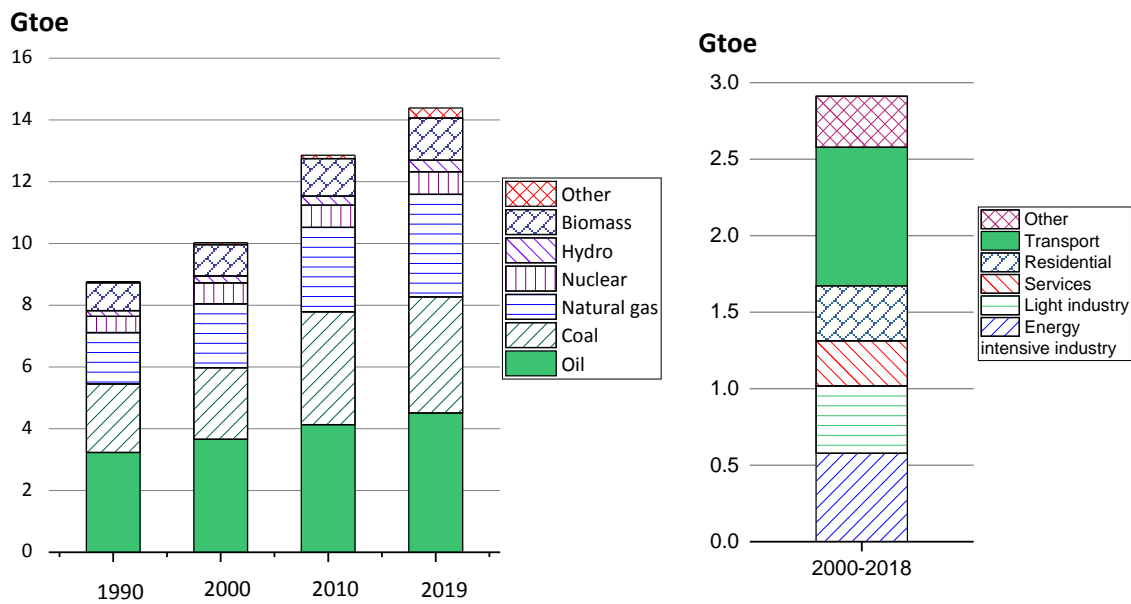


**Figure 1.2.** Total energy supply by source [left] (data from [6,7]) and change in final energy consumption by sector (2000-2018) [right] (data from [8]).

The increase in the final energy consumption between 2000 and 2018 is summarized in Figure 1.2. It can be observed that more than 30 % of the increase in the energy consumption is caused by transport. In this sector the consumption of oil is predominant, with values above 90 % [9].

The relevance of oil in the total energy consumption is evident, but involves significant drawbacks, along with its impact in CO<sub>2</sub> emissions. Disturbances such as armed conflicts, new discoveries and extraction technologies or strategic shifts can result in sharp price fluctuations [10]. In Figure 1.3 the instability of the crude oil price can be observed for both Brent (reference for European markets) and WTI (West Texas Intermediate, reference of U.S. markets). Moreover, the oil production forecast



predicts a near-term peak and subsequent terminal decline due to the physical depletion of the resources [11].

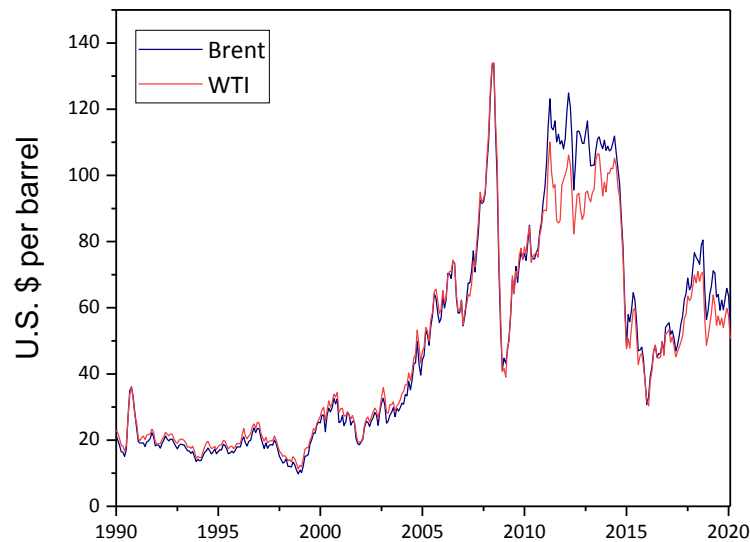


**Figure 1.3.** Global price of Brent crude and WTI crude [12,13].

Therefore, there is strong necessity of replacing conventional oil as raw material for fuels and chemicals. In this sense, biomass is presented as the only renewable energy source of organic carbon that can be used as precursor to products such as value-added chemicals, carbon-based functional materials or liquid fuels [14] in addition to provide a sustainable supply of electricity and heat [15]. The following section will deepen more in this renewable source.

## 1.2 Biomass, a renewable feedstock for the energetic transition

The European Union Directive 2009/28/EC defined biomass as “biodegradable fraction of products, waste and residues from biological origin from agriculture (including vegetal and animal substances), forestry and related industries including fisheries and aquaculture, as well as the biodegradable fraction of industrial and municipal waste” [16]. This involves any material of biological origin, available in non-fossilized form, including arable crops, plants, forestry, animal by-products, biological waste from households, agriculture, animals and food/feed production [15].

Biomass is a carbon-neutral energy source. The released CO<sub>2</sub> during the conversion and combustion of biomass is counter balanced by the CO<sub>2</sub> previously absorbed during its growth. This involves a zero-net balance of CO<sub>2</sub> emissions [15,17].

The most appealing characteristic of this resource is its versatility: it can be used as raw material to produce sustainable electricity or heat supply but also it is the only source of organic carbon in nature, which can be used as feedstock of transport fuel or value-added chemicals. Relatively little attention has been paid to biomass as a chemical feedstock, comparing to the considerable emphasis given to biomass as source of electricity and heat so far [15]. Moreover, biomass resources are common and widespread across the world, unlike other renewable sources [18]. Additionally, it can be easily stored, transported and utilized, giving flexibility to be used when required, depending on the energy demand of the place [19].

Bioenergy (use of biomass explicitly for energy use) is a complex energy system, where multitude variety of feedstock, technology pathways and products need to be contemplated. It is the largest renewable energy source across the world and is responsible of the two-third of renewable energy mix [20].

In 2017 55.6 EJ of biomass was utilized for energy purpose. Primary solid fuel (wood chips, wood pellets, fuelwood for cooking and heating, etc.) was the most used form of biomass, reaching 86 % of the total supply, followed by liquid biofuels (7 %) (see Figure 1.4). Biogas, municipal waste and industrial waste provided the remaining 7 %. Although most of this biomass was expended in the sector of direct heating, since 2000, the global energy supply from biomass has increased 30 %, mostly due to the fact that the supply of liquid biofuels was quadrupled during this period. Thus, in 2017 the 70 % of the total consumption was employed in residential, commercial, agriculture, etc. sectors for heating and cooking [20].

The consumption of biomass differs depending on the stage of development of each area. On the one hand, in developed countries this resource is used to produce liquid fuels (bioethanol and biodiesel), combined heat and power generation and heat in residential areas. On the other hand, in developing countries, biomass may represent

opportunities for domestic industrial development and economic growth. Finally, in least developed countries, especially in rural areas without access to electricity or other energy sources, it is used as the predominant domestic fuel [21].

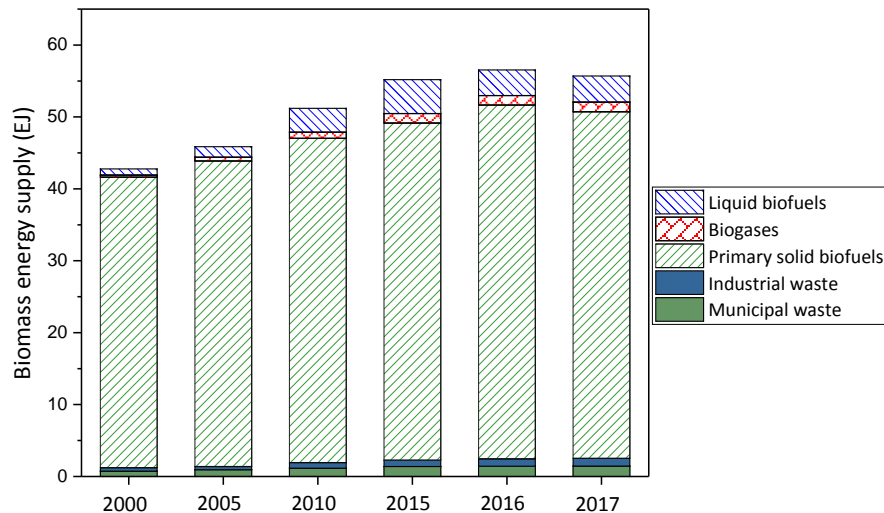


**Figure 1.4.** Biomass global energy supply (data from [20]).

Although biomass has been exploited mainly as a direct energy source so far, especially for heat generation; this energy can also be obtained from other renewable sources. Moreover, bioenergy production will be limited by the biomass supply. Thus, there is a need for optimizing its consumption. For these reasons, and taking into account that biomass is the only renewable source that can replace petrochemical-type products, an investment in biomass conversion processes into valuable products needs to be done, rather than just burning it [15,22]. In this sense, the biorefinery concept has gained relevance in the last decades and will be analysed in the subsequent section.

### 1.3 The biorefinery concept

The National Renewable Energy Laboratory (NREL), which depends on U.S. Department of Energy's Office of Energy Efficiency and Renewable Energy, defined the biorefinery as a facility that integrates biomass conversion processes and equipment to produce fuels, power and chemicals from biomass. The biorefinery concept is analogous to today's oil refinery. An oil refinery produces high-specification fuels and chemicals

from non-renewable crude oils and similarly, a biorefinery enables the conversion of renewable biomass into value-added chemicals, energy and fuels [15,23].

The biorefinery implies multistep processes. First, the feedstock needs to be selected, depending on the required characteristic of the biomass. Next step involves pretreatments (such as extraction) for further processing. Afterwards, biomass is subjected to different conversion processes, which can be biochemical, thermochemical and/or hydrolysis/catalytic [15,22,24].

### **Biochemical conversion**

The carbohydrates (hemicellulose and cellulose) from biomass are converted into sugars, which can be further converted into biofuels and value-added chemicals. The most common biological conversions are fermentation or anaerobic digestion, which are carried out in absence of oxygen. The first process involves microorganisms and enzymes, which are able to produce alcohols (ethanol, butanol or methanol, among others) and organic acids (including, for instance, butyrate acid and acetate acid) from fermentable substrate. Conversely, in anaerobic digestion microorganisms break down complex organic material to produce biogas (methane and CO<sub>2</sub>) [15,22].

### **Thermochemical conversion**

This type of process involves controlled heating to convert biomass into desired chemicals, fuels and/or power. The main pathways are: combustion (complete oxidation), gasification (partial oxidation) and pyrolysis (absence of oxygen). In combustion process, heat and power are generated from the exothermic reaction between oxygen and hydrocarbons from biomass, where the feedstock is converted into H<sub>2</sub>O and CO<sub>2</sub>. In gasification, the available oxygen is approximately one-third of the oxygen needed for complete combustion. This process produces a mixture of CO, CO<sub>2</sub> and H<sub>2</sub>, commonly known as syngas. Lastly, pyrolysis converts the biomass at high temperatures but in absence of oxygen into solid (bio-char), liquid (bio-oils) and gaseous products. Both liquid and gas products can be further converted into valuable fuels and chemicals [22].

**Hydrolysis and catalytic conversion**

This pathway is appropriate if a higher selectivity is desired in the biomass processing. First, the isolation of the monomers is required, which is a complex and expensive step. Subsequently, these monomers can be efficiently processed at relatively mild conditions by different catalytic systems. Wide variety of value-added chemicals and biofuels can be obtained from these processes [25].

The catalytic conversion of biomass has gained attention in the last decades, attributed to the wide variety of interesting chemicals that can be obtained by selective and active catalytic systems. There is a need of replacing the conventional catalytic generation of petrochemical products by developing new catalytic routes for the production of chemicals in biorefineries.

The broad variety of biomass resources provides a heterogeneous raw material with a wide chemical complexity. Four types of biomass can be highlighted due to their economic interest: oleaginous (containing oil or lipids), saccharides (or sugary), starchy and lignocellulosic biomass [24]. For this reason, a preliminary detailed and accurate characterization of biomass feedstock is required to select the proper biomass, depending on the conversion process and the desired final product.

Lignocellulosic biomass has been recognized as the most prosperous feedstock in biorefinery to produce valuable chemicals, fuels and power, due to its low cost and abundancy in agricultural residues and waste streams [24,25]. The structure can be described as a skeleton of cellulose (40-50 wt %), embedded in a cross-linked matrix of hemicellulose (25-35 wt %) within a lignin-based structure (15-20 wt %) [15,25].

**Cellulose**

Cellulose is a high molecular weight polysaccharide constituted of glucose monomers (hexose), creating a linear and crystalline structure. A treatment for isolating the glucose is needed for further transformation of this monomer into value added chemicals including polyols, organic acids and furan derived compounds [26].

### **Hemicellulose**

Hemicellulose is composed by short-branched heteropolymers composed of 5 carbon (pentose) and 6 carbon (hexose) sugars or sugar acids. The most abundant monomer is xylose, which once extracted can be converted into a wide variety of chemicals, such as ethanol via fermentation or furfural by a dehydration process [25,27].

### **Lignin**

Lignin is an amorphous, three-dimensional, highly cross-linked polymeric structure of aromatic units, which provides structural rigidity and a hydrophobicity to plants. This component has been used to produce energy, but the research for valorising this feedstock has recently gained attention, focusing on the separation, purification, fragmentation and functionalization to produce lignin-based high-value products [24,27].

These components develop a complex, robust and heterogeneous structure [14] which needs to be broken into its constituent parts to be efficiently processed [25] (see Figure 1.5). This can be solved by a suitable physical and/or chemical pretreatment of the biomass to achieve an efficient depolymerisation of lignocellulose [14]. These preprocessings serve to depolymerize the lignin seal, which surrounds the hemicellulose and cellulose fractions, and therefore the carbohydrates can be accessible. Subsequently, enzymatic or acid hydrolysis of cellulose and hemicellulose is performed to acquire the desired monomers [25].

The multiple possibilities of the lignocellulosic biomass have been underlined. Moreover, this feedstock does not present the most contentious issue that the existing first-generation biofuels exhibit: “fuel vs food”. These biofuels are produced directly from food crops that can also be consumed as human food, which means that the increase on fuel demand will drop the volume of crops destined for global food markets [28].

Due to the complexity of lignocellulosic biomass, most of the catalytic routes involve the conversion of this renewable feedstock into several versatile platform molecules,

which are further transformed into a variety of important chemicals. Thereby, next section will highlight the most important platform chemicals and building blocks derived from this raw material.

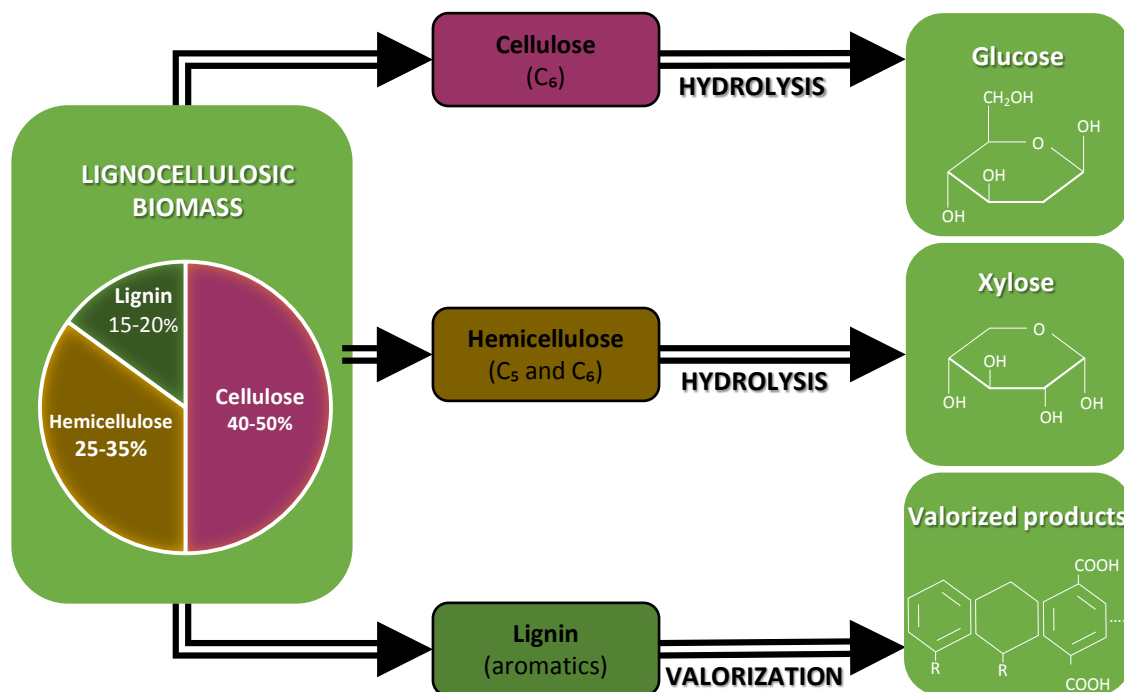


**Figure 1.5.** Lignocellulose composition: cellulose, hemicellulose and lignin (adapted from [14]).

## 1.4 Top platform molecules derived from lignocellulosic biomass carbohydrates

The depolymerisation of cellulose and hemicellulose into simple sugars, cellulose and xylose, is of paramount importance for lignocellulosic biomass valorization. This step is optimized and controlled by an active and selective catalytic system. These sugars can be further converted into platform molecules, which are useful for the production of chemicals and fuels [23].

In 2010 Bozell and Petersen [29] developed a list of biobased product opportunities from carbohydrates, updating the previous publication of the US Department of Energy (DOE) in 2004. In the report, the most interesting and promising compounds (platform molecules) and technologies for biorefinery are identified. A short review of

each chemical will be now described, giving special attention to 5-hydroxymethylfurfural (HMF) due to the opportunities this platform molecule provides.

*Ethanol:* It is produced by the fermentation of sugars obtained from biomass. This is the most important biochemical transformation of biomass to produce biofuels. Ethanol can be further dehydrated to ethylene or oxidized to produce acetic acid and ethyl acetate [29].

*Furfural:* Xylose (present in hemicellulose) can be dehydrated to produce furfural. This compound has a highly functionalized molecular structure which makes it attractive for the production of value-added chemicals and fuels. It can be converted into C<sub>4</sub> chemicals, by means of selective oxidation (e.g. maleic acid), and/or C<sub>5</sub> chemicals, via selective hydrogenation and/or hydrogenolysis, including potential fuel components such as 2-methylfuran (2-MF) and 2-methyltetrahydrofuran (2-MTHF) [30].

*5-hydroxymethylfurfural (HMF):* The dehydration of glucose (present in cellulose) produces this target molecule, which can be further converted into value added-chemicals and biofuels. Due to the importance of this molecule, additional extended information will be described below.

*Furan-2,5-dicarboxylic acid (FDCA):* It is produced by the oxidation of HMF. It has been proposed as an important molecule because it can substitute conventional terephthalic and isophthalic acids in the production of polyamides, polyesters and polyurethanes to obtain a greener process [26,29].

*Glycerol and derivatives:* Glycerol is nowadays produced as a by-product in the conversion of fats and oils when biodiesel is produced. Moreover, it can also be produced by fermentation of sugars or hydrogenation of carbohydrates. It can be further converted into a wide variety of chemicals and polymers by different processes such as reduction, dehydration and fermentation. For instance, is commonly used as a polyol for the production of alkyd resins [29,31].



**Biohydrocarbons:** Production of hydrocarbons from biorefinery sugars by biochemical routes has gained attention because they provide a direct drop-in connection between conventional petrochemical industry and biorefining. Isoprene is a high value hydrocarbon and its production is the most studied in this type of processes. Moreover, the bioproduction of long chain hydrocarbons has been deeply examined.

**Organic acids:** Lactic acid, succinic acid and levulinic acid are obtained from the fermentation or chemical conversion of sugars. They have been widely studied because they are precursors for petrochemical products such as solvents (1,4-butanediol, tetrahydrofuran) or biobased polymers [29].

**Sugar alcohols:** Xylitol and sorbitol are commercially produced by catalytic hydrogenation of xylose and glucose, respectively. Moreover, biochemical reduction has also been investigated, although it cannot yet compete with chemical reduction. These alcohols are promising intermediates for the production of hydrocarbons or isosorbide [29].

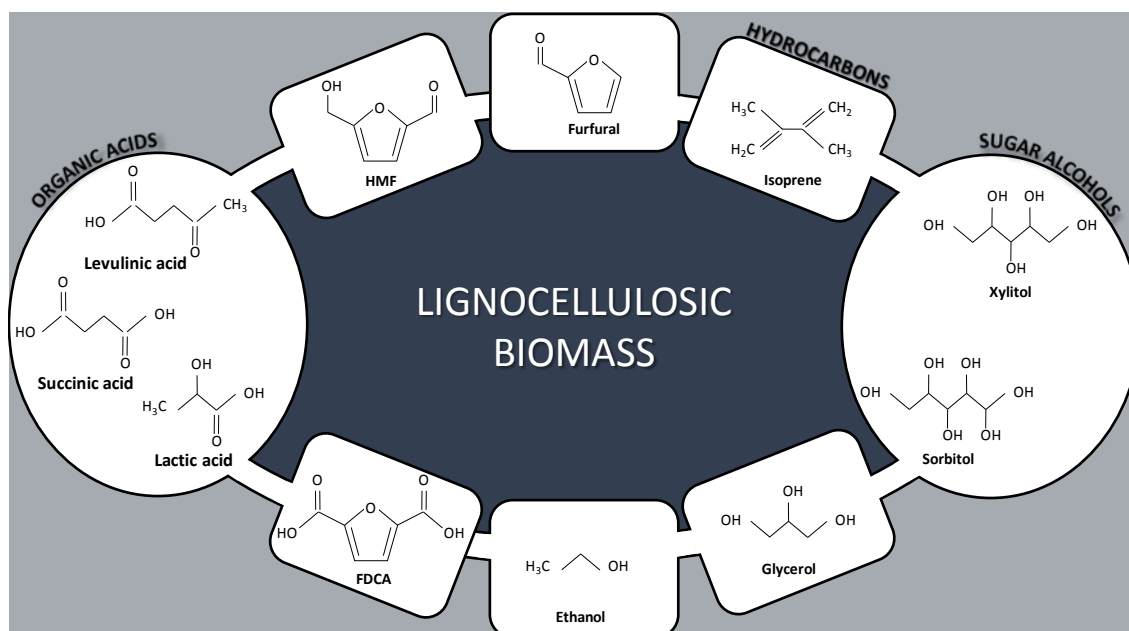


**Figure 1.6.** Platform molecules obtained from lignocellulosic biomass.

### **5-hydroxymethylfurfural (HMF)**

5-hydroxymethylfurfural (HMF) is the most important platform molecule from renewable feedstock for the next-generation plastic and biofuel production. It is called as the “sleeping giant” of renewable intermediate chemicals for having an enormous market potential [26,31]. The HMF derivatives are precursors in the synthesis of materials such as polyesters, polyamides and polyurethane [26]. Moreover, HMF can be converted into biofuels which can be substitutes or additives of conventional fuels [32].

The HMF can be obtained from lignocellulosic biomass generally in three steps: i) hydrolysis of cellulose into glucose, ii) isomerization of glucose into fructose, iii) dehydration of fructose into HMF (see Figure 1.7) [33]. The latter sugar molecule is highly reactive and it can undergo conversion into levulinic and formic acids (FA), step that needs to be avoided to obtain high yields of HMF [29]. Moreover, HMF decomposition must be avoided and for that purpose, ionic liquid media or some specific organic solvents can be employed. Thus, high yields of HMF can be achieved; however, the separation of HMF, for further use, from the reaction mixture is not easy. One option to overcome these difficulties and optimize the extraction of HMF is the use of biphasic systems [29].

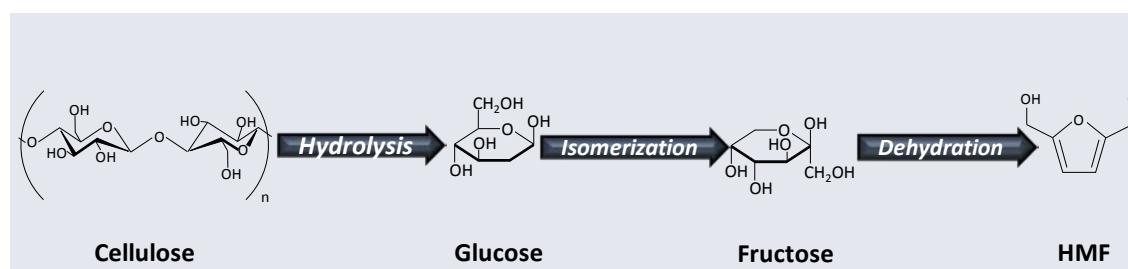


**Figure 1.7.** Formation steps of HMF from cellulose.

Depending on the type of catalyst, the processes are divided into homogeneous (the catalyst and the reaction media are in the same state phase) and heterogeneous (the catalyst and the reaction media are in different state phase). Even though homogeneous inorganic acid and metal chloride catalysts demonstrated high catalytic activity, the use of homogeneous catalysts present several drawbacks. Being in the

same phase that the reaction media, it is difficult to separate the catalyst from the products or reaction system. Moreover, the corrosive nature of inorganic acids involve high maintenance costs due to the damage of the materials and the resulting final waste liquid requires further treatment due to its environmental impact. One solution to avoid these problems is the use of solid acid catalysts (heterogeneous catalysis). In this sense, carbon-based materials, molecular sieves, ion-exchanged resins and heteropoly acids have been extensively studied for the acidic dehydration of glucose to form HMF [33].

The additional conversion of this platform molecule can produce a broad variety of chemicals, such as furan-based derivatives (2,5-diformylfuran (DFF), 2,5-furan carboxylic acid (FDCA), 2,5-bis(hydroxymethyl)furan (BHMF), 2,5-dimethylfuran (DMF), 2,5-dimethyltetrahydrofuran (DMTHF)), and ring-opening products (levulinic acid (LA), 1,2,6-hexanetriol (HTO), 1,6-hexanediol (HDO)).

The partial and selective oxidation of HMF to furan-based products produces DFF. This compound is used in the synthesis of fungicides, drugs and polymeric materials. Further oxidation of DFF leads to the production of FDCA, which is a potential substitute of terephthalic or isophthalic acids in the manufacture of polyamides, polyesters and polyurethanes, as explained above [26].

Another route is the opening of the furan ring. By a Brønsted acid catalyst HMF can be rehydrated into levulinic acid (LA), which is an interesting platform molecule for the production of biofuels, lubricants or plasticizers and thermoplastics or polyols [29,33]. Moreover, the hydrogenation-ring-opening reaction of HMF produces HTO. This compound is applied in the production of drugs and cosmetics as a humidity regulator and viscosity controlling agent [33]. Lastly, HDO is one of the most important diol obtained from lignocellulosic biomass, which is used for the production of polyester and polyurethane. Different reaction pathways have been reported in the open literature, that include direct hydrogenation of HMF to HDO or step hydrogenation through different intermediates [14,31].

Furthermore, BHMF is the hydrogenation product of the aldehyde group in HMF. This chemical is a versatile molecule for the generation of polymers, drugs, etc. Additionally, the hydrogenolysis of HMF produces DMF, which has gained attention because it is a suitable biofuel candidate and an important intermediate in the chemical industry. The deeper reduction of DMF produces DMTHF, another promising biofuel and potential alternative to conventional tetrahydrofuran solvent [32,34].

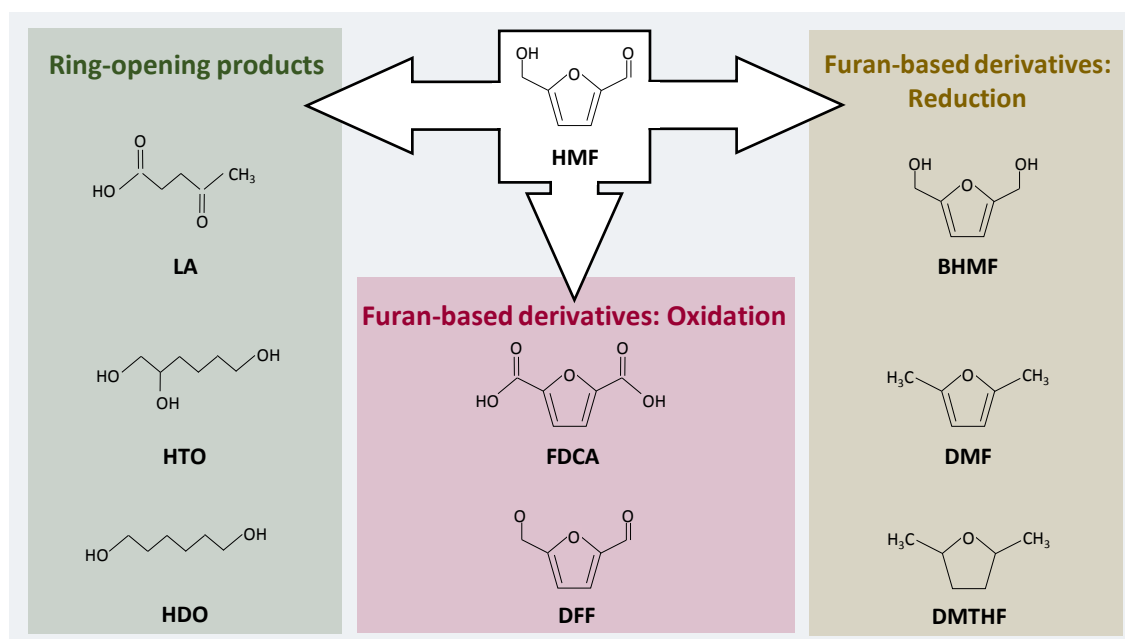


**Figure 1.8.** HMF derived products (furan-based derivatives and ring-opening products).

Due to the multiple options HMF provides, the present PhD thesis focuses on the production of DMF and DMTHF. To understand the importance of these chemical compounds, the next section is dedicated to explain the excellent properties these biofuels offer.

## 1.5 DMF and DMTHF properties and applications

DMF has been extensively studied and the properties of this biofuel have been precisely defined by several authors. On the contrary, DMTHF has gained attention in the last years, and therefore, the research status of this fuel is not as advanced as that

of the DMF. The physical properties of DMF and DMTHF, which are suitable for liquid fuels, are compared with the characteristics of conventional gasoline and ethanol. Although it is already known that the latter presents various restrictions (low energy density, high volatility and high energy consumption in the production stage [35]) it has been also chosen for this comparison as it is the only renewable liquid fuel currently produced in large quantities [36].

It must be remarked that DMF exhibits more suitable properties than bioethanol for replacing conventional gasoline (see Table 1.1). The energy density of DMF ( $31.5 \text{ kJ/cm}^3$ ) is almost 40 % higher than the one from ethanol, and comparable to the one of gasoline ( $32.2 \text{ kJ/cm}^3$ ). Moreover, due to its immiscibility with water (unlike ethanol), absorption of atmospheric steam, and therefore its contamination, is avoided [37]. Furthermore, the higher boiling point of DMF ( $92\text{-}94 \text{ }^\circ\text{C}$ ) makes this fuel less volatile and more convenient for transportation [38]. Lastly, DMF consumes one-third of the energy in its production, compared to the required energy in the fermentation process of bioethanol fabrication [39].

**Table 1.1.** Properties of conventional gasoline and different biofuels.

	<b>Conventional gasoline</b> [40]	<b>Ethanol</b> [40]	<b>DMF</b> [40]	<b>DMTHF</b> [41]
<b>Energy density (<math>\text{kJ/cm}^3</math>)</b>	30-33	21.4	30.1	31
<b>RON</b>	88-98	109	119	82
<b>Boiling point (<math>^\circ\text{C}</math>)</b>	27-225	78	94	90
<b>Water soluble</b>	Insoluble	Highly soluble	Insoluble	Insoluble

Due to the similar physicochemical properties of DMF and gasoline, DMF exhibits very similar combustion and emissions characteristics (CO, HC,  $\text{NO}_x$ , particulate matter) to gasoline [37]. Because of these similarities, the adaptation between this biofuel and current DISI technologies would not be difficult [35].

Similarly to DMF, DMTHF presents characteristics which overcome the limitations of bioethanol, such as higher energy density and boiling point and lower miscibility in

water [42]. In addition, it can be blended with gasoline up to 60 % by volume without deleterious engine performance [43].

Even though the most studied applications of DMF and DMTHF are as substitutes or additives of conventional gasoline, these chemicals can be utilized for other purposes. DMF can also be a renewable source of furan based compounds, which have extensive use in solvent and pharmaceutical industry. Moreover, it is an intermediate for *p*-xylene production, one of the highest volume bulk chemical derived from petroleum [44,45]. DMTHF is also a valuable organic solvent, which can serve as an alternative to conventional tetrahydrofuran solvent. Besides, it can be converted into other high value-added chemicals such as 2,5-hexanediol and 2,4-hexadiene [32,46].

Once the valuable properties of these molecules have been explained, the catalytic production of HMF into biofuels DMF and DMTHF will be discussed in the following section.

## 1.6 Biofuels production from hydrogenolysis of HMF

The catalytic hydrogenolysis of HMF into DMF and DMTHF is an effective and promising approach, which has attracted increasing attention in the last decade due to the excellent properties these biofuels offer [32,47].

HMF is composed of an aldehyde group ( $\text{-C=O}$ ) and a hydroxyl group ( $\text{-OH}$ ) attached to a furan ring. This molecule can follow different reaction pathways when a hydrogenation/hydrogenolysis process is carried out, which causes a complicated reaction network, as it can be observed in Figure 1.9. Ring-opening and C–C cleavage need to be avoided to provide high selectivity to desired biofuels. For that purpose, selective, active and stable catalysts need to be found.

For the production of DMF and DMTHF from HMF, hydrogenation and hydrogenolysis reactions take place. HMF possess both C=C and C=O bonds, which can be hydrogenated over proper catalysts. The direct hydrogenation of HMF produces BHMF (hydrogenation of C=O bond of the aldehyde group) and further hydrogenation of

BHMF yields 2,5-bis(hydroxymethyltetrahydro)furan (BHMTFH) due to the hydrogenation of C=C bonds of the furan-ring. This reaction takes place over the surface of metal catalyst, which absorbs the substrate and activates hydrogen molecules to form active hydrogen species that reduces the double bond. Depending on the desired product, controlled hydrogenation of C=O or C=C needs to be carried out. Additionally, hydrogenolysis reaction is needed to obtain the desired DMF and DMTHF products. Particularly, C–O bond cleavage is required. Some authors explained this cleavage as a combination of dehydration and hydrogenation process to transform C–OH group into a C–H group. This is considered an indirect hydrogenolysis of C–O bond [34,48].

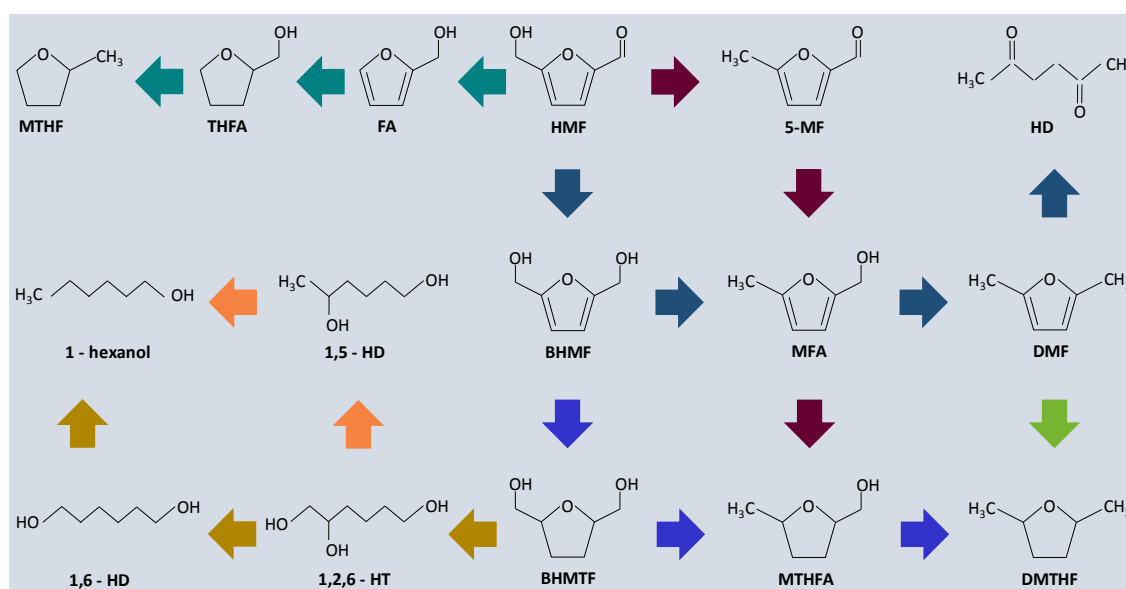


**Figure 1.9.** Reaction pathway of HMF hydrogenolysis and hydrogenation (addapted from [49]).

DMF can be obtained through two possible pathways. Path 1 involves the conversion of HMF to BHMF by the hydrogenation of the aldehyde group and further double hydrogenolysis of C–O to produce 5-methyl furfuryl alcohol (MFA) in a first step and finally DMF in a second step. Path 2 includes a hydrogenolysis as initial step to produce 5-methylfurfural (5-MF). Then, the aldehyde group is hydrogenated to produce MFA and lastly, a hydrogenolysis step produces DMF. Although there is a certain discrepancy in the literature, most of the studies revealed that Path 1 is the main route for DMF production. The difference on the observed pathway could be caused by the diverse nature and properties of the catalytic systems [47].

Similarly, DMTHF production can undergo two different pathways, as stated in literature. In Path 1 DMF undergoes further hydrogenation of the furan ring to produce DMTHF. Alternatively, in Path 2, the furan ring is hydrogenated from BHMF to produce BHMTHF and a sequential double hydrogenolysis of C–O produces 5-methyl tetrahydrofurfuryl alcohol (MTHFA) in a first step and DMTHF in a final second step [50].



**References**

- [1] European Commission. A Clean Planet for all. A European long-term strategic vision for a prosperous, modern, competitive and climate neutral economy. 2018.
- [2] International Energy Agency (IEA). CO2 emissions from fuel combustion. 2019.
- [3] CO2 emissions – Global Energy Review 2019 – Analysis - IEA n.d. <https://www.iea.org/reports/global-energy-review-2019/co2-emissions#abstract> (accessed May 9, 2020).
- [4] BP. Carbon emissions | Energy economics | Home n.d. <https://www.bp.com/en/global/corporate/energy-economics/energy-outlook/carbon-emissions.html> (accessed May 10, 2020).
- [5] BP. BP Energy Outlook 2019 edition. 2019.
- [6] International Energy Agency (IEA). Data & Statistics n.d. [https://www.iea.org/data-and-statistics?country=WORLD&fuel=Energy supply&indicator=Total primary energy supply \(TPES\) by source](https://www.iea.org/data-and-statistics?country=WORLD&fuel=Energy supply&indicator=Total primary energy supply (TPES) by source) (accessed March 27, 2020).
- [7] IEA. Annexes – Global Energy Review 2019 – Analysis - IEA n.d. <https://www.iea.org/reports/global-energy-review-2019/annexes#data-tables> (accessed May 9, 2020).
- [8] Change in final energy consumption by sector, 2000-2018, and by scenario to 2040 – Charts – Data & Statistics - IEA n.d. <https://www.iea.org/data-and-statistics/charts/change-in-final-energy-consumption-by-sector-2000-2018-and-by-scenario-to-2040> (accessed May 11, 2020).
- [9] International Energy Agency. World energy balances: An Overview. J Chem Inf Model 2019;53:1689–99. <https://doi.org/10.1017/CBO9781107415324.004>.
- [10] Monadjemi MS. Oil Prices and the Global Economy. J Econ Public Financ

- 2016;2:353. <https://doi.org/10.22158/jepf.v2n2p353>.
- [11] UK Energy-Research-Centre. Global Oil Depletion. 2009. <https://doi.org/ISBNnumber1-903144-0-35>.
- [12] International Monetary Fund, Global price of WTI Crude (POILWTIUSDM) | FRED | St. Louis Fed n.d. <https://fred.stlouisfed.org/series/POILWTIUSDM> (accessed March 30, 2020).
- [13] International Monetary Fund, Global price of Brent Crude (POILBREUSDM) | FRED | St. Louis Fed n.d. <https://fred.stlouisfed.org/series/POILBREUSDM> (accessed March 30, 2020).
- [14] Jing Y, Guo Y, Xia Q, Liu X, Wang Y. Catalytic Production of Value-Added Chemicals and Liquid Fuels from Lignocellulosic Biomass. *Chem* 2019;5:2520–46. <https://doi.org/10.1016/j.chempr.2019.05.022>.
- [15] Roddy DJ. Biomass in a petrochemical world. *Interface Focus* 2013;3. <https://doi.org/10.1098/rsfs.2012.0038>.
- [16] The European Parliament and The Council. Renewable energy directive. vol. 1. 2008.
- [17] Perea-Moreno MA, Samerón-Manzano E, Perea-Moreno AJ. Biomass as renewable energy: Worldwide research trends. *Sustain* 2019;11:1–21. <https://doi.org/10.3390/su11030863>.
- [18] Vinterbäck J. Global Potential of Sustainable Biomass for Energy Svetlana Ladanai. *Technology* 2009.
- [19] Holm-Nielsen JB. Introduction to biomass supply chains. Elsevier Ltd; 2016. <https://doi.org/10.1016/B978-1-78242-366-9.00001-0>.
- [20] World-Bioenergy-Association. Global Bioenergy Statistics 2019. 2019.
- [21] World-Energy-Council. World Energy Resources 2016. 2016.

- [22] Rabaçal M, Ferreira AF, Silva CAM, Costa M. Biorefineries. Targeting energy, high value products and waste valorization. 2017.
- [23] Melero JA, Iglesias J, Garcia A. Biomass as renewable feedstock in standard refinery units. Feasibility, opportunities and challenges. *Energy Environ Sci* 2012;5:7393–420. <https://doi.org/10.1039/c2ee21231e>.
- [24] Jr V, Pathway R. Biomass and Green Chemistry. 2018. <https://doi.org/10.1007/978-3-319-66736-2>.
- [25] Alonso DM, Bond JQ, Dumesic JA. Catalytic conversion of biomass to biofuels. *Green Chem* 2010;12:1493–513. <https://doi.org/10.1039/c004654j>.
- [26] Kohli K, Prajapati R, Sharma BK. Bio-based chemicals from renewable biomass for integrated biorefineries. *Energies* 2019;12. <https://doi.org/10.3390/en12020233>.
- [27] Sani RK. Biorefining of biomass to biofuels: opportunities and perception. vol. 4. 2018. <https://doi.org/10.1007/978-3-319-67678-4>.
- [28] Behera BK, Varma A. Bioenergy for sustainability and security. 2018. <https://doi.org/10.1007/978-3-319-96538-3>.
- [29] Bozell JJ, Petersen GR. Technology development for the production of biobased products from biorefinery carbohydrates - The US Department of Energy's "top 10" revisited. *Green Chem* 2010;12:539–54. <https://doi.org/10.1039/b922014c>.
- [30] Li X, Jia P, Wang T. Furfural: A Promising Platform Compound for Sustainable Production of C4 and C5 Chemicals. *ACS Catal* 2016;6:7621–40. <https://doi.org/10.1021/acscatal.6b01838>.
- [31] Isikgor FH, Becer CR. Lignocellulosic biomass: a sustainable platform for the production of bio-based chemicals and polymers. *Polym Chem* 2015;6:4497–559. <https://doi.org/10.1039/c5py00263j>.
- [32] Gao Z, Li C, Fan G, Yang L, Li F. Nitrogen-doped carbon-decorated copper

- catalyst for highly efficient transfer hydrogenolysis of 5-hydroxymethylfurfural to convertibly produce 2,5-dimethylfuran or 2,5-dimethyltetrahydrofuran. *Appl Catal B Environ* 2018;226:523–33. <https://doi.org/10.1016/j.apcatb.2018.01.006>.
- [33] Li X, Xu R, Yang J, Nie S, Liu D, Liu Y, et al. Production of 5-hydroxymethylfurfural and levulinic acid from lignocellulosic biomass and catalytic upgradation. *Ind Crops Prod* 2019;130:184–97. <https://doi.org/10.1016/j.indcrop.2018.12.082>.
- [34] Xia H, Xu S, Hu H, An J, Li C. Efficient conversion of 5-hydroxymethylfurfural to high-value chemicals by chemo- and bio-catalysis. *RSC Adv* 2018;8:30875–86. <https://doi.org/10.1039/C8RA05308A>.
- [35] Wang C, Xu H, Daniel R, Ghafourian A, Herreros JM, Shuai S, et al. Combustion characteristics and emissions of 2-methylfuran compared to 2,5-dimethylfuran, gasoline and ethanol in a DISI engine. *Fuel* 2013;103:200–11. <https://doi.org/10.1016/j.fuel.2012.05.043>.
- [36] Da Silva JL, Aznar M. Thermophysical properties of 2,5-dimethylfuran and liquid-liquid equilibria of ternary systems water + 2,5-dimethylfuran + alcohols (1-butanol or 2-butanol or 1-hexanol). *Fuel* 2014;136:316–25. <https://doi.org/10.1016/j.fuel.2014.07.039>.
- [37] Zhong S, Daniel R, Xu H, Zhang J, Turner D, Wyszynski ML, et al. Combustion and Emissions of 2, 5-Dimethylfuran in a Direct-Injection Spark-Ignition Engine 2010:2891–9. <https://doi.org/10.1021/ef901575a>.
- [38] Daniel R, Tian G, Xu H, Wyszynski ML, Wu X, Huang Z. Effect of spark timing and load on a DISI engine fuelled with 2,5-dimethylfuran. *Fuel* 2011;90:449–58. <https://doi.org/10.1016/j.fuel.2010.10.008>.
- [39] Tian G, Daniel R, Li H, Xu H, Shuai S, Richards P. Laminar burning velocities of 2,5-dimethylfuran compared with ethanol and gasoline. *Energy and Fuels* 2010;24:3898–905. <https://doi.org/10.1021/ef100452c>.

- [40] Christensen E, Yanowitz J, Ratcliff M, McCormick RL. Renewable oxygenate blending effects on gasoline properties. *Energy and Fuels* 2011;25:4723–33. <https://doi.org/10.1021/ef2010089>.
- [41] Grochowski MR, Yang W, Sen A. Mechanistic study of a one-step catalytic conversion of fructose to 2,5-dimethyltetrahydrofuran. *Chem - A Eur J* 2012;18:12363–71. <https://doi.org/10.1002/chem.201201522>.
- [42] Li H, Fang Z, Smith RL, Yang S. Efficient valorization of biomass to biofuels with bifunctional solid catalytic materials. *Prog Energy Combust Sci* 2016;55:98–194. <https://doi.org/10.1016/j.pecs.2016.04.004>.
- [43] Rout PK, Nannaware AD, Prakash O, Kalra A, Rajasekharan R. Synthesis of hydroxymethylfurfural from cellulose using green processes: A promising biochemical and biofuel feedstock. *Chem Eng Sci* 2016;142:318–46. <https://doi.org/10.1016/j.ces.2015.12.002>.
- [44] Kazi FK, Patel AD, Serrano-Ruiz JC, Dumesic JA, Anex RP. Techno-economic analysis of dimethylfuran (DMF) and hydroxymethylfurfural (HMF) production from pure fructose in catalytic processes. *Chem Eng J* 2011;169:329–38. <https://doi.org/10.1016/j.cej.2011.03.018>.
- [45] Li C, Cai H, Zhang B, Li W, Pei G, Dai T, et al. Tailored one-pot production of furan-based fuels from fructose in an ionic liquid biphasic solvent system. *Chinese J Catal* 2015;36:1638–46. [https://doi.org/10.1016/S1872-2067\(15\)60927-5](https://doi.org/10.1016/S1872-2067(15)60927-5).
- [46] Li T, Ong SSG, Zhang J, Jia C, Sun J, Wang Y, et al. One-pot conversion of carbohydrates into furan derivatives in biphasic tandem catalytic process. *Catal Today* 2020;339:296–304. <https://doi.org/10.1016/j.cattod.2018.11.052>.
- [47] Wang X, Liang X, Li J, Li Q. Catalytic hydrogenolysis of biomass-derived 5-hydroxymethylfurfural to biofuel 2, 5-dimethylfuran. *Appl Catal A Gen* 2019;576:85–95. <https://doi.org/10.1016/j.apcata.2019.03.005>.

- [48] Schlaf M. Selective deoxygenation of sugar polyols to  $\alpha,\omega$ -diols and other oxygen content reduced materials—a new challenge to homogeneous ionic hydrogenation and hydrogenolysis catalysis. *J Chem Soc Dalton Trans* 2006:4645–53. <https://doi.org/10.1039/b608007c>.
- [49] Tang X, Wei J, Ding N, Sun Y, Zeng X, Hu L, et al. Chemoselective hydrogenation of biomass derived 5-hydroxymethylfurfural to diols: Key intermediates for sustainable chemicals, materials and fuels. *Renew Sustain Energy Rev* 2017;77:287–96. <https://doi.org/10.1016/j.rser.2017.04.013>.
- [50] Mitra J, Zhou X, Rauchfuss T. Pd/C-catalyzed reactions of HMF: Decarbonylation, hydrogenation, and hydrogenolysis. *Green Chem* 2015;17:307–13. <https://doi.org/10.1039/c4gc01520g>.

## **CHAPTER 2: State of art**

---





---

## Table of contents

2.1 DMF PRODUCTION DIRECTLY FROM BIOMASS AND SUGARS.....	59
2.2 DMF PRODUCTION FROM HMF .....	66
2.2.1 <i>Reaction pathway</i> .....	66
2.2.2 <i>Catalytic system</i> .....	70
2.2.2.1 Noble metal monometallic catalysts .....	71
2.2.2.2 Non-noble metal monometallic catalysts.....	75
2.2.2.3 Bimetallic catalysts .....	79
2.3 DMTHF PRODUCTION .....	83



As specified in Chapter 1, this PhD thesis is focused on the production of DMF and DMTHF from HMF. These organic compounds offer excellent properties to be exploited as substitutive or additive of conventional fuels. In the last years, different catalytic systems have been studied for the production of these biofuels. In this second chapter, an extended bibliographic review is presented, including different investigations carried out recently. Firstly, researches focused on the production of DMF directly from biomass have been explained. Subsequently, investigations of the production of DMF from HMF have been described. Finally, the studies focused on DMTHF production have been outlined.

## 2.1 DMF production directly from biomass and sugars

In 2007 Roman-Leshkov et al. [1] described a pioneering process to obtain DMF directly from fructose. The system was divided in two different stages: i) sugar dehydration into HMF and ii) hydrogenolysis of HMF to DMF (see Figure 2.1). In the first step, a biphasic system was used (R1). In the aqueous phase, the fructose was converted to HMF by a homogeneous acid catalyst (HCl) at 180 °C and the produced HMF was extracted by an organic solvent. The use of NaOH in the aqueous phase optimized the extraction of HMF, improving the ratio  $[HMF]_{org}/[HMF]_{aq}$ . Different organic solvents were employed and there was no difference in the obtained results. 1-butanol was selected for further investigations, since this solvent can be produced by the fermentation of biomass-derived carbohydrates (green solvent). The achieved conversion of fructose reached 88 %, with a HMF yield of 82 %. The extracting phase was then purified by vacuum evaporation at low temperature (E1) to separate volatile impurities, which are recycled to the biphasic reactor, from lower relative volatile components (1-butanol and HMF). Next, HMF is converted to DMF over a bimetallic CuRu/C catalyst in both liquid-phase (autoclave reactor) and vapour-phase (flow reactor) systems. Monometallic Cu was able to produce DMF, although it was deactivated by chloride ions, which were not completely removed in the purification step. By contrast, Ru monometallic catalyst was resistant to chloride ions but did not carry out the hydrogenolysis step, obtaining principally BHMTFH. Therefore, the

bimetallic CuRu catalyst was used showing both the hydrogenolysis behaviour of copper and the chlorine resistance of ruthenium. The reaction was studied in liquid and vapour phase at 220 °C. The maximum yield of DMF obtained in the liquid phase at 6.8 bar of H<sub>2</sub> was 61 %, due to the fact that impurities of NaCl slightly lowered the activity of the bimetallic catalyst. However, the vapour phase hydrogenolysis reached DMF yields of 76-79 % since NaCl does not evaporate under the aforementioned conditions and therefore did not contaminate the catalytic system. Finally, the more volatile products (DMF and water) were separated from the solvent and the reaction intermediates (S1), recycling the latter stream back to the hydrogenolysis reactor. Subsequently, DMF was separated spontaneously from water by means of simple condensation.

This innovative work was the starting point of other numerous investigations on the direct production of DMF from lignocellulosic biomass.

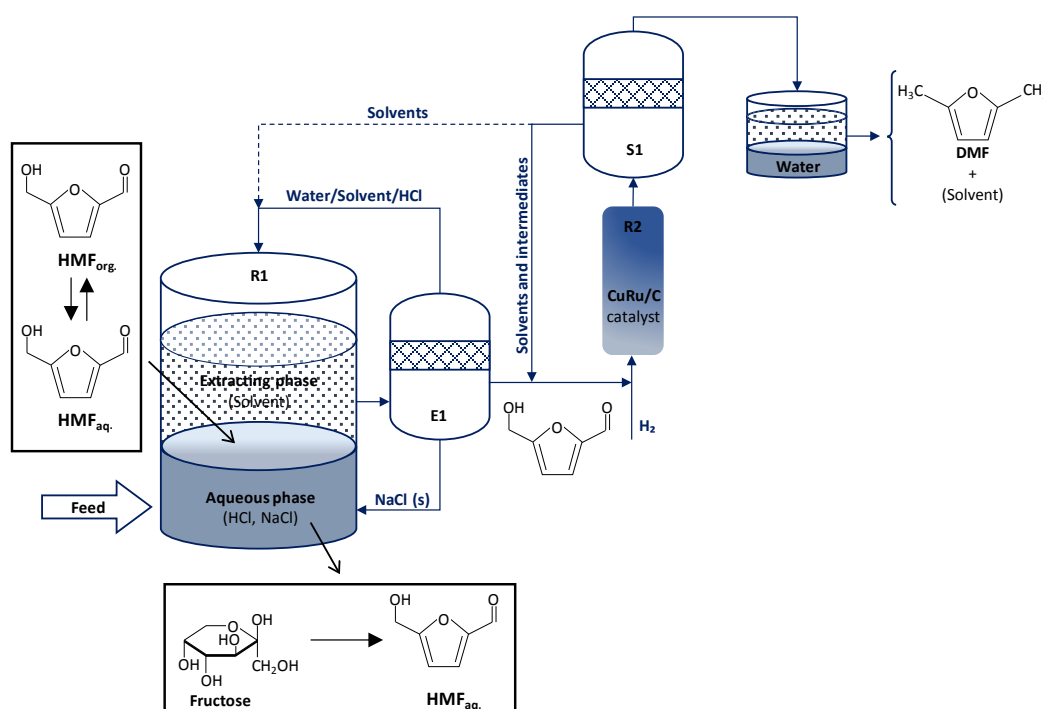


**Figure 2.1.** Schematic diagram for the conversion of fructose to DMF (proposed by Roman-Leshkov et al. [1]).

Based on this work, Binder and Raines [2] studied the production of DMF directly from untreated corn stover in N,N-dimethylacetamide (DMA). Lithium chloride (LiCl) was

used as a promising solvent and a maximum yield of 9 % of DMF (based on the cellulose content of the corn stover) was achieved. As in the previous investigation, the process was carried out in two steps, involving the transformation of the feedstock into HMF by  $\text{CrCl}_3\text{-HCl}$  homogeneous catalyst, followed by the hydrogenolysis to DMF by  $\text{Cu-Ru/C}$  catalyst in 1-butanol in the presence of  $\text{H}_2$ . The most important drawback of this system is the toxicity of the chromium salt along with the mineral acid used as catalyst in the first step. Moreover, the obtained global yield is quite low. Zhang et al. [3] tried to solve the toxicity problem, synthesizing and optimising a  $\text{SO}_4^{2-}/\text{ZrO}_2\text{-TiO}_2$  catalyst for the glucose and xylose mixture dehydration in a biphasic  $\text{H}_2\text{O}/1\text{-butanol}$  system. The extracting solvent containing HMF and furfural was separated and it underwent a further purification step. The hydrogenolysis step was then performed at  $260\text{ }^\circ\text{C}$  by  $\text{Ru/C}$  catalyst, reaching a DMF yield of 32.7 % after 1.5 h on stream in a Parr reactor.

Thananattachon and Rauchfuss [4] studied the dehydration and hydrogenolysis processes of DMF from fructose using FA as an acid catalyst,  $\text{H}_2$  source and deoxygenation agent. In contrast, these authors carried out the process in one unique step, using the so called “one-pot synthesis”. The sugar was kept stirring with the acid at  $150\text{ }^\circ\text{C}$  during 2 h. The obtained solution, containing HMF and its formate ester (FMF), was cooled down to room temperature and diluted in tetrahydrofuran (THF). Moreover,  $\text{H}_2\text{SO}_4$  and  $\text{Pd/C}$  catalysts were added before warming the solution up to  $70\text{ }^\circ\text{C}$ , which was stirred for additional 15 h. The progress of the reaction was followed by the conversion of the intermediaries, MFA and its monoformate ester FMMF (see Figure 2.2). After the overall process, 51 % of DMF yield was reached.

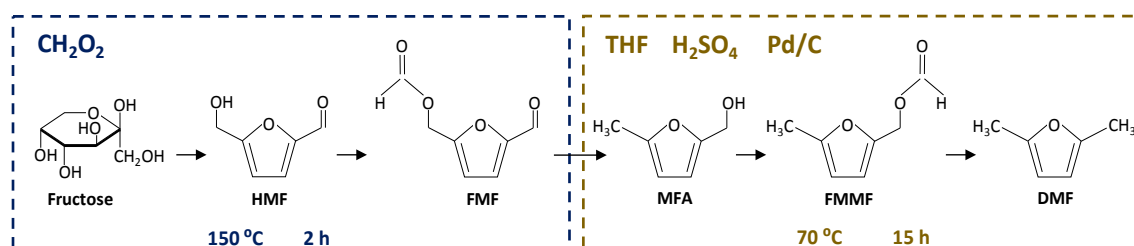


**Figure 2.2.** One-pot process to generate DMF from fructose (adapted from [4]).

Similarly, Chidambaran and Bell [5] studied the glucose dehydration into HMF and its posterior hydrogenolysis to DMF in one-pot synthesis based on ionic liquids (IL). These liquids are salts that melt below 100 °C and provide liquids composed by cations and anions exclusively [6]. The addition of acetonitrile to either 1-butyl-3-methylimidazolium chloride (BMIMCl) or 1-ethyl-3-methylimidazolium chloride (EMIMCl) reduced the tendency of glucose to form humins (both IL exhibited similar activities). Different solid and liquid acids were tested for the dehydration step, obtaining 99 % conversion of glucose and achieving a yield of HMF of 98 % with the solid 12-molybdophosphoric acid (12-MPA) at 120 °C after 3 h of reaction. The mixture was cooled down to 50 °C and 12-MPA was removed and replaced by Pd/C catalyst in order to carry out the hydrogenolysis step of HMF to DMF. This step was performed under 120 °C and 62 bar of H<sub>2</sub> pressure (high H<sub>2</sub> pressure was required due to the low solubility of H<sub>2</sub> in IL) achieving a HMF conversion of 46 % and a DMF yield of 30 % after 1 h. This noticeable decrease of DMF yield, comparing with other investigations, can be attributable to lower temperature and reaction time, as well as low solubility of H<sub>2</sub> in IL. A similar case was studied by De's group [7], obtaining a DMF yield of 24 % from the micro algae derived agar. Brønsted acid IL catalyst ([DMA]<sup>+</sup>[CH<sub>3</sub>SO<sub>3</sub>]<sup>-</sup>) was initially used for the dehydration step to obtain HMF at 150 °C. Then, FA (used as deoxygenating agent and H<sub>2</sub> source for hydrogenolysis step) was added for the formilation of HMF into 5-(formyloxymethyl) furfural (FMF), which was further converted into DMF by loading Ru/C, H<sub>2</sub>SO<sub>4</sub> and THF solvent for the hydrogenolysis step at 75 °C. The process was optimized by microwave (MW)-assisted transformation, increasing the DMF final yield 10 points, up to 34 % and reducing 10 times the reaction time under the same operation conditions.

Continuing with those studies using IL-s, Li et al. [8] investigated the direct conversion of fructose to DMF using a biphasic ionic liquid/solvent system (BMIMCl/THF). The dehydration of the fructose was carried out at 130 °C for 30 minutes adding the ionic liquid (IL) to the reaction media. Afterwards, the *in situ* hydrodeoxygenation was performed including another solvent to the system, THF. Thus, the negative effect of the high viscosity of IL is compensated and the mass transfer is favoured in the reaction media. Moreover, Ru/C catalyst was also added and stirred for 5 h at 220 °C

and 50 bar of H<sub>2</sub> pressure, obtaining DMF and DMTHF yields of 50 % and 20 %, respectively.

To avoid the use of ionic liquids, Upare and coworkers [9] studied two heterogeneous catalytic reactions: i) fructose dehydration into HMF over Amberlyst-15 in 1-butanol and, ii) the subsequent vapour-phase hydrogenolysis over Ru-Sn/ZnO catalyst. This second step was carried out using directly the obtained solution in the first step and the achieved overall DMF yield was 92 % under atmospheric pressure and 240 °C. Following the idea of the direct use of dehydration products into hydrogenolysis reaction, Wang's group [10] proposed a process where real lignocellulosic biomass was firstly transformed into HMF by Sn-Mont catalyst combined with NbOPO<sub>4</sub> to tune-up Lewis and Brønsted acid sites. Lewis acid sites are required for the isomerization step while Brønsted sites are responsible for the hydrolysis and dehydration processes. This first step was carried out in a biphasic system using THF and H<sub>2</sub>O-NaCl as solvents. Depending on the type of lignocellulosic biomass employed as feedstock, the achieved furfural and HMF yields were in the range of 50-70 % and 30-40 %, respectively. The organic phase was further treated by Ru/Co<sub>3</sub>O<sub>4</sub> at 170 °C and 10 bar of H<sub>2</sub> pressure, reaching DMF and 2-methylfuran (2-MF) yields above 90 % from HMF and furfural, correspondingly. In this bimetallic catalyst, Ru was favourable for hydrogenation step and CoO<sub>x</sub> species for C–O bond cleavage.

An important effort was carried out by Saha et al. [11] for the optimization of hydrogenolysis step, obtaining high yields of DMF when feeding the reactor with HMF in THF with ZnCl<sub>2</sub>-Pd/C catalyst. The synergy of both metals was effective for the hydrogenolysis step. Moreover, the reaction system was tested using fructose as raw material, obtaining a total yield of DMF of 22 % after 8 h of reaction at 150 °C and 8 bar of H<sub>2</sub> pressure. The low fructose conversion to HMF by ZnCl<sub>2</sub> containing Lewis acid sites could be the reason of the low global yield of DMF.

Insyani and colleagues [12] synthesized a multifunctional heterogeneous catalyst based on metal-organic frameworks (MOFs). Pd nanoparticles were loaded into Zr-metal organic framework (UiO-66) treated with HCl and sulfonated graphene oxide (SGO). The effective combination of SGO properties (Brønsted acid sites and

hydrophilic surface) and UiO-66 treated with HCl characteristics (high porosity, acidity and surface area) enhanced the fructose adsorption and dehydration to HMF. Moreover, Pd nanoparticles were responsible for the hydrogenolysis of HMF to DMF. The reaction was carried out in THF at 160-180 °C and under 10 bar of H<sub>2</sub> pressure for 3 h, achieving a DMF yield of 70.5 % and 45.3 % when using fructose and glucose as feedstock, respectively. Further optimization of the catalytic system was carried out, maximizing the yield towards DMF [13]. This enhancement was achieved modifying the UiO-66 with -NH<sub>2</sub>. Moreover, adding Cu to the metallic active phase resulted in the formation of a bimetallic Cu-Pd alloy, which promoted consecutive C=O hydrogenation and C-OH hydrogenolysis, producing DMF yield of 73 % after 2 h of reaction at 200 °C and 10 bar using sucrose as feedstock.

More recently, Zhang's group [14] studied a simple catalytic system using ethanol as reaction media, commercial PdCl<sub>2</sub> catalyst and poly(methylhydrosiloxane) (PMHS) as H<sub>2</sub> donor. Acid sites are needed for the dehydration of fructose to HMF. In this case, HCl was *in situ* generated from PMHS and PdCl<sub>2</sub> in an alcoholic solvent, acting as Brønsted acid sites. The reached DMF yield was 88 % when using fructose as substrate at 120 °C after 2.5 h. Moreover, the maximum yield obtained from glucose as feedstock was 41 %, under the aforementioned conditions. To enhance the glucose to fructose isomerization step, AlCl<sub>3</sub> was added into the system, promoting as Lewis acid sites, which were in charge of accelerating the isomerization procedure, increasing the yield to 53 %.

The above mentioned investigations with different catalytic systems, reaction conditions and activity results are summarized in Table 2.1.



**Table 2.1:** DMF direct production from biomass

Feedstock	Catalyst	H <sub>2</sub> donor	Solvent	T (°C)	Time	DMF yield (%)	Reference
Fructose HMF	HCl Cu-Ru/C	H <sub>2</sub>	H <sub>2</sub> O-NaCl / BuOH BuOH	180 220	3 min 10 h	82 (HMF) 76-79 (VP)	[1]
Corn stover	CrCl <sub>3</sub> -HCl Cu-Ru/C	H <sub>2</sub>	DMA / LiCl BuOH	140 220	1 h 10 h	9	[2]
Glucose + xylose	SO <sub>4</sub> <sup>-</sup> / ZrO <sub>2</sub> -TiO <sub>2</sub> Ru/C	H <sub>2</sub>	H <sub>2</sub> O / BuOH Ru/C	180 260	3 h 1.5 h	32.7	[3]
Fructose	FA H <sub>2</sub> SO <sub>4</sub> and Pd/C	FA	FA THF	150 70	2 h 15 h	51	[4]
Glucose	12-MPA Pd/C	H <sub>2</sub>	BMIMCl or EMIMCl	120 120	3 h 1 h	30	[5]
Agar	[DMA] <sup>+</sup> [CH <sub>3</sub> SO <sub>3</sub> ] <sup>-</sup> H <sub>2</sub> SO <sub>4</sub> and Ru/C	FA	DMA / LiCl THF	150 75	2 h 17 h	24	[7]
Fructose	BMIMCl Ru/C	H <sub>2</sub>	BMIMCl BMIMCl / THF	130 220	30 min 5 h	50	[8]
Fructose	Amberlyst-15 Ru-Sn/ZnO	H <sub>2</sub>	BuOH	100 240	5 h 100 h	83	[9]
Lignocellulosic biomass	Sn-Mont and NbOPO <sub>4</sub> Ru/Co <sub>3</sub> O <sub>4</sub>	H <sub>2</sub>	H <sub>2</sub> O-NaCl / THF THF	160 170	2 h 24 h	27-36	[10]
Fructose <sup>a</sup>	ZnCl <sub>2</sub> -Pd/C	H <sub>2</sub>	THF	150	8 h	22	[11]
Glucose <sup>a</sup> Fructose <sup>a</sup>	Pd/UiO-66@SGO	H <sub>2</sub>	THF	160- 180	3 h	45.3 70.5	[12]
Sucrose <sup>a</sup>	Cu-Pd/UiO- 66(NH <sub>2</sub> )@SGO	H <sub>2</sub>	THF	200	2 h	73	[13]
Glucose <sup>a</sup>	PdCl <sub>2</sub> + AlCl <sub>3</sub>	PMHS	Ethanol	120	2.5 h	53	[14]

<sup>a</sup> Dehydration+hydrogenolysis consecutively at same reaction conditions. Others: first row for dehydration data and second for hydrogenolysis data.

## 2.2 DMF production from HMF

In the previous section, the direct conversion of biomass into DMF has been reported. Similarly, in the subsequent section, the reaction pathways and catalytic systems for the production of DMF from HMF have been described.

### 2.2.1 Reaction pathway

Different reaction mechanisms have been reported for HMF hydrogenolysis to produce DMF. The pathway and product distribution are strongly dependent on the nature of the employed catalyst and the reaction conditions. Most of the studies follow mainly two routes (see Figure 2.3): 1) selective hydrogenolysis of the hydroxyl group to form 5-MF, followed by the hydrogenation of the aldehyde group to form MFA. Finally, the hydrogenolysis of  $-OH$  provides the desired product DMF. Alternatively, route 2) begins with the hydrogenation of the aldehyde group to form BHMF followed by the hydrogenolysis of the hydroxyl group to obtain MFA, from which finally DMF can be produced by its  $-OH$  hydrogenolysis.

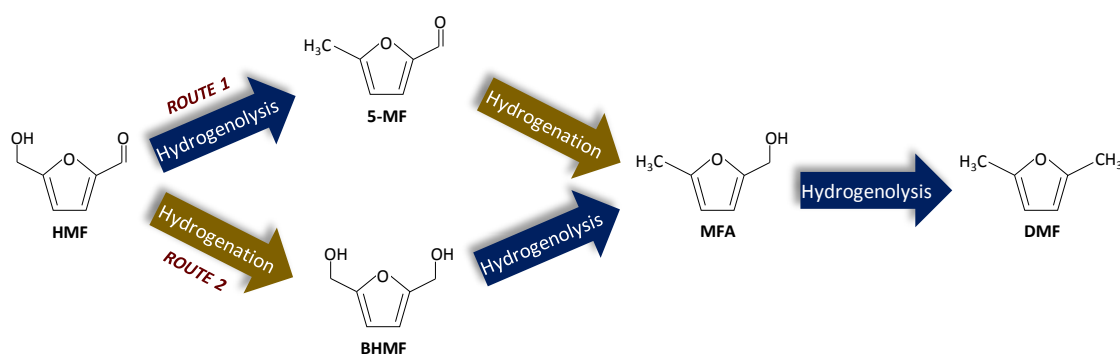


**Figure 2.3.** Main reaction pathways for the hydrogenolysis of HMF to DMF.

#### **Route 1) 5-MF as main intermediate**

To study the reaction sequence of HMF hydrogenolysis, Chidambaram and Bell [5] studied the use of the reaction intermediates ( 5-MF, MFA and BHMF) as reagents using a Pd/C catalyst. 5-MF was highly reactive to form MFA and, when reaction time increased, DMF was obtained. However, when BHMF was fed in the reactor, MFA was

the main product, producing slight amount of DMF. To understand the behaviour of BHMF in the reaction system, increasing amounts of this compound were incorporated to a mixture containing a fixed quantity of MFA, concluding that BHMF inhibits the conversion of MFA to DMF due to the competitive adsorption of them on the surface of Pd.

The complete mechanism to form DMF and DMTHF from fructose employing hydroiodic acid (HI) and  $\text{RhI}_3$  was studied by Grochowski et al. [15]. HI was in charge of the dehydration step to form HMF. Under inert atmosphere (He) the reaction was stopped when 5-MF was formed and they did not observe any further hydrogenation. However, when hydrogen gas was added to the reaction system, DMF and 2,5-hexanedione (HD) were formed, meaning that HI performed as dehydration and hydrogenolysis agent whereas Rh acted as hydrogenation agent. Longer reaction times implied a decrease of both products and formation of an equal amount of DMTHF. Thus, the formation of DMTHF was a direct result of the disappearance of both DMF and HD (see Figure 2.4, blue pathway). Similarly, Zhang and colleagues [14] studied the formation of DMF through hydrogenolysis of 5-MF but proposed a new route for the formation of DMTHF. Remarkably, ring-hydrogenation product of MFA, MTHFA, was detected during the reaction and further confirmed as an intermediate of DMTHF production (see Figure 2.4, green pathway).

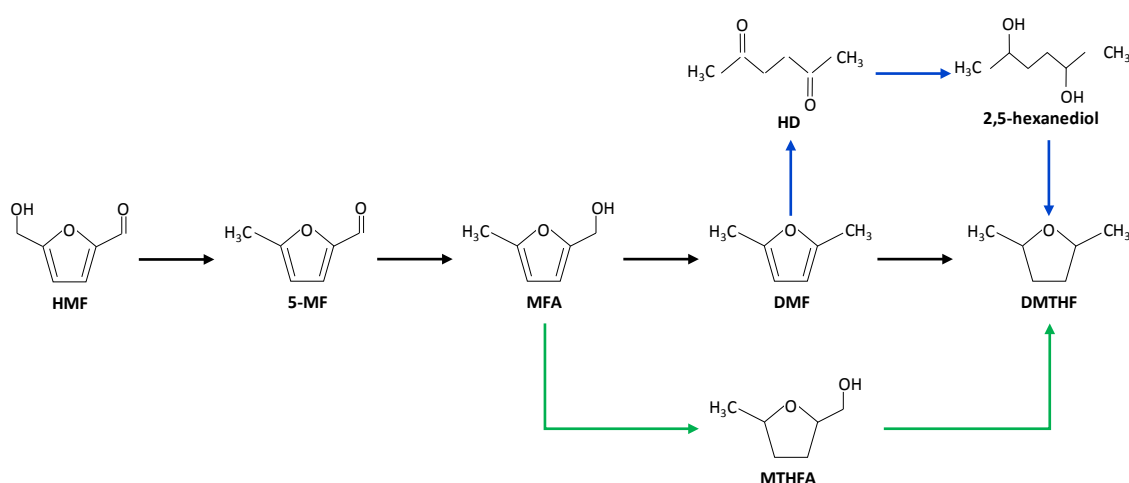


**Figure 2.4.** Reaction pathway of HMF to DMF and DMTHF with 5-MF as intermediate.

Tzeng et al. [16] studied the effect of the electronic structure of Ru nanoparticles on the reaction pathway. Ru catalysts of different porous textures on carbonaceous materials were tested. Non-porous carbon exhibited Ru metallic particles which were able to hydrogenate the aldehyde group obtaining BHMF as main product. In contrast, microporous materials presented Ru<sup>0</sup>/RuO<sub>x</sub> particles. This incomplete reduction might be due to high interaction between the metal and the support or caused by a limitation of mass transfer of H<sub>2</sub>. The synergy of both metallic and oxidized sites involved the hydrogenation and hydrogenolysis steps, obtaining high yields of DMF with 5-MF as by-product.

Other authors confirmed the production of DMF via 5-MF by Cu-Pd bimetallic catalysts [13], by CuZnCo complex [17] (where Cu-Co alloy acted as hydrogenolysis agent and ZnO as hydrogenation agent) and, by Ni/ZSM-5 [18]. All of them concluded that the transformation of 5-MF to MFA is the rate determining step.

### **Route 2) BHMF as main intermediate**

Another possible route for the hydrogenolysis of HMF to DMF is the hydrogenation to BHMF in the first step, followed by MFA production to finally obtain DMF. To validate the formation of BHMF, Saha et al. [11] performed an experiment using this chemical as the starting substrate catalysed by ZnCl<sub>2</sub>-Pd/C, achieving high conversion and producing high DMF yields. MFA was not detected, meaning that the last hydrogenolysis step was rapidly carried out. In the same way, Upare and colleagues [9] concluded that the hydrogenolysis step of BHMF to produce MFA was much lower than the subsequent hydrogenolysis to DMF.

Recently, Li et al. [19] studied the synergistic effect of metallic Co and CoO<sub>x</sub> acidic sites in the hydrogenolysis of HMF. Metallic Co was responsible for the hydrogenation step and CoO<sub>x</sub> was in charge of activating the C–O bond, obtaining DMF through BHMF hydrogenation.

This reaction pathway was approved by other authors via different catalytic systems. Using Ru/Co<sub>3</sub>O<sub>4</sub> [10] or a nitrogen-doped carbon decorated Cu based catalyst [20] DMF was produced from HMF via BHMF and MFA, followed by a further hydrogenation step

towards DMTHF. It must be mentioned that in the first system DMF etherification products were also detected.

Some authors detected both 5-MF and BHMF during the reaction. Solanki and co-workers [21] tried to find the exact reaction sequence by taking BHMF and 5-MF intermediates as starting compounds. They obtained high yields of DMF with no considerable difference when varying the substrate, deducing that both pathways were followed in parallel. In the same line, Chen et al. [22] reasoned that the conversion of HMF into DMF follows two analogous routes (BHMF hydrogenation and 5-MF hydrogenolysis) to form DMF and MFA, which was further hydrogenated into MTHFA. Similarly, Liao and colleagues [23] proposed a double parallel route due to the synergy of Pd and CoS sites, which are in charge of the hydrogenation of  $-CHO$  and the hydrogenolysis of  $-HO$ , respectively.

Esteves et al. [24] studied the product distribution varying the acidity of the support on Cu based catalyst. Lewis and Brønsted acid sites followed BHMF route, while weak and moderate acidic catalysts showed the formation of 5-MF during the reaction.

Interestingly, some investigations established a parallel pathway of hydrogenolysis and etherification reactions in the formation of DMF. Jae and colleagues [25] detected etherified compounds during the reaction over Ru/C catalyst. The acidic functional groups on activated carbon were presumably responsible for the etherification reactions. The hydrogenolysis reaction of HMF was conducted by the hydrogenolysis of BHMF to form DMF through MFA and occurred combined with etherification reactions, which also produced DMF, as it can be observed in see Figure 2.5 (green pathway). Analogously, Han et al. [26] demonstrated the parallel production of DMF through both hydrogenolysis and etherification. In this case, the hydrogenolysis route followed the hydrogenolysis of 5-MF and further hydrogenation of MFA to form DMF (see Figure 2.5, blue pathway).

Lastly, some groups investigated the reaction pathway through etherification in the absence of hydrogenolysis intermediates such as BHMF, 5-MF or MFA. Braun and colleagues [27] identified the formation of two condensates, determining a reaction

mechanism that involved the etherification of HMF in ethanol to produce DMF. Similarly, De's group [7] studied the transformation of HMF to DMF by Ru/C catalyst in FA and H<sub>2</sub>SO<sub>4</sub>. The investigation revealed that this reaction occurred via the formation of HMF formate ester (FMF), as shown above in Figure 2.2.

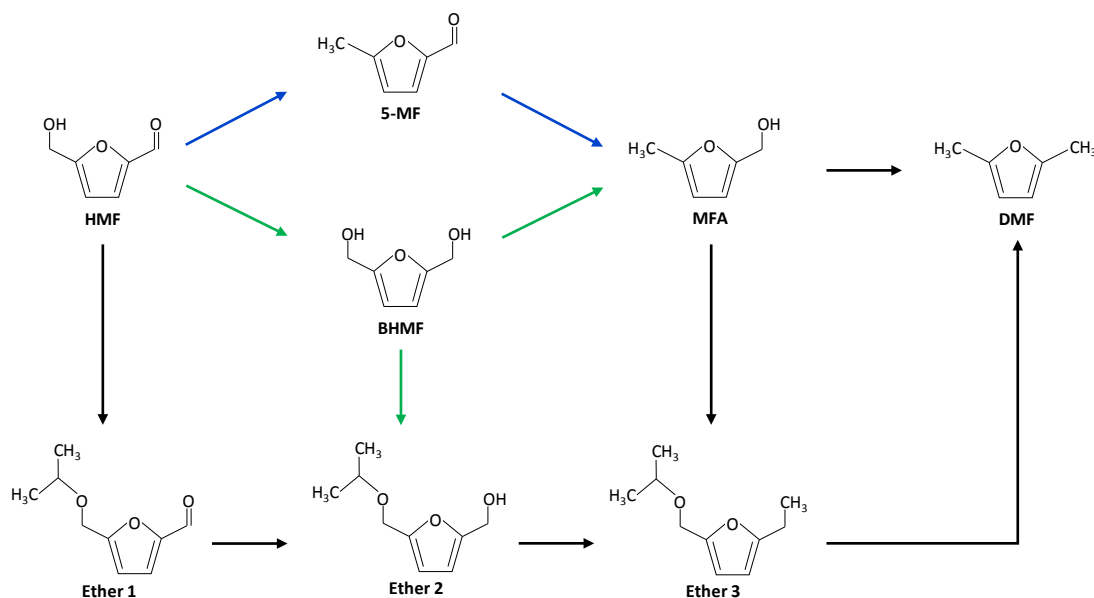


**Figure 2.5.** HMF hydrogenolysis and etherification pathway to DMF.

Therefore, different reaction pathways can be followed to obtain DMF from HMF. BHMf or 5-MF are the most common intermediates, implying firstly the hydrogenation of the aldehyde group or the hydrogenolysis of the hydroxyl group, respectively.

### 2.2.2 Catalytic system

It has been previously stated that HMF possess an aldehyde group, a hydroxyl group and a furan ring, which makes a highly reactive molecule. Moreover, numerous products can be obtained from the hydrogenation-hydrogenolysis reaction of this molecule. One of the key challenges for upgrading HMF is to get a high desired product selectivity to avoid undesired side reactions. Therefore, a highly efficient, selective and stable catalytic system needs to be found. In general, most of the studied systems are based on batch discontinuous reactors. However, only a limited number of investigations have been carried out in fixed-bed continuous flow reactors. In the next

sections, different catalytic systems for the production of DMF have been described. On the one hand, monometallic catalytic systems based on noble metals such as Ru, Pd or Pt have been studied. On the other hand, non-noble Ni and Cu monometallic catalysts have been examined to reduce the high costs that noble metals imply. Lastly, bimetallic catalysts based in noble and/or non-noble metals have been investigated.

### 2.2.2.1 Noble metal monometallic catalysts

Noble metals exhibit remarkable, and in many cases unique, catalytic performance in numerous reaction systems. Therefore, Ru, Pd and Pt have been extensively studied for the hydrogenolysis reaction of HMF.

#### **Ru based monometallic catalysts**

Numerous investigations have studied catalytic systems of Ru supported on carbon materials. Commercial Ru/C catalyst was employed by Hu et al. [28] in THF, which acted as a solvent without playing any active role in the reaction. Moreover, the acid sites observed in the support were responsible for side reactions such as etherification reactions and Ru was in charge of the hydrogenolysis of HMF to DMF. The reaction conditions were optimized obtaining a DMF yield of 94 % after 2 h of reaction at 200 °C and 20 bar of H<sub>2</sub> pressure. Longer reaction times and higher temperatures or pressures led to ring-opening and over-hydrogenated products. Similarly, Jae's group [25] investigated the role of commercial Ru/C using 2-propanol as H<sub>2</sub> donor and solvent to avoid the consumption of H<sub>2</sub>. The reaction variables were adjusted and the yield of DMF reached 81 % at 190 °C and 20.4 bar of N<sub>2</sub> after 6 h. Carbon nanotubes (CNTs) were synthesized by Priecel and colleagues [29], enhancing the performance of ruthenium by a combination of higher porosity of CNTs and the electronic promotion within the nanotubes, which increased the reducibility of the metal. Lower temperature (150 °C) and reaction time (1 h) were needed to obtain a maximum DMF yield of 83.5 % at 20 bar of H<sub>2</sub> in dioxane. Interestingly, some authors verified the beneficial synergy of metallic Ru and RuO<sub>x</sub> for the production of DMF. Jae et al. [30] examined the partial oxidation of Ru by mild oxidation treatment at 130 °C, generating a partially oxidized Ru surface necessary for the hydrogenolysis reaction, achieving a

DMF yield of 72 %. Recently, Tzeng and coworkers [16] investigated Ru supported on microporous, mesoporous and non porous carbon, concluding that the hydrogenolysis reaction was highly correlated with the electronic structure of Ru nanoparticles. Ru supported in non-porous carbon was completely reduced. In contrast, RuO<sub>x</sub> species were detected in microporous and mesoporous supports. These last catalysts achieved high yields of DMF (nearly 70 %) at mild reaction conditions, 5 bar of H<sub>2</sub> and 125 °C after 1 h.

Moreover, zeolite and metal oxide supports have also been considered for this reaction. Nagpure et al. investigated Ru catalyst over NaY zeolite [31] and hydrotalcite (HT) [32]. The Lewis acid sites detected in NaY increased the deoxygenation ability of the catalyst, maximizing the DMF yield up to 78 % after 1 h at 220 °C and 15 bar of H<sub>2</sub>. When hydrotalcite was used as support, the yield decreased to 58 %. The pressure was slightly reduced to 10 bar, since higher values resulted in over-hydrogenated products. Lastly, Raut and colleagues [33] synthesized a mesoporous ZrO<sub>2</sub>-MCM-41 support containing acid sites that apparently could enhance the dehydration of CH<sub>2</sub>-OH, achieving 90 % of DMF yield at 160 °C and 15 bar of H<sub>2</sub> after 1 h.

### **Pd based monometallic catalysts**

Monometallic palladium is also investigated as a promising noble metal in the DMF production. As well as Ru catalysts, carbon materials showed interesting behavior as catalytic support. Mitra et al. [34] studied the effect of FA on the product distribution over commercial Pd/C in dioxane. In absence of FA, HMF underwent decarbonylation to furfuryl alcohol (C<sub>5</sub>). However, in presence of FA, decarbonylation of HMF is suppressed, enhancing the hydrogenolysis to DMF. Therefore, FA facilitates the conversion of HMF to DMF by acting as H<sub>2</sub> source and inhibiting decarbonylation to C<sub>5</sub>, reaching 85 % DMF yield after 15 h on stream at 120 °C in an autoclave reactor. Commercial Pd/C was also employed by Chatterjee and coworkers [35] in a supercritical carbon dioxide (scCO<sub>2</sub>) and water system. A complete miscibility of reagents was obtained by scCO<sub>2</sub>, which is highly used in the chemical reactions involving gasses. Moreover, the acidity of scCO<sub>2</sub>-H<sub>2</sub>O benefited the hydrogenolysis reaction. Optimization of the reaction variables was carried out in a batch reactor,



obtaining 100 % of DMF yield at 80 °C and H<sub>2</sub> and CO<sub>2</sub> partial pressures of 10 bar and 100 bar, respectively, after 2 h of reaction time. The CO<sub>2</sub> pressure variation completely altered the product distribution, being able to produce high yields of MTHFA and DMTHF when adapting the pressure. This variation affects to the phase behaviour and hence, the product distribution can be tuned-up (see Figure 2.6).

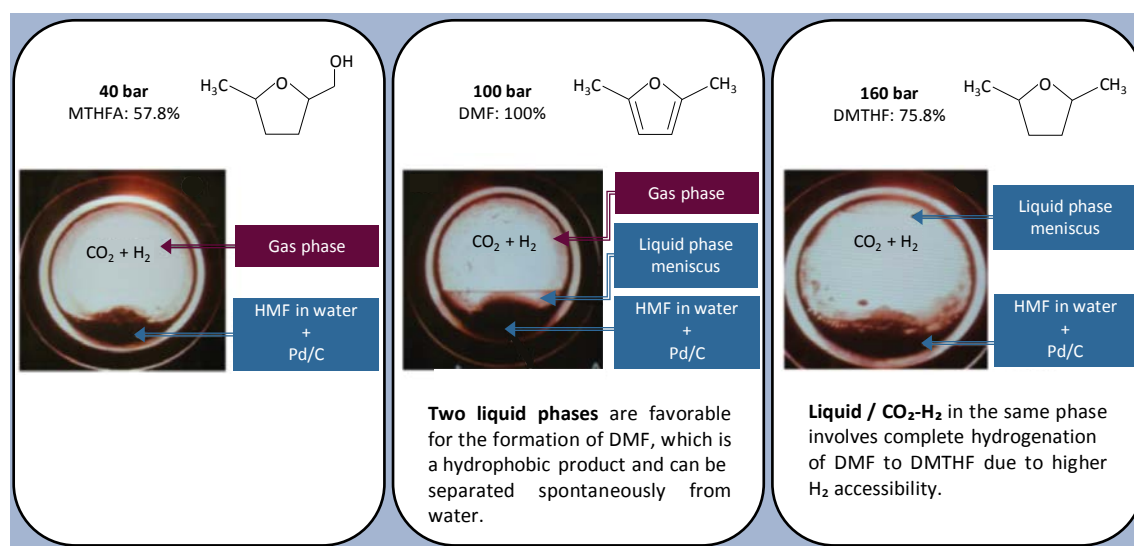


**Figure 2.6.** Phase observation over different pressures and main product of each division [35].

Pd catalyst supported on Fe<sub>2</sub>O<sub>3</sub> was synthesized by Scholz's group [36], using 2-propanol as H<sub>2</sub> donor in a continuous flow at 25 bar of N<sub>2</sub> and 180 °C. The *in situ* reduced Pd catalyst was able to obtain 70 % of DMF yield. Recently, Zhang et al. [14] studied the hydrogenolysis of HMF over commercial PdCl<sub>2</sub> catalyst and PMHS acting as H<sub>2</sub> donor. HCl was *in situ* liberated from both catalyst and H<sub>2</sub> source in alcoholic solvents such as ethanol. At room temperature and atmospheric pressure, the reached yield rose up to 89 % after 30 minutes.

### **Pt based monometallic catalysts**

Most of the platinum-based catalysts are developed with the addition of another noble or non-noble metal, resulting in bimetallic catalysts, which will be discussed later in section 2.2.2.3. However, some authors studied the performance of monometallic Pt catalysts.

Shi et al. [37] reached 73.2 % DMF yield with complete HMF conversion at 120 °C and 30 bar of H<sub>2</sub> over Pt supported on reduced graphene oxides (rGO). The suitable performance of the catalyst was attributed to the highly dispersed Pt nanoparticles, to the micropore-free configuration and to the flat structured Pt/rGO, which enabled the selective adsorption of HMF, accelerating its reaction rate.

**Table 2.2.** Activity results of monometallic noble metal catalysts.

Catalyst	Solvent	P (bar)	T (°C)	Time (h)	Conversion (%)	Yield (%)	Ref.
Ru/C	THF	20	200	2	100	94	[28]
Ru/C	2-propanol	20 (N <sub>2</sub> )	190	6	100	81	[25]
Ru/CNT	Dioxane	20	150	1	96.5	83.5	[29]
Ru-RuO <sub>2</sub> /C	2-propanol	20 (N <sub>2</sub> )	130	6	100	72	[30]
Ru/C	2-propanol	5	125	1	100	70	[16]
Ru/NaY	THF	15	220	1	100	78	[31]
Ru/HT	2-propanol	10	220	1	100	58	[32]
Ru/ZrO <sub>2</sub> -MCM-41	THF	15	160	1	99	90	[33]
Pd/C	Dioxane	2	120	15	95	85	[34]
Pd/C	Water+CO <sub>2</sub>	10 (H <sub>2</sub> ) 100 (CO <sub>2</sub> )	80	2	100	100	[35]
Pd/Fe <sub>2</sub> O <sub>3</sub>	2-propanol	25 (N <sub>2</sub> )	180	0.5	100	70	[36]
PdCl <sub>2</sub>	Ethanol	-	25	0.5	100	89	[14]
Pt/rGO	BuOH	30	120	2	100	73.2	[37]
Pt/C + ZrO <sub>2</sub> /SBA-15 <sup>a</sup>	1-propanol	33	180	-	100	77.6	[38]

<sup>a</sup> Continuous flow

Batch and continuous flow reactors were employed by Luo and colleagues [38] to investigate the hydrogenolysis over Pt/C catalyst. The batch experiments revealed that DMF showed its highest concentration at the beginning of the reaction (27.2 %), decreasing steadily with time of reaction as a result of the formation of ring-opening and over-hydrogenated products. This implied that shorter contact time were needed. Thus, when using the continuous reactor higher DMF yields could be obtained (60 %) since this reaction system allows choosing the suitable contact time by modifying the space velocity. The reaction was carried out sequentially, producing partially hydrogenated compounds and ethers from HMF and producing DMF afterwards.

Assuming that DMF was produced from the ethers, high concentrations of these last compounds was tried to obtain by the addition of ZrO<sub>2</sub>/SBA-15. This catalyst was previously studied, providing high conversion of HMF towards different ethers. Therefore, it was placed on the flow reactor before the Pt/C catalyst, involving the production of ethers by ZrO<sub>2</sub>/SBA-15 followed by the conversion of the ethers into DMF by Pt/C. This modification improved the DMF yield up to 77.6 %.

The explained catalytic systems, reaction conditions and obtained activity results in the different studies based on monometallic noble metal catalysts have been summarized in Table 2.2.

#### 2.2.2.2 Non-noble metal monometallic catalysts

The effective and selective performance of noble metals has been explained in the previous section. However, their application is restricted because of their limited availability and high costs [39].

The development of efficient and non-precious metal-based catalytic system for this hydrogenolysis process is of great importance, from the large-scale industrialization [40,41] point of view.

##### **Ni based monometallic catalysts**

Gyngazova's group [42] synthesized monometallic Ni supported on carbon (Ni/C) by incipient-wetness impregnation method, which is attractive due to its technical simplicity and low cost. The optimization of the variables was carried out to avoid the formation of polymeric side products, reaching a DMF yield of 70 % and almost 80 % of HMF conversion at 45 bar of H<sub>2</sub> and 180 °C after 2 h of reaction. Based also on carbon materials, Goyal et al. [39] developed a more sophisticated mesoporous nitrogen-rich carbon (NrC) support. The high HMF conversion (99.9 %) and DMF yield (98.7 %) were attributed to the strong interfacial interaction between Ni and nitrogen atoms of the support, which enhanced the total Ni reduction. Ni nanoparticles (below 5 nm) highly dispersed on the support were observed when the metal loading was 5 %. Higher metal loading involved an increase of the particle size, reducing DMF selectivity. Mani

and coworkers [43] created a functional nickel-carbon composite based on squaric acid-zinc complex and porous carbon (Ni@SAZn\_PC), achieving a cube shaped morphology and high porosity. The catalyst was tested in a continuous flow reactor reaching 79 % of HMF conversion and 68 % of DMF at 6 bar of H<sub>2</sub> and 150 °C.

Commercial Ni Raney was employed by Kong and colleagues [41]. The difference on product distribution was related to the variation of the temperature. The catalyst enabled the hydrogenation to BHMF at low temperatures and its hydrogenolysis to DMF at high temperatures (see Figure 2.7). The high yield obtained was ascribed to the weak acidity of Raney Ni. The same group investigated the reaction over Ni/Al<sub>2</sub>O<sub>3</sub> [44]. The modulation of surface metal-acid bifunctional sites (by varying the calcination temperature) and reaction conditions altered the product distribution. Lower calcination temperatures involved excessive metal sites that promote C=C hydrogenation. Moreover, low temperature and high pressure values blocked the hydrogenolysis reaction. Thus, BHMF yield of 96.2 % was obtained at 60 °C and 60 bar of H<sub>2</sub> when the catalyst was calcined at 450 °C. When a higher calcination temperature (850 °C) was set, a balanced surface acid/metallic sites was obtained. Hence, together with a slightly higher reaction temperature (180 °C) and a lower pressure (12 bar) hydrogenolysis to DMF and DMTHF was obtained in a tank reactor. In such conditions, the DMF yield reached 91.5 % in 4 h of reaction time; longer reaction times (20 h) implied high DMTHF yield (97.4 %).

Recently, Guo et al. [18] employed ZSM-5 zeolite to synthesize Ni/ZSM-5 by solid-phase grinding method. The synergistic effect of acid sites and metal sites on the catalyst surface was responsible for the excellent production of DMF (86.5 %). An appropriate ratio of metal sites and acidic sites was essential for the selective hydrogenolysis of HMF.

Other supports such as zirconium phosphate (Ni/ZrP) [45], Co<sub>3</sub>O<sub>4</sub> [46] and perovskites [40] have been studied for the hydrogenolysis of HMF to produce DMF in batch reactors.

### Cu based monometallic catalysts

Diverse metal oxides have been investigated as supports of Cu monometallic catalysts for hydrogenolysis reactions. Hansen et al. [47] synthesized monometallic Cu supported on porous metal oxide (PMO) by coprecipitation of a mixture of Al, Mg and Cu precursors, obtaining a Cu-doped hydrotalcite like compound. The reaction was carried out in supercritical methanol at 260 °C resulting in 48 % of DMF yield after 3 h. Another studied metal oxide was ZnO. Zhu et al. [48] tested different Cu loadings obtaining the highest yield when the (Cu:Zn) molar ratio was equal 2. This ratio offered the most proper combination of high surface Cu concentration and suitable acidity. The same behaviour as explained before with Ni-Raney was observed; low reaction temperatures involved the hydrogenation of HMF to BHTMF and by contrast, high temperatures implied hydrogenolysis to DMF (see Figure 2.7).

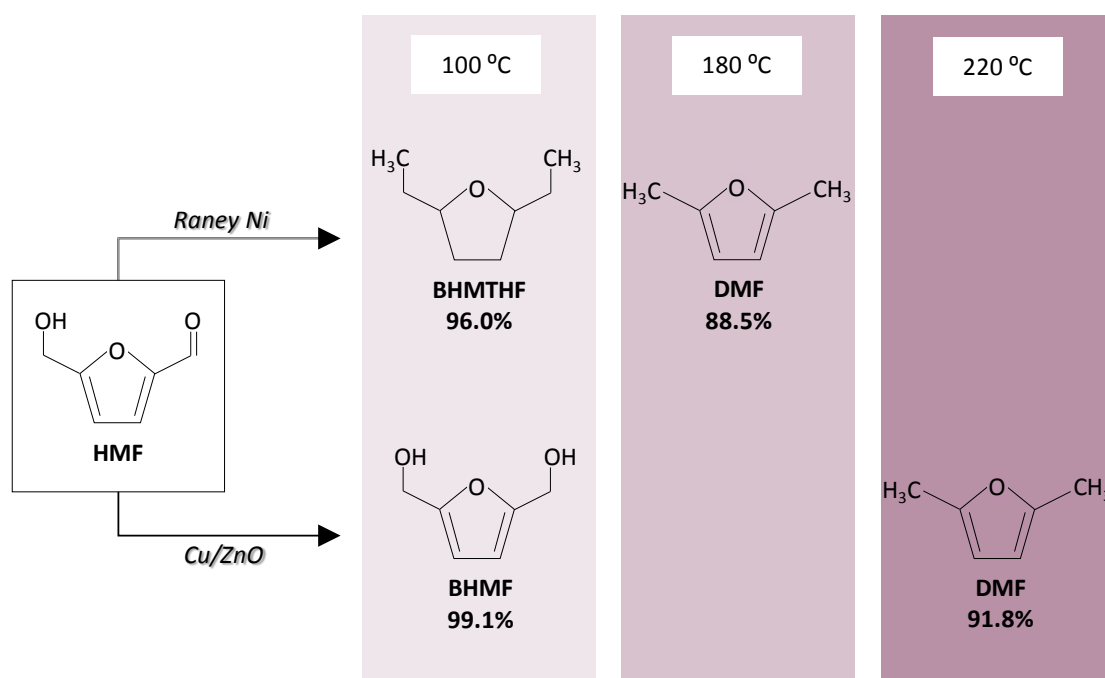


**Figure 2.7.** Difference on product distribution depending on the reaction temperature

The synergistic effect of ZnO Lewis acidic sites and Cu<sup>0</sup> active species was studied by Bottari et al. [49]. The Cu<sup>0</sup> particles were responsible for hydrogenation/hydrogenolysis, being the particle size a crucial parameter. They determined that Cu particle size < 150 nm is needed for the optimal production of DMF. Thus, they were

able to reach a DMF yield of 89 % at 200 °C using cyclopentyl methyl ether (CPME) as solvent.

**Table 2.3.** Activity results of monometallic non-noble metal catalysts

Catalyst	Solvent	P (bar)	T (°C)	Time (h)	Conversion (%)	Yield (%)	Ref.
Ni/C	THF	45	180	2	80	70	[42]
Ni/NrC	Water	30	200	6	99.9	98.7	[39]
Ni/SAZn_PC <sup>a</sup>	Ethanol	6	150	-	79	68	[43]
Raney Ni	1,4-dioxane	15	180	15	100	88.5	[41]
Ni/Al <sub>2</sub> O <sub>3</sub>	1,4-dioxane	12	180	4	100	91.5	[44]
Ni/ZSM-5	THF	2.5	180	7	90	86.5	[18]
Cu/PMO	MeOH	-	260	3	100	48	[47]
Cu/ZnO	1,4-dioxane	15	220	5	100	91.8	[48]
Cu/ZnO	CPME	20	200	6	100	89	[49]
Cu/Al <sub>2</sub> O <sub>3</sub>	MeOH	1 (N <sub>2</sub> )	240	6	100	73.9	[50]
Cu/Al <sub>2</sub> O <sub>3</sub>	THF	20	150	10	100	85	[24]

<sup>a</sup> Continuous flow

Different supports were evaluated by Zhang et al. [50] in a microbatch reactor (14 ml). In all the cases, methanol was used as H<sub>2</sub> donor, thus, the catalyst needed to be active for the hydrogenolysis reaction but also for the *in situ* H<sub>2</sub> production from methanol. Monometallic Cu supported on Al<sub>2</sub>O<sub>3</sub> exhibited the best catalytic activity (73.9 % DMF yield) attributable to the elevated H<sub>2</sub> production, small Cu crystallite size and strong acidity. Similarly, Esteves and colleagues [24] also studied the effect of various supports. They concluded that high copper dispersion and Lewis acid sites of the support were crucial for the activation of oxygen of hydroxyl group in HMF. Alumina containing catalyst showed the best performance, reaching a complete conversion and a DMF yield of 85 %.

In Table 2.3 the results of DMF production and the operating conditions using Ni and Cu catalysts are summarized.

### 2.2.2.3 Bimetallic catalysts

Different bimetallic (noble and non-noble) catalysts designed for the production of DMF have been recently reported.

Gao et al. [51] centred their study on Ru-Co nanoparticles (NP) homogeneously dispersed on  $\text{CoO}_x$  microspheres, which possessed abundant surface defects, such as oxygen vacancies and  $\text{Co}^{2+}$  species. High DMF yield (96.5 %) was obtained by the synergistic effect of Ru-Co NP, highly active sites, and abundant surface defects. These characteristics led to an effective activation of C=O and C–O bonds, promoting the hydrogenolysis of the hydroxyl group.

Other authors have investigated this reaction using Pd-based bimetallic catalysts. Nishimura and coworkers [52] selectively produced DMF by Pd-Au/C. X-ray diffraction (XRD) results revealed the existence of Pd-Au alloy particles and Au isolated particles, indicating the need of both active sites for the conversion of HMF to DMF. Moreover, the co-existence of a strong acid (HCl), which performed as homogeneous catalyst, optimized the efficiency of the catalytic system, reaching a DMF yield of 96 %. To reduce the noble metal consumption and avoid the use of acidic precursors, Talpade and colleagues [53] developed a bimetallic Fe-Pd/C nanocatalyst. Partially oxidized Fe and reduced Pd atoms led a DMF yield of 85 %. Moreover, the oxidized Fe presented magnetic properties to the catalyst, performing an easier recovery of the catalyst. More recently, Liao's group [23] studied a bimetallic Pd-Co catalyst supported on sulphur-modified carbon nanotubes (S-CNT). The high activity of Pd-Co/S-CNT was attributed to the synergetic effect of active Pd and  $\text{Co}_9\text{S}_8$ , which were responsible for the hydrogenation of the aldehyde group and the hydrogenolysis of the hydroxyl group, respectively. It was demonstrated that Pd- $\text{Co}_9\text{S}_8$  was much more active than Pd-CoO in the hydrogenolysis reaction of HMF to DMF, reaching a maximum yield of 83.7 % of DMF at mild reaction conditions (120 °C and 3 bar).

As it is explained above, monometallic Pt catalysts have not been widely studied. However, the incorporation of another noble or non-noble metal to Pt-based catalyst has gained attention over the last years. Wang et al. [54] incorporated Pt-Co bimetallic

nanoparticles in hollow carbon nanospheres (HCS), reaching a DMF yield of 98 % after 2 h at 180 °C, where the hydrogenolysis was the rate-determining step. Moreover, different commercial Pt/carbon catalysts were tested, reaching considerable lower yields. However, altering these catalysts with Co (forming Pd-Co alloy) improved the DMF yield up to 98 %, proving that the alloy is essential for the production of desired product. Similarly, Wang's group [55] deposited Pt-Co bimetallic nanoparticles over carbon nanotubes (CNT) by atomic layer deposition. Pt enhanced the hydrogenation of C=O bond and Co promoted the selectivity to DMF and inhibited the production of undesired byproducts. Moreover, the graphene layer on CNT transferred electrons to Pt nanoparticles, involving an increase of the charge density on Pd, improving C=O activation. Recently, Ledesma and colleagues [56] synthesized a Pt-Ir alloy supported on CMK-3 and SBA-15. This alloy combines the hydrogenating capacity of Pt and hydrogenolysis ability of Ir. Moreover, the Pt high activity involved the generation of undesired byproducts, which was prevented by adding the second metal. The highest DMF yield (86 %) was obtained by Pt-Ir supported on CMK-3 due to the neutral nature of this support, that avoids the C=C cleavage, and the high dispersion achieved on the mesoporous carbon support.

An efficient nonprecious nickel-tungsten carbide catalyst on active carbon (Ni-W<sub>2</sub>C/C) was reported by Huang et al. [57]. Ni particles showed an excellent hydrogenation capacity and W<sub>2</sub>C an exceptional deoxygenation ability, achieving 96 % of DMF yield with the optimized loading ratio of 7 % Ni and 30 % W<sub>2</sub>C. Yu's group [58] determined that Ni-Fe supported on carbon nanotubes (CNT) showed higher activity than the same metals supported on activated carbon. Moreover, the Ni-Fe alloy species favoured the cleavage of C—O bond, reaching DMF yields exceeding 90 %. Besides, this catalyst presented a magnetic nature, that generates a simpler separation, as explained above. Based on sulphur-modified catalysts, a non-noble catalytic system was synthesized by Han et al. [59] by evaporation-induced self-assembly (EISA) method. The obtained Ni-MoO/Al<sub>2</sub>O<sub>3</sub> catalyst was sulfided by dimethyl disulphide (DMDS) as sulphiding agent, obtaining an ordered mesoporous alumina supported nickel-molybdenum sulphide catalyst. The activity depended on the content of NiMoS coordinated unsaturated sites (CSU). Moreover, 2-propanol solvent promoted the formation of



intermediate ether compounds, which were easier to be hydrogenolyzed. Under mild reaction conditions, 130 °C and 10 bar of H<sub>2</sub>, the reached DMF yield was 95 % after 6 h. Continuing with Ni-based bimetallic catalysts, Yang and coworkers [60] obtained the same activity results (DMF yield of 95 %) at identical reaction parameters as Han's group by Ni-Co/C catalyst. The high activity obtained with this catalyst was attributed to the synergistic effect between Ni and CoO<sub>x</sub> species. The optimization of Ni loading was needed because excessive Ni content provoked over-hydrogenated products. A subsequent investigation was carried out by Yang et al. [61] employing the same catalyst but using FA as hydrogen donor, reaching 90 % of DMF yield at 210 °C under self-generated pressure. Recently, Chen et al. [62] efficiently dispersed Co and Ni-Fe alloy species on the surface of boron nitride (BN). Fe species were beneficial for the adsorption of the furan ring but they showed low hydrogenation ability. However, Ni species possessed excellent hydrogenation capacity. Thus, the Ni-Fe alloy presented a favourable synergist effect. Moreover, the addition of Co enhanced the selectivity to DMF, concluding that three metals were crucial factors to achieve high yields of DMF, reaching 94 % of DMF yield at 20 bar of H<sub>2</sub> pressure and 180 °C. The XRD and temperature programmed reduction with hydrogen (H<sub>2</sub>-TPR) results indicated that isolated Co and Ni-Fe alloy were formed on the support surface.

Cu-based bimetallic catalysts have been considered by several authors. Srivastava and colleagues [63] studied the bimetallic Cu-Co catalyst over various supports (CeO<sub>2</sub>, ZrO<sub>2</sub> and Al<sub>2</sub>O<sub>3</sub>). Cu-Co/CeO<sub>2</sub> produced mainly BHMF due to large Cu particles. By comparison, Cu-Co/ZrO<sub>2</sub> exhibited low selectivity due to the generation of over-hydrogenated and ring-opening products, caused by the strong acidic sites of the support. The best activity was achieved by Cu-Co/Al<sub>2</sub>O<sub>3</sub>, as a result of combination of highly dispersed Cu and partially reduced CoO<sub>x</sub> and suitable weak acidic sites, reaching a DMF yield of 78 % after 8 h of reaction at 220 °C and 30 bar of H<sub>2</sub>. Similar catalytic system was studied by Guo et al. [64]. The bimetallic Cu-Co/Al<sub>2</sub>O<sub>3</sub> was modified with N-graphene (NGr). The achieved optimum DMF yield (99 %) was a consequence of highly effective catalyst for C–O cleavage and C=O bond hydrogenation but exhibited an inactive capacity for the hydrogenation of C=C bond, avoiding DMTHF or BHMTFH production. Identical metals were employed by Chen et al. [65] but supported on

carbon. Monometallic Cu catalyst was not able to achieve the hydrogenolysis step, obtaining high yields of BHMF. However, the Co species improved the catalytic performance of copper species by the synergistic effect between metals, achieving the hydrogenolysis step to produce DMF.

The aforementioned investigations were focused on discontinuous batch reactors. Nevertheless, Luo and colleagues [66] studied the hydrogenolysis of HMF to DMF over bimetallic catalysts in continuous flow reactors. They synthesized Pt-based bimetallic catalysts supported on carbon by sorvothermal method and tested in a liquid-phase flow reactor. High yields (> 95 %) were achieved by Pt-Ni, Pt-Zn and Pt-Cu nanocrystals. The alloying metal prevented the ring-opening or ring-hydrogenated byproducts.

The above mentioned investigations based on bimetallic catalysts are summarized in Table 2.4, including the catalytic system, operation conditions and activity results.

**Table 2.4.** Activity results of bimetallic catalysts.

Catalyst	Solvent	P (bar)	T (°C)	Time (h)	Conversion (%)	Yield (%)	Ref.
Ru-Co/CoO <sub>x</sub>	1,4-dioxane	5	200	2	100	96.5	[51]
Pd-Au/C	THF	1	60	12	99	96	[52]
Pd-Fe/C	THF	20	150	2	100	85	[53]
Pd-Co/S-CNT	THF	3	120	13	96	83.7	[23]
Pt-Co/HCS	BuOH	10	180	2	100	98	[54]
Pt-Co/CNT	BuOH	10	160	8	100	90	[55]
Pt-Ir/CMK-3	THF	15	120	4	98	86	[56]
Ni-W <sub>2</sub> C/C	THF	40	180	3	100	96	[57]
Ni-Fe/CNT	BuOH	300	200	3	100	91.3	[58]
NiMoS/Al <sub>2</sub> O <sub>3</sub>	2-propanol	10	130	6	100	95	[59]
Ni-Co/C	THF	10	130	24	99	95	[60]
Ni-Co/C	FA	1 (N <sub>2</sub> )	210	24	99	90	[61]
NiFeCo/BN	THF	20	180	4.5	100	94	[62]
Cu-Co/Al <sub>2</sub> O <sub>3</sub>	THF	30	220	8	100	78	[63]
Cu-Co/NGr/Al <sub>2</sub> O <sub>3</sub>	THF	20	180	16	99	99	[64]
Cu-Co/C	Ethanol	50	180	8	100	99.4	[65]
Pt-M/C <sup>a</sup>	1-propanol	33	200	-	95	95	[66]

<sup>a</sup> Continuous flow: M = Ni, Zr or Cu.

## 2.3 DMTHF production

The production of DMTHF has gained attention in the very last years; therefore, there is a modest number of investigations focused on its production. As described in Figure 2.4, DMTHF can be obtained following different routes. The most studied pathway is the hydrogenation of the furan ring of DMF to produce DMTHF. Another possibility is that the hydrogenation of the furan ring is produced in a previous step, where MFA is converted into MTHFA to subsequently be transformed into DMTHF. In the last route, the furan ring of DMF can be opened to HD, which is further hydrogenated to 2,5-hexanediol and finally, DMTHF is generated.

Yang et al. [67] studied the transformation of fructose, glucose and cellulose to DMTHF in a biphasic system. A homogeneous catalyst constituted of rhodium salt and hydroiodic acid (HI) under H<sub>2</sub> atmosphere was employed. The addition of an organic solvent enhanced the production of DMTHF due to the extraction of unstable reaction intermediates out of the aqueous phase. The desired product yield was enlarged by increasing the temperature and decreasing the amount of acid, obtaining a maximum DMTHF yield of 81 %, 70 % and 54 % when fructose, glucose and cellulose were tested as raw materials. Subsequently, the same research group investigated the role of both Rh and the HI in the production of DMTHF from fructose [15]. They concluded that HI acts as a dehydration agent in the conversion of fructose to HMF and as a reducing reagent to consecutively produce 5-MF. Moreover, HI enables the hydration of DMF to HD, an important intermediate to produce DMTHF. The I<sub>2</sub> produced in the reduction steps is converted back to HI by Rh. This metal is additionally responsible for the hydrogenation of unsaturated C=C and C=O. Even if high yields of DMTHF are obtained with this catalytic system, the high cost of Rh and the corrosive nature of HI make the process uneconomical. Similarly, Li's group [68] investigated the fructose conversion to DMTHF in a biphasic system. A hydrophilic (Brønsted acid: H<sub>2</sub>SO<sub>4</sub>) and hydrophobic catalyst (Pt/C) were added into immiscible organic/water system. The dehydration of fructose to HMF was catalysed by H<sub>2</sub>SO<sub>4</sub> in the aqueous phase, and then, to DMTHF by Pd/C at the water/organic interface. Higher amount of diethyl ether (EtOEt) solvent improved the extraction of HMF. The maximum yield of DMTHF

obtained was 70 % in water-EtOEt biphasic system at 130 °C after 12 h. The addition of dimethyl sulfoxide (DMSO) provoked the decrease of Pd/C activity, involving the production of DMF and 5-MF and the decrease in DMTHF generation.

The same heterogeneous catalyst (Pt/C) was employed by Jackson and colleagues [69]. The catalyst was poisoned by sulphur (sulfided Pt/C) to increase the selectivity of DMTHF from HD by enhancing the rate of ring closing of HD. The reaction was carried out in ethanol, which stabilized fructose against dehydration to HMF, allowing hydrodeoxygenation to take place. The ring-opening of fructofuranose lead to HD, further hydrogenated to 2,5-hexanediol, which ring closes to DMTHF. The achieved DMTHF yield reached 50 % at 103 bar and 175 °C.

The conversion of DMTHF from HMF was studied by Gao et al. [20] using nitrogen-doped decorated copper-based catalyst (NC-Cu/MgAlO) reaching a DMTHF yield of 94.6 % at 220 °C after 200 min. Cyclohexanol was used as both hydrogen donor and solvent in N<sub>2</sub> atmosphere. The surface basic sites promoted the activation of hydroxyl group in cyclohexanol and subsequent release of active hydrogen. Moreover, the highly dispersed Cu<sup>0</sup> and Cu<sup>+</sup> species efficiently transferred the hydrogen and activated both carbonyl and hydroxyl group. Recently, Chen et al. [70] achieved 97 % yield of DMTHF after 10 h of reaction under mild conditions (130 °C and 30 bar) catalysed by Ni/SBA-15. HMF was rapidly converted into DMF and in a second stage, the furan ring hydrogenation occurred in a slower rate.

The aforementioned research results based on the production of DMTHF are summarized in Table 2.5.

According to this background, an important effort has been carried out to study the hydrogenolysis of HMF to DMF and DMTHF with a variety of catalytic systems (monometallic and bimetallic catalysts based on noble and non-noble metals) in monophasic and biphasic systems using diverse solvents at different reaction conditions. However, most of the investigations are focused on batch type reactors, implying discontinuous systems. Considering the lack of research data for continuous systems, this PhD thesis focuses on the production of DMF and DMTHF in a continuous

fixed-bed reactor. This type of continuous process provide higher efficiencies and lower production costs [71] and are preferable for use on an industrial scale.

**Table 2.5.** Catalytic activity of DMTHF production.

Catalyst	Feed	Solvent	P (bar)	T (°C)	Time (h)	Yield (%)	Ref.
HI + Rh	Fructose	Water + chloro- benzene	20.7	140	16	81	[67]
	Glucose					70	
	Cellulose					54	
H <sub>2</sub> SO <sub>4</sub> +Pd/C	Fructose	Water + EtOEt	27.6	130	12	70	[68]
Sulfided Pt/C	Fructose	Ethanol	103	175	2	50	[69]
NC-Cu/MgAlO	HMF	Cyclo- hexanol	1 (N <sub>2</sub> )	220	3.33	94.6	[20]
Ni/SBA-15	HMF	1,4-dioxane	30	130	10	97	[70]

**References**

- [1] Roman-Leshkov Y, Barrett CJ, Liu ZY, Dumesic JA. Production of dimethylfuran for liquid fuels from biomass-derived carbohydrates. *Nature* 2007;447:982–5.
- [2] Binder JB, Raines RT. Simple chemical transformation of lignocellulosic biomass into furans for fuels and chemicals. *J Am Chem Soc* 2009;131:1979–85. <https://doi.org/10.1021/ja808537j>.
- [3] Zhang J, Lin L, Liu S. Efficient production of furan derivatives from a sugar mixture by catalytic process. *Energy and Fuels* 2012;26:4560–7. <https://doi.org/10.1021/ef300606v>.
- [4] Thananattachon T, Rauchfuss TB. Efficient production of the liquid fuel 2,5-dimethylfuran from fructose using formic acid as a reagent. *Angew Chemie - Int Ed* 2010;49:6616–8. <https://doi.org/10.1002/anie.201002267>.
- [5] Chidambaram M, Bell AT. A two-step approach for the catalytic conversion of glucose to 2,5-dimethylfuran in ionic liquids. *Green Chem* 2010;12:1253–62. <https://doi.org/10.1039/C004343E>.
- [6] Welton T. Ionic liquids in catalysis. *Coord Chem Rev* 2004;248:2459–77. <https://doi.org/10.1016/j.ccr.2004.04.015>.
- [7] De S, Dutta S, Saha B. One-pot conversions of lignocellulosic and algal biomass into liquid fuels. *ChemSusChem* 2012;5:1826–33. <https://doi.org/10.1002/cssc.201200031>.
- [8] Li C, Cai H, Zhang B, Li W, Pei G, Dai T, et al. Tailored one-pot production of furan-based fuels from fructose in an ionic liquid biphasic solvent system. *Chinese J Catal* 2015;36:1638–46. [https://doi.org/10.1016/S1872-2067\(15\)60927-5](https://doi.org/10.1016/S1872-2067(15)60927-5).
- [9] Upare PP, Hwang DW, Hwang YK, Lee U-H, Hong D-Y, Chang J-S. An integrated process for the production of 2,5-dimethylfuran from fructose. *Green Chem* 2015;17:3310–3. <https://doi.org/10.1039/C5GC00281H>.

- [10] Wang J, Liu X, Hu B, Lu G, Wang Y. Efficient catalytic conversion of lignocellulosic biomass into renewable liquid biofuels via furan derivatives. *RSC Adv* 2014;4:31101–7. <https://doi.org/10.1039/c4ra04900d>.
- [11] Saha B, Bohn CM, Abu-Omar MM. Zinc-assisted hydrodeoxygenation of biomass-derived 5-hydroxymethylfurfural to 2,5-dimethylfuran. *ChemSusChem* 2014;7:3095–101. <https://doi.org/10.1002/cssc.201402530>.
- [12] Insyani R, Verma D, Kim SM, Kim J. Direct one-pot conversion of monosaccharides into high-yield 2,5-dimethylfuran over a multifunctional Pd/Zr-based metal-organic framework@ sulfonated graphene oxide catalyst. *Green Chem* 2017;19:2482–90. <https://doi.org/10.1039/c7gc00269f>.
- [13] Insyani R, Verma D, Cahyadi HS, Kim SM, Kim SK, Karanwal N, et al. One-pot di- and polysaccharides conversion to highly selective 2,5-dimethylfuran over Cu-Pd/Amino-functionalized Zr-based metal-organic framework (UiO-66(NH<sub>2</sub>))@SGO tandem catalyst. *Appl Catal B Environ* 2019;243:337–54. <https://doi.org/10.1016/j.apcatb.2018.10.036>.
- [14] Zhang J, Dong K, Luo W. PdCl<sub>2</sub>-catalyzed hydrodeoxygenation of 5-hydroxymethylfurfural into 2,5-dimethylfuran at room-temperature using polymethylhydrosiloxane as the hydrogen donor. *Chem Eng Sci* 2019;201:467–74. <https://doi.org/10.1016/j.ces.2019.03.011>.
- [15] Grochowski MR, Yang W, Sen A. Mechanistic study of a one-step catalytic conversion of fructose to 2,5-dimethyltetrahydrofuran. *Chem - A Eur J* 2012;18:12363–71. <https://doi.org/10.1002/chem.201201522>.
- [16] Tzeng TW, Lin CY, Pao CW, Chen JL, Nuguid RJG, Chung PW. Understanding catalytic hydrogenolysis of 5-hydroxymethylfurfural (HMF) to 2,5-dimethylfuran (DMF) using carbon supported Ru catalysts. *Fuel Process Technol* 2020;199:106225. <https://doi.org/10.1016/j.fuproc.2019.106225>.
- [17] Zhang Z, Yao S, Wang C, Liu M, Zhang F, Hu X, et al. CuZnCoO<sub>x</sub> multifunctional catalyst for in situ hydrogenation of 5-hydroxymethylfurfural with ethanol as

- hydrogen carrier. J Catal 2019;373:314–21.  
<https://doi.org/10.1016/j.jcat.2019.04.011>.
- [18] Guo D, Liu X, Cheng F, Zhao W, Wen S, Xiang Y, et al. Selective hydrogenolysis of 5-hydroxymethylfurfural to produce biofuel 2, 5-dimethylfuran over Ni/ZSM-5 catalysts. Fuel 2020;274:117853. <https://doi.org/10.1016/j.fuel.2020.117853>.
- [19] Li D, Liu Q, Zhu C, Wang H, Cui C, Wang C, et al. Selective hydrogenolysis of 5-hydroxymethylfurfural to 2,5-dimethylfuran over Co<sub>3</sub>O<sub>4</sub> catalyst by controlled reduction. J Energy Chem 2019;30:34–41.  
<https://doi.org/10.1016/j.jechem.2018.03.008>.
- [20] Gao Z, Li C, Fan G, Yang L, Li F. Nitrogen-doped carbon-decorated copper catalyst for highly efficient transfer hydrogenolysis of 5-hydroxymethylfurfural to convertibly produce 2,5-dimethylfuran or 2,5-dimethyltetrahydrofuran. Appl Catal B Environ 2018;226:523–33.  
<https://doi.org/10.1016/j.apcatb.2018.01.006>.
- [21] Solanki BS, Rode C V. Selective hydrogenolysis of 5-(hydroxymethyl)furfural over Pd/C catalyst to 2,5-dimethylfuran. J Saudi Chem Soc 2019;23:439–51.  
<https://doi.org/10.1016/j.jscs.2018.08.009>.
- [22] Chen N, Zhu Z, Ma H, Liao W, Lü H. Catalytic upgrading of biomass-derived 5-hydroxymethylfurfural to biofuel 2,5-dimethylfuran over Beta zeolite supported non-noble Co catalyst. Mol Catal 2020;486:110882.  
<https://doi.org/10.1016/j.mcat.2020.110882>.
- [23] Liao W, Zhu Z, Chen N, Su T, Deng C, Zhao Y, et al. Highly active bifunctional Pd-Co<sub>9</sub>S<sub>8</sub>/S-CNT catalysts for selective hydrogenolysis of 5-hydroxymethylfurfural to 2,5-dimethylfuran. Mol Catal 2020;482:110756.  
<https://doi.org/10.1016/j.mcat.2019.110756>.
- [24] Esteves LM, Brijaldo MH, Oliveira EG, Martinez JJ, Rojas H, Caytuelero A, et al. Effect of support on selective 5-hydroxymethylfurfural hydrogenation towards 2,5-dimethylfuran over copper catalysts. Fuel 2020;270:117524.



<https://doi.org/10.1016/j.fuel.2020.117524>.

- [25] Jae J, Zheng W, Lobo RF, Vlachos DG. Production of dimethylfuran from hydroxymethylfurfural through catalytic transfer hydrogenation with ruthenium supported on carbon. *ChemSusChem* 2013;6:1158–62. <https://doi.org/10.1002/cssc.201300288>.
- [26] Han W, Tang M, Li J, Li X, Wang J, Zhou L, et al. Selective hydrogenolysis of 5-hydroxymethylfurfural to 2,5-dimethylfuran catalyzed by ordered mesoporous alumina supported nickel-molybdenum sulfide catalysts. *Appl Catal B Environ* 2020;268:118748. <https://doi.org/10.1016/j.apcatb.2020.118748>.
- [27] Braun M, Antonietti M. A continuous flow process for the production of 2,5-dimethylfuran from fructose using (non-noble metal based) heterogeneous catalysis. *Green Chem* 2017;19:3813–9. <https://doi.org/10.1039/c7gc01055a>.
- [28] Hu L, Tang X, Xu J, Wu Z, Lin L, Liu S. Selective Transformation of 5 - Hydroxymethylfurfural into the Liquid Fuel 2 , 5-Dimethylfuran over Carbon-Supported Ruthenium. *Ind Eng Chem Res* 2014.
- [29] Priece P, Endot NA, Carà PD, Lopez-Sanchez JA. Fast Catalytic Hydrogenation of 2,5-Hydroxymethylfurfural to 2,5-Dimethylfuran with Ruthenium on Carbon Nanotubes. *Ind Eng Chem Res* 2018;57:1991–2002. <https://doi.org/10.1021/acs.iecr.7b04715>.
- [30] Jae J, Zheng W, Karim AM, Guo W, Lobo RF. The Role of Ru and RuO<sub>2</sub> in the Catalytic Transfer Hydrogenation of 5-Hydroxymethylfurfural for the Production of 2 , 5-Dimethylfuran 2014;791:848–56. <https://doi.org/10.1002/cctc.201300945>.
- [31] Nagpure AS, Lucas N, Chilukuri S V. Efficient Preparation of Liquid Fuel 2,5-Dimethylfuran from Biomass-Derived 5-Hydroxymethylfurfural over Ru-NaY Catalyst. *ACS Sustain Chem Eng* 2015;3:2909–16. <https://doi.org/10.1021/acssuschemeng.5b00857>.

- [32] Nagpure AS, Venugopal AK, Lucas N, Manikandan M, Thirumalaiswamy R, Chilukuri S. Renewable fuels from biomass-derived compounds: Ru-containing hydrotalcites as catalysts for conversion of HMF to 2,5-dimethylfuran. *Catal Sci Technol* 2015;5:1463–72. <https://doi.org/10.1039/c4cy01376j>.
- [33] Raut AB, Nanda B, Parida KM, Bhanage BM. Hydrogenolysis of Biomass-Derived 5-Hydroxymethylfurfural to Produce 2,5-Dimethylfuran Over Ru-ZrO<sub>2</sub>-MCM-41 Catalyst. *ChemistrySelect* 2019;4:6080–9. <https://doi.org/10.1002/slct.201901145>.
- [34] Mitra J, Zhou X, Rauchfuss T. Pd/C-catalyzed reactions of HMF: Decarbonylation, hydrogenation, and hydrogenolysis. *Green Chem* 2015;17:307–13. <https://doi.org/10.1039/c4gc01520g>.
- [35] Chatterjee M, Ishizaka T, Kawanami H. Hydrogenation of 5-hydroxymethylfurfural in supercritical carbon dioxide-water: A tunable approach to dimethylfuran selectivity. *Green Chem* 2014;16:1543–51. <https://doi.org/10.1039/c3gc42145g>.
- [36] Scholz D, Aellig C, Hermans I. Catalytic transfer hydrogenation/hydrogenolysis for reductive upgrading of furfural and 5-(hydroxymethyl)furfural. *ChemSusChem* 2014;7:268–75. <https://doi.org/10.1002/cssc.201300774>.
- [37] Shi J, Wang Y, Yu X, Du W, Hou Z. Production of 2,5-dimethylfuran from 5-hydroxymethylfurfural over reduced graphene oxides supported Pt catalyst under mild conditions. *Fuel* 2016;163:74–9. <https://doi.org/10.1016/j.fuel.2015.09.047>.
- [38] Luo J, Arroyo-Ramírez L, Gorte RJ, Tzoulaki D, Vlachos DG. Hydrodeoxygenation of HMF over Pt/C in a continuous flow reactor. *AIChE* 2015;61:590–7. <https://doi.org/10.1002/aic.14660>.
- [39] Goyal R, Sarkar B, Bag A, Siddiqui N, Dumbre D, Lucas N, et al. Studies of synergy between metal – support interfaces and selective hydrogenation of HMF to DMF in water. *J Catal* 2016;340:248–60. <https://doi.org/10.1016/j.jcat.2016.05.012>.

- [40] Chen MY, Chen CB, Zada B, Fu Y. Perovskite type oxide-supported Ni catalysts for the production of 2,5-dimethylfuran from biomass-derived 5-hydroxymethylfurfural. *Green Chem* 2016;18:3858–66. <https://doi.org/10.1039/c6gc00432f>.
- [41] Kong X, Zhu Y, Zheng H, Dong F, Zhu Y, Li YW. Switchable synthesis of 2,5-dimethylfuran and 2,5-dihydroxymethyltetrahydrofuran from 5-hydroxymethylfurfural over Raney Ni catalyst. *RSC Adv* 2014;4:60467–72. <https://doi.org/10.1039/c4ra09550b>.
- [42] Gyngazova MS, Negahdar L, Blumenthal LC, Palkovits R. Experimental and kinetic analysis of the liquid phase hydrodeoxygenation of 5-hydroxymethylfurfural to 2,5-dimethylfuran over carbon-supported nickel catalysts. *Chem Eng Sci* 2017;173:455–64. <https://doi.org/10.1016/j.ces.2017.07.045>.
- [43] Mani CM, Braun M, Molinari V, Antonietti M, Fechler N. A High-Throughput Composite Catalyst based on Nickel Carbon Cubes for the Hydrogenation of 5-Hydroxymethylfurfural to 2,5-Dimethylfuran. *ChemCatChem* 2017;9:3388–94. <https://doi.org/10.1002/cctc.201700506>.
- [44] Kong X, Zheng R, Zhu Y, Ding G, Zhu Y, Li YW. Rational design of Ni-based catalysts derived from hydrotalcite for selective hydrogenation of 5-hydroxymethylfurfural. *Green Chem* 2015;17:2504–14. <https://doi.org/10.1039/c5gc00062a>.
- [45] Zhu C, Liu Q, Li D, Wang H, Zhang C, Cui C, et al. Selective Hydrodeoxygenation of 5-Hydroxymethylfurfural to 2,5-Dimethylfuran over Ni Supported on Zirconium Phosphate Catalysts. *ACS Omega* 2018;3:7407–17. <https://doi.org/10.1021/acsomega.8b00609>.
- [46] Yang P, Cui Q, Zu Y, Liu X, Lu G, Wang Y. Catalytic production of 2,5-dimethylfuran from 5-hydroxymethylfurfural over Ni/Co<sub>3</sub>O<sub>4</sub> catalyst. *Catal Commun* 2015;66:55–9. <https://doi.org/10.1016/j.catcom.2015.02.014>.

- [47] Hansen TS, Barta K, Anastas PT, Ford PC, Riisager A. One-pot reduction of 5-hydroxymethylfurfural via hydrogen transfer from supercritical methanol. *Green Chem* 2012;14:2457–61. <https://doi.org/10.1039/c2gc35667h>.
- [48] Zhu Y, Kong X, Zheng H, Ding G, Zhu Y, Li YW. Efficient synthesis of 2,5-dihydroxymethylfuran and 2,5-dimethylfuran from 5-hydroxymethylfurfural using mineral-derived Cu catalysts as versatile catalysts. *Catal Sci Technol* 2015;5:4208–17. <https://doi.org/10.1039/c5cy00700c>.
- [49] Bottari G, Kumalaputri AJ, Krawczyk KK, Feringa BL, Heeres HJ, Barta K. Copper-Zinc Alloy Nanopowder: A Robust Precious-Metal-Free Catalyst for the Conversion of 5-Hydroxymethylfurfural. *ChemSusChem* 2015;8:1323–7. <https://doi.org/10.1002/cssc.201403453>.
- [50] Zhang Z, Wang C, Gou X, Chen H, Chen K, Lu X, et al. Catalytic in-situ hydrogenation of 5-hydroxymethylfurfural to 2,5-dimethylfuran over Cu-based catalysts with methanol as a hydrogen donor. *Appl Catal A Gen* 2019;570:245–50. <https://doi.org/10.1016/j.apcata.2018.11.029>.
- [51] Gao Z, Fan G, Liu M, Yang L, Li F. Dandelion-like cobalt oxide microsphere-supported RuCo bimetallic catalyst for highly efficient hydrogenolysis of 5-hydroxymethylfurfural. *Appl Catal B Environ* 2018;237:649–59. <https://doi.org/10.1016/j.apcatb.2018.06.026>.
- [52] Nishimura S, Ikeda N, Ebitani K. Selective hydrogenation of biomass-derived 5-hydroxymethylfurfural (HMF) to 2,5-dimethylfuran (DMF) under atmospheric hydrogen pressure over carbon supported PdAu bimetallic catalyst. *Catal Today* 2014;232:89–98. <https://doi.org/10.1016/j.cattod.2013.10.012>.
- [53] Talpade AD, Tiwari MS, Yadav GD. Selective hydrogenation of bio-based 5-hydroxymethyl furfural to 2,5-dimethylfuran over magnetically separable Fe-Pd/C bimetallic nanocatalyst. *Mol Catal* 2019;465:1–15. <https://doi.org/10.1016/j.mcat.2018.12.009>.
- [54] Wang G-H, Hilgert J, Richter FH, Wang F, Bongard H-J, Spliethoff B, et al.

- Platinum–cobalt bimetallic nanoparticles in hollow carbon nanospheres for hydrogenolysis of 5-hydroxymethylfurfural. *Nat Mater* 2014;13:293–300.
- [55] Wang X, Liu Y, Liang X. Hydrogenolysis of 5-hydroxymethylfurfural to 2,5-dimethylfuran over supported Pt-Co bimetallic catalysts under mild conditions. *Green Chem* 2018;20:2894–902. <https://doi.org/10.1039/c8gc00716k>.
- [56] Ledesma B, Juárez J, Mazarío J, Domine M, Beltramone A. Bimetallic platinum/iridium modified mesoporous catalysts applied in the hydrogenation of HMF. *Catal Today* 2019:1–10. <https://doi.org/10.1016/j.cattod.2019.06.037>.
- [57] Huang YB, Chen MY, Yan L, Guo QX, Fu Y. Nickel-tungsten carbide catalysts for the production of 2,5-dimethylfuran from biomass-derived molecules. *ChemSusChem* 2014;7:1068–72. <https://doi.org/10.1002/cssc.201301356>.
- [58] Yu L, He L, Chen J, Zheng J, Ye L, Lin H, et al. Robust and recyclable nonprecious bimetallic nanoparticles on carbon nanotubes for the hydrogenation and hydrogenolysis of 5-hydroxymethylfurfural. *ChemCatChem* 2015;7:1701–7. <https://doi.org/10.1002/cctc.201500097>.
- [59] Han W, Tang M, Li J, Li X, Wang J, Zhou L, et al. Selective hydrogenolysis of 5-hydroxymethylfurfural to 2,5-dimethylfuran catalyzed by ordered mesoporous alumina supported nickel-molybdenum sulfide catalysts. *Appl Catal B Environ* 2020;268:118748. <https://doi.org/10.1016/j.apcatb.2020.118748>.
- [60] Yang P, Xia Q, Liu X, Wang Y. High-yield production of 2,5-dimethylfuran from 5-hydroxymethylfurfural over carbon supported Ni–Co bimetallic catalyst. *J Energy Chem* 2016;25:1015–20. <https://doi.org/10.1016/j.jechem.2016.08.008>.
- [61] Yang P, Xia Q, Liu X, Wang Y. Catalytic transfer hydrogenation/hydrogenolysis of 5-hydroxymethylfurfural to 2,5-dimethylfuran over Ni-Co/C catalyst. *Fuel* 2017;187:159–66. <https://doi.org/10.1016/j.fuel.2016.09.026>.
- [62] Chen N, Zhu Z, Su T, Liao W, Deng C, Ren W, et al. Catalytic hydrogenolysis of hydroxymethylfurfural to highly selective 2,5-dimethylfuran over FeCoNi/h-BN

- catalyst. Chem Eng J 2020;381:122755. <https://doi.org/10.1016/j.cej.2019.122755>.
- [63] Srivastava S, Jadeja GC, Parikh J. Influence of supports for selective production of 2,5-dimethylfuran via bimetallic copper-cobalt catalyzed 5-hydroxymethylfurfural hydrogenolysis. Cuihua Xuebao/Chinese J Catal 2017;38:699–709. [https://doi.org/10.1016/S1872-2067\(17\)62789-X](https://doi.org/10.1016/S1872-2067(17)62789-X).
- [64] Guo W, Liu H, Zhang S, Han H, Liu H, Jiang T, et al. Efficient hydrogenolysis of 5-hydroxymethylfurfural to 2,5-dimethylfuran over a cobalt and copper bimetallic catalyst on N-graphene-modified Al<sub>2</sub>O<sub>3</sub>. Green Chem 2016;18:6222–8. <https://doi.org/10.1039/c6gc02630c>.
- [65] Chen B, Li F, Huang Z, Yuan G. Carbon-coated Cu-Co bimetallic nanoparticles as selective and recyclable catalysts for production of biofuel 2,5-dimethylfuran. Appl Catal B Environ 2017;200:192–9. <https://doi.org/10.1016/j.apcatb.2016.07.004>.
- [66] Luo J, Lee JD, Yun H, Wang C, Monai M, Murray CB, et al. Base metal-Pt alloys: A general route to high selectivity and stability in the production of biofuels from HMF. Appl Catal B Environ 2016;199:439–46. <https://doi.org/10.1016/j.apcatb.2016.06.051>.
- [67] Yang W, Sen A. One-Step catalytic transformation of carbohydrates and cellulosic biomass to 2,5-dimethyltetrahydrofuran for liquid Fuels. ChemSusChem 2010;3:597–603. <https://doi.org/10.1002/cssc.200900285>.
- [68] Li T, Ong SSG, Zhang J, Jia C, Sun J, Wang Y, et al. One-pot conversion of carbohydrates into furan derivatives in biphasic tandem catalytic process. Catal Today 2020;339:296–304. <https://doi.org/10.1016/j.cattod.2018.11.052>.
- [69] Jackson MA, Appell M, Blackburn JA. Hydrodeoxygenation of Fructose to 2,5-Dimethyltetrahydrofuran Using a Sulfur Poisoned Pt/C Catalyst. Ind Eng Chem Res 2015;54:7059–66. <https://doi.org/10.1021/acs.iecr.5b00766>.

- [70] Chen S, Ciotonea C, De Oliveira Vigier K, Jérôme F, Wojcieszak R, Dumeignil F, et al. Hydroconversion of 5-Hydroxymethylfurfural to 2,5-Dimethylfuran and 2,5-Dimethyltetrahydrofuran over Non-promoted Ni/SBA-15. *ChemCatChem* 2020;12:2050–9. <https://doi.org/10.1002/cctc.201902028>.
- [71] Pastor-Pérez L, Gu S, Sepúlveda-Escribano A, Reina TR. Bimetallic Cu–Ni catalysts for the WGS reaction – Cooperative or uncooperative effect? *Int J Hydrogen Energy* 2019;44:4011–9. <https://doi.org/10.1016/j.ijhydene.2018.12.127>.





## **CHAPTER 3: Objectives and scope of the thesis**

---



This PhD thesis focuses on the production of green biofuels. The Chapter 1 evidenced the need of replacing conventional petroleum-based fuels. Moreover, it was emphasized that green fuels produced from biomass are a promising alternative. In this sense, the recent studies on the production of DMF and DMTHF (biofuels which can be substitutive or additive of conventional fuels) were described in Chapter 2.

The main objective of this PhD thesis is the **development of advanced catalytic technologies for biofuels production from selective hydrogenolysis of biomass-derived platform molecule using a fixed bed reactor**. This work aims to have an academic interest, being useful for the scientific community, and provide a contribution in the field of sustainable processes and applied catalysis in biorefineries, especially in the area of hydrogenolysis reactions.

For this research, the hydrogenolysis of HMF to produce DMF and DMTHF was studied, due to the promising characteristics these biofuels present. Many studies have centred their attention on the study of catalysts based on noble metals, due to the suitable characteristics they present. However, the high price and reduced availability of these metals involve the need of studying new advanced catalytic systems based on non-noble metals. Moreover, most of the investigations carried out in this area are performed on batch type reactors. Nevertheless, from an industrial point of view, the continuous processes provide higher efficiencies and lower production costs. For these reasons, the current PhD thesis research will be carried out in a continuous fixed-bed reactor. Additionally, avoiding the use of noble metals will reduce the costs of the process. Therefore, Cu based catalysts will be synthesized due to the high hydrogenation capacity and C—O hydrogenolysis capacity this non-noble metal exhibits.

In order to achieve the main objective of this thesis successfully, some partial goals were established using different active metals and catalyst support materials:

- A continuous update of the new relevant published investigations will be carried out, once the state-of-the-art revision is included in the previous chapter.

- Set up and start up of the experimental lab scale facility in order to develop the corresponding activity studies. A precise functioning of the system is required to achieve reliable results.
- *Catalyst screening.* Considering the low amount of investigations carried out in the hydrogenolysis of HMF in continuous fixed bed reactors, a screening of different catalysts will be carried out. Based on Cu/ZrO<sub>2</sub>, different catalysts will be synthesized and tested. On the one hand, the support will be modified by CeO<sub>2</sub> to improve its characteristics. Moreover, the addition of Ru (noble metal) and Ni (non-noble metal) will be studied to see if their addition enhances the catalytic activity of the system.
- *A deep study of the catalytic behaviour* of the most promising catalysts observed in the catalyst screening will be performed. An analysis of the correlation between the hydrogenolysis activity results and the catalysts physicochemical properties will be carried out. For this purpose, fresh and used catalysts will be examined by different characterization techniques (ICP-OES, N<sub>2</sub>-physisorption, H<sub>2</sub>-TPR, NH<sub>3</sub>-TPD, CHN, XRD, XPS and STEM). This extensive investigation should promote the comprehension of the factors affecting positively and negatively the hydrogenolysis reaction.
- *Ni-Cu bimetallic interaction study.* The promising bimetallic Ni-Cu interaction will be profoundly studied in Ni-Cu/ZrO<sub>2</sub> based catalysts. For this purpose, different metal content of Ni and/or Cu will be loaded to the support. Moreover, the impregnation method will be varied. On the one hand, both metals will be co-impregnated in the same step. On the other hand, the metals will be impregnated in sequential steps (first impregnating one metal and then the second metal).
- *Biomass-derived carbon as catalytic support.* Biomass-derived carbon produced from agroforestry residues will be studied as catalytic support to examine the possible use of this valorised residue. The results obtained with the catalysts synthesized with biomass-derived carbon will be compared with the catalysts supported on commercial carbon to understand the potential of the valorised carbon.

Therefore, a selective and stable catalytic system for the hydrogenolysis of HMF to DMF and DMTHF could favour the intensification of biofuels production. Moreover, this PhD thesis focuses on the cost minimization of the process, employing non-noble metals and working on a fixed bed reactor. Nevertheless, the process is yet away from being scaled-up to the industry.



## **CHAPTER 4: Experimental**

---





---

## Table of contents

4.1 CATALYST PREPARATION.....	107
4.1.1 ZrO <sub>2</sub> based catalysts .....	107
4.1.2 Carbon based catalysts .....	109
4.2 APPARATUS AND PROCEDURE.....	110
4.2.1 Continuous reaction system.....	110
4.2.2 Analysis .....	112
4.2.3 Measurement of the reaction progress .....	112
4.3 CATALYST CHARACTERIZATION.....	113
4.3.1 Textural properties – N <sub>2</sub> physisorption .....	113
4.3.2 Inductively Coupled Plasma Optical Emission Spectroscopy (ICP-OES) .....	114
4.3.3 Temperature-Programmed Reduction with Hydrogen (H <sub>2</sub> -TPR) .....	114
4.3.4 Temperature-Programmed Desorption with Ammonia (NH <sub>3</sub> -TPD).....	115
4.3.5 X-ray Diffraction (XRD).....	115
4.3.6 Scanning Transmission Electron Microscopy (STEM).....	115
4.3.7 X-ray Photoelectron Spectroscopy (XPS).....	116
4.3.8 Elemental analysis (CHN).....	117



In this chapter the experimental procedure of the catalysts synthesis and the catalytic activity test have been described. Moreover, the analysis of the obtained products and the characterization techniques employed to understand the physicochemical characteristics of the catalysts have been outlined.

## 4.1 Catalyst preparation

The catalyst synthesis is one of the key factors in this PhD thesis. Wet impregnation method was employed for the preparation of the catalysts, due to its simplicity, low cost and fast preparation time this technique provides [1]. The synthesized catalysts were classified considering the employed support, discerning between ZrO<sub>2</sub> based catalysts and carbon based catalysts.

### 4.1.1 ZrO<sub>2</sub> based catalysts

#### **Monometallic catalysts**

The catalysts were synthesized by wetness impregnation (WI) method. Zirconium nitrate, ZrO(NO<sub>3</sub>)·H<sub>2</sub>O (Sigma-Aldrich, 99 %), and the corresponding metal nitrate, Cu(NO<sub>3</sub>)<sub>2</sub>·H<sub>2</sub>O (Alfa Aesar, 98 %) or Ni(NO<sub>3</sub>)<sub>2</sub>·6H<sub>2</sub>O (Sigma-Aldrich 99.99 %), were dissolved in deionized water. The solution was stirred in a rotatory evaporator at room temperature for 2 h. Subsequently, it was warmed up to 60 °C and the water was evaporated employing a vacuum system. The samples were dried overnight at 110 °C and calcined in air at 250 °C for 2 h. An scheme is showed in Figure 4.1.

The samples obtained with this method are denominated as xCuZr or yNiZr, where x and y represent the metal content (wt %) of Cu and Ni, respectively.

#### **Co-impregnated bimetallic catalysts**

The same method as explained for monometallic catalyst was performed to prepare bimetallic catalysts. The difference was that Zr, Ni and Cu nitrates were at the same

time dissolved in deionized water. The followed procedure was identical to the one described above.

The samples are named as  $y\text{Ni}x\text{CuZr}$ , where  $x$  and  $y$  represent the metal content (wt %) of Cu and Ni, respectively.

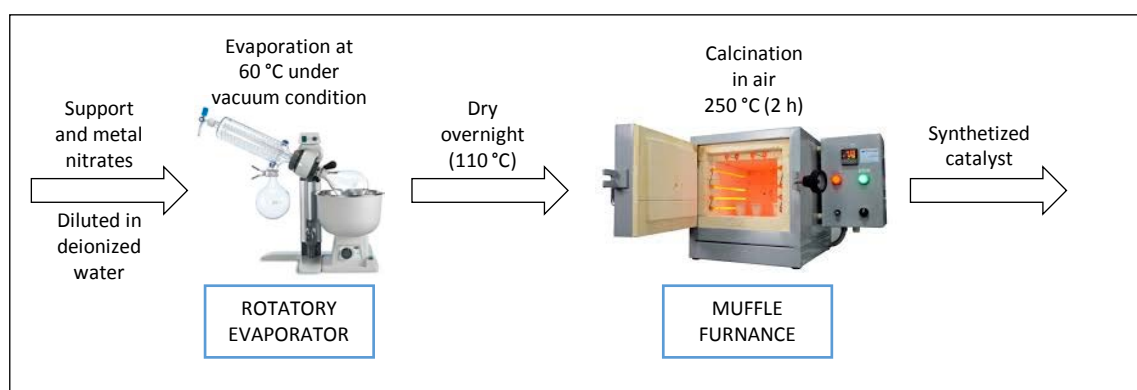


**Figure 4.1.** Catalyst preparation scheme.

### **Bimetallic catalyst impregnated in sequential steps**

In this case, the metals were integrated in two steps. The first metal was incorporated following the aforementioned monometallic procedure precisely. After the impregnation, drying and calcination steps, the second metal was introduced. In this case, the remaining metal was impregnated, dried and calcined in the same conditions. Thus, in this case, the catalyst underwent a double calcination.

The impregnation in sequential steps was employed for synthesizing bimetallic Ru-Cu and Ni-Cu catalysts. In the first case, Cu was added in a first step and Ru in a second step. The obtained catalyst was labelled as  $u\text{Ru}-x\text{CuZr}$ , where  $u$  represents the metal content (%) of Ru. In the case of nickel, the catalysts prepared in two steps are designed as  $y\text{Ni}-x\text{CuZr}$  when copper was first impregnated and as  $x\text{Cu}-y\text{NiZr}$  when nickel was first impregnated.

### **ZrO<sub>2</sub> support modification with CeO<sub>2</sub>**

The ZrO<sub>2</sub> support was modified by loading 5 and 20 wt% of CeO<sub>2</sub>. The zirconium and cerium nitrates, CeN<sub>3</sub>O<sub>9</sub>·6H<sub>2</sub>O (Alfa Aesar, 99.5 %), were dissolved in deionized water

and followed the procedure explained in monometallic catalyst section. The synthesized support was identified as  $z\text{CeZr}$ , where  $z$  represents the metal loading of  $\text{CeO}_2$ .

#### 4.1.2 Carbon based catalysts

In general, the impregnation procedure of these catalysts was similar to  $\text{ZrO}_2$  based catalysts. The main difference relied on the support preparation and the thermal treatment.

##### **Carbon support preparation**

Two different carbon supports were employed: commercial activated carbon (PanReac, granulated n°2) and biomass-derived carbon supplied by EnviroHemp company, based on different agroforestry resources. 40 wt % of kaolin (Merck) was added to improve the mechanical properties of these supports [2]. The kaolin was impregnated in the carbon by wetness impregnation to improve the mechanical characteristic of the carbons (WI). Subsequently, it was dried overnight and treated thermally in a  $\text{N}_2$  atmosphere at 500 °C for 2 h. The commercial carbon support was denominated as CC and biomass-derived carbon as BC.

##### **Carbon support preparation with acidic pretreatment**

The commercial and biomass-derived carbons were initially pretreated with acid. The support was stirred for 1 h at 80 °C in 10 wt %  $\text{HNO}_3$  solution [3]. The carbon was filtered and washed several times with deionized water. Subsequently, NaOH was employed to neutralize the solution. Finally, the carbon was treated at 180 °C in air for 6 h to remove the volatile components [4].

The pretreated carbon was mixed with kaolin and thermally treated as detailed above in “*carbon support preparation*” section. The treated commercial carbon support was denominated as TCC and treated biomass-derived carbon as TBC.

### **Monometallic catalysts**

Monometallic Ni and Cu catalysts were prepared by wetness impregnation. 15 wt % of metal was impregnated in non pretreated commercial and biomass-derived carbon. After drying overnight, the catalyst was thermally treated at 500 °C for 2 h at N<sub>2</sub> atmosphere. The obtained catalysts were denoted as Ni/CC, Ni/BC, Cu/CC and Cu/BC.

### **Bimetallic catalysts**

Ni-Cu bimetallic catalysts were prepared varying the support: treated and non-treated commercial and biomass-derived carbon.

15 wt % of Cu was impregnated in the support by wetness impregnation. After drying overnight, the catalyst was treated in N<sub>2</sub> atmosphere at 500 °C for 2 h. In a second step, 15 wt % of Ni was loaded following the same method. Consecutively, the catalyst was dried overnight and thermally treated as mentioned above. The obtained catalysts were designated as Ni-Cu/CC, Ni-Cu/BS, Ni-Cu/TCC and Ni-Cu/TBC.

## 4.2 Apparatus and procedure

The synthesized catalysts were tested in a continuous fixed-bed reactor to examine their catalytic activity. In the following section, the reaction system and the analysis of the obtained products have been explained.

### 4.2.1 Continuous reaction system

The hydrogenolysis reaction of HMF was carried out in a continuous fixed-bed reactor in vapour-phase (Microactivity Reference PID Eng&Tech bench scale plant). Previous to the hydrogenolysis reaction, the catalytic bed was placed in the centre of the reactor. For that purpose, before and after the catalytic bed the reactor was filled with inert silicon carbide (SiC). The catalyst (0.42 - 0.5 mm diameter particle size) was diluted in SiC ( $m_{\text{catalyst}}/m_{\text{SiC}} = 1/9$ ) to avoid temperature gradients in the catalytic bed. The

reaction system (schematized in Figure 4.1) was composed of three different sections: feed system, reaction system and condensation system (peltier).

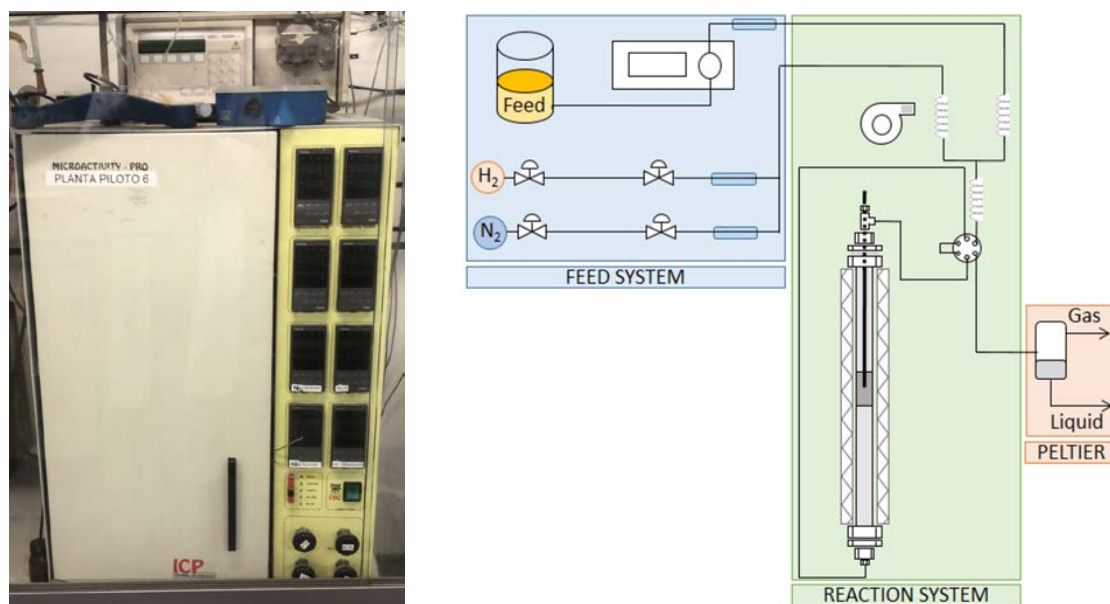


**Figure 4.2.** Continuous reaction system: pilote plant (left) and scheme (right)

### **Feed system**

HMF (Sigma-Aldrich, 99 %) was diluted in 1-butanol (PanReac, 99.5 %) – 1.5 wt % – and fed to the reactor by a HPLC pump (Gilson), being the weight hour space velocity (WHSV -  $\text{g HMF}/\text{g}_{\text{cat}}\cdot\text{h}$ ) in the reaction equal to  $0.15 \text{ h}^{-1}$ . Simultaneously, 100 ml/min of  $\text{H}_2$  were flown into the reactor, measured by a mass-flow controller (Bronkhorst). In addition,  $\text{N}_2$  gas was also available for the heating and cooling steps.

### **Reaction system**

The aforementioned feed was evaporated and mixed with  $\text{H}_2$  before incoming to the reactor, a stainless steel cylinder of 0.9 cm i.d. and 30 cm length. The catalytic bed was placed in the middle of the tube, which was thermally controlled placing a thermocouple in the centre of the catalytic bed. The catalyst was reduced before the beginning of the reaction, while working up to the reaction operating conditions.

### **Liquid-Gas condensation**

After the reaction the vapour stream was flowed into the condenser where, by means of the peltier effect, the obtained products were separated as liquids from the  $\text{H}_2$ .

### 4.2.2 Analysis

The obtained liquid product and the feed were analysed by different chromatographs. On the one hand, a high-performance liquid chromatograph (HPLC 1260 Infinity equipped with a refractive index detector (RID) and Hi-Plex H column) was employed to analyse the HMF concentration. On the other hand, a gas chromatograph (Agilent 6804 GC equipped with a flame ionization detector (FID) and using a SupraWax 280 capillary column) was used to analyse other obtained products (DMF, DMTHF, etc.). Lastly, the identification of the unknown products was carried out by a GC-MS chromatograph (Agilent 6890 GC equipped with a mass selective detector – 5973 Network – and using a DB-FFAP column).



**Figure 4.3.** Chromatographs employed in the analysis: HPLC (left) and GC-FID (right)

### 4.2.3 Measurement of the reaction progress

The products were collected every hour and analysed by using the abovementioned analytical equipment. The obtained liquid at 23 h was analysed as the overall production during the night. The activity results were determined by HMF conversion and DMF or DMTHF yield, defined as follows (where  $N$  is the molar flow rate given as mol/min):

$$\text{conversion (\%)} = \frac{N_{\text{HMF}}^{\text{in}} - N_{\text{HMF}}^{\text{out}}}{N_{\text{HMF}}^{\text{in}}} \cdot 100 \quad (1)$$

$$\text{yield (\%)} = \frac{N_{\text{DMF/DMTHF}}^{\text{out}}}{N_{\text{HMF}}^{\text{in}}} \cdot 100 \quad (2)$$



## 4.3 Catalyst characterization

In this last section, the characterization techniques utilized for the analysis of the physicochemical properties of the catalysts are described. These characteristics are important for the understanding of the catalytic activity. The utilized techniques are listed below:

- Textural properties – N<sub>2</sub> physisorption.
- Inductively Coupled Plasma Optical Emission Spectroscopy (ICP-OES).
- Temperature Programmed Reduction with Hydrogen (H<sub>2</sub>-TPR).
- Temperature Programmed Desorption with Ammonia (NH<sub>3</sub>-TPD).
- X-ray Diffraction (XRD).
- Scanning Transmission Electron Microscopy (STEM).
- X-ray Photoelectron Spectroscopy (XPS).
- Elemental analysis (CHN).

### 4.3.1 Textural properties – N<sub>2</sub> physisorption

N<sub>2</sub>-adsorption-desorption isotherms were obtained at -198 °C using an Autosorb-1-C/TCD (Quantachrome, USA) instrument to calculate the textural properties (surface area, pore volume, and average pore diameter). The calcined supports and catalysts were previously *in situ* outgassed at 150 °C for 4 h under high vacuum.

Surface area was calculated using Brunauer, Emmet, and Teller (BET) method. Moreover, average pore diameter was determined employing Barret, Joyner, and Halenda (BJH) method applied to the desorption branch of the isotherms.

### 4.3.2 Inductively Coupled Plasma Optical Emission Spectroscopy (ICP-OES)

The chemical composition of the calcined catalysts was determined by ICP-OES technique using a Perkin Elmer Optima 3300-DV equipment. Before the measurement, the samples (50-100 mg) were digested using a Milestone microwave digestion system (Ethos 1) in different acid solutions:

- \* 2 mL of HCl (Panreac, 37 %), 3 mL of HNO<sub>3</sub> (Panreac, 65 %) and 3 mL of HF (Panreac, 48 %) for catalysts employed in the initial screening.
- \* 6 mL of HCl and 2 mL of HNO<sub>3</sub> for bimetallic catalysts supported on ZrO<sub>2</sub> and carbon supported catalysts.

The digestion process consisted in heating the samples from room temperature to 180 °C with a heating ramp of 7 °C/min and keeping the temperature for 30 min. Subsequently, the obtained liquid, which contains the complete decomposed sample, was filtered and diluted up to 100 mL with deionized water. Some samples were further diluted with deionized water to achieve a concentration of the solution within the instrument detection range. The final solution was analysed to calculate the metallic content present in the catalyst.

### 4.3.3 Temperature-Programmed Reduction with Hydrogen (H<sub>2</sub>-TPR)

The reducibility of the calcined catalysts was determined by H<sub>2</sub>-TPR. Measurements were carried out in a Micromeritics AutoChem 2920 II instrument equipped with a thermal conductivity detector (TCD). The samples were *in situ* pretreated heating them to 200 °C under helium atmosphere with a heating rate of 10 °C/min and maintaining the temperature for 2 h to desorb the physisorbed impurities. The samples were cooled down to 50 °C before heating the samples under a reducing atmosphere (5% v/v H<sub>2</sub> diluted in Ar) up to 850 °C at a rate of 10 °C/min. The TCD recorded the changes in H<sub>2</sub> concentration; therefore, the H<sub>2</sub> consumption, corresponding to the reducibility of the surface species, could be examined.

#### 4.3.4 Temperature-Programmed Desorption with Ammonia (NH<sub>3</sub>-TPD)

The acidity of the fresh reduced catalysts was examined by NH<sub>3</sub>-TPD. Measurements were also performed in a Micromeritics AutoChem 2920 II instrument equipped with a TCD. Prior to the analysis, the calcined samples were *in situ* reduced at 275 °C for 1 h by flushing H<sub>2</sub> (5 % v/v H<sub>2</sub> diluted in Ar) to simulate the reduction conditions carried out before the activity tests. The physisorbed impurities were later desorbed by flowing He for 30 min. After this step, catalysts were cooled down to 100 °C, and NH<sub>3</sub> (10 % v/v NH<sub>3</sub> diluted in He) was fed to the sample for 30 min. The physisorbed NH<sub>3</sub> was subsequently removed by increasing the sample temperature to 150 °C with He for 60 min. Finally, samples were heated up to 850 °C with He at a rate of 10 °C/min and the release of NH<sub>3</sub> was recorded by the TCD.

#### 4.3.5 X-ray Diffraction (XRD)

X-ray diffraction patterns of fresh reduced and used catalysts were obtained by using a Seifert XRD 3000 diffractometer equipped with a PW 2200 Bragg-Brentano  $\theta/2\theta$  goniometer, bent graphite monochromator, and automatic slit, using Cu K radiation (0.15418 nm) and 0.028° steps scanning. The samples were reduced *ex situ* before the measurements in a H<sub>2</sub> flow for 1 h at 275 °C. The Scherrer equation was used to calculate the average crystallite size of the crystalline species.

#### 4.3.6 Scanning Transmission Electron Microscopy (STEM)

Elemental maps of the samples were obtained to calculate the mean particle size of the catalysts. The catalysts were *ex situ* reduced before the measurements in a H<sub>2</sub> flow for 1 h at 275 °C. On the one hand, a FEI Titan Cubed G2 60-300 transmission electron microscope at 300 kV was used, equipped with a Schottky X-FEG field emission electron gun, a monochromator, and a CEOS GmbH spherical aberration (C<sub>s</sub>) corrector on the image side. On the other hand, a Super-X EDX system was used under a

high-angle annular dark-field (HAADF) detector for Z contrast imaging under STEM conditions (camera length of 115 mm) using a pixel size of 2 nm, a dwell time of 900 s, and an image size of 512 x 512 pixels. The TEM samples were prepared by dispersion into an ethanol solvent and maintaining the suspension in an ultrasonic bath for 15 min. A drop of suspension was then spread onto a TEM Cu grid (300 mesh) covered by a perforated carbon film, followed by drying under vacuum. In addition, EDX microanalyses were carried out with a Super-X EDX system, using a probe current of 240 pA and a semi-convergence angle of 10 mrad. HAADF STEM images were collected with an inner detector radius of 63.5 mrad.

For the catalysts supported in carbon the morphology was studied by Transmission Electron Microscopy (TEM), using a FEI Talos F200X equipment (Thermo Fisher Scientific). This equipment combines outstanding high-resolution S/TEM and TEM imaging with industry-leading energy dispersive X-ray spectroscopy (EDS) signal detection, and 3D chemical characterization with compositional mapping. The samples were dispersed in ethanol and a drop of the suspension was put on a Cu grid (300 mesh).

The metallic dispersion was calculated from the measurement of the size of 200 particles according to the method described by Borodziński and Bonarowska [5]. In the procedure, the atomic ratio of the particles is required. For monometallic catalysts, the atomic ratio of metallic Ni and Cu was employed. However, in the case of bimetallic catalysts, the atomic ratio was calculated based on the the assumption that the contribution of each metal to the atomic ratio is associated to the metallic content of Ni and Cu obtained by ICP-OES, as previously reported [6].

#### 4.3.7 X-ray Photoelectron Spectroscopy (XPS)

Prior to the measurements, the fresh catalysts were *ex situ* reduced at 275 °C for 1 h. Moreover, used catalysts were also characterized. The atomic ratios and the oxidation state of the surface species were studied using a VG Escalab 200R spectrometer equipped with a hemispherical electron analyser and an Al K1 ( $h = 1486.6$ ) 120 W X-ray

source. A stainless-steel sample holder was used to deposit the samples. First, the samples were degassed at 300 °C in a pretreatment chamber. The spectrometer base pressure was typically 9-10 Torr (0.0133 bar). The spectra were collected with a pass energy of 20 eV, which is usually considered a high-resolution condition.

#### 4.3.8 Elemental analysis (CHN)

Different carbons utilized as catalyst support were analysed by elemental analysis. Calibration samples were prepared as follows: 5 tin capsules were packed with 5 acetanilide test samples varying in mass. The mass of samples was chosen so as to make the absolute content of the detected elements cover all their expected concentration range in the analysed samples. Samples to be analysed were placed in tin capsules, weighed and packed carefully.

The prepared calibration and analysis samples were placed in the auto-sampler, from they were periodically tipped into a vertical quartz reactor heated at a temperature of 980 °C with a constant flow of helium stream. A few seconds before introduction, the helium stream was enriched with high purity oxygen. The combustion gas mixture was driven through a tungsten oxide zone to achieve a complete quantitative oxidation, followed by a reduction step in a copper zone to reduce nitrogen oxides to nitrogen. The resulting components N<sub>2</sub>, CO<sub>2</sub>, H<sub>2</sub>O, were separated in a chromatographic column and detected by a TCD. The resulting signals, proportional to the amount of eluted gasses, were analysed by Callidus® software, which automatically provides the sample elemental composition report.

**References**

- [1] Deraz NM. The comparative jurisprudence of catalysts preparation methods: I. precipitation and impregnation methods. *J Ind Environ Chem* 2018;2:19–21.
- [2] Du X, Kong X, Chen L. Influence of binder on catalytic performance of Ni/HZSM-5 for hydrodeoxygenation of cyclohexanone. *Catal Commun* 2014;45:109–13. <https://doi.org/10.1016/j.catcom.2013.10.042>.
- [3] Zhao Z, Lu W, Feng C, Chen X, Zhu H, Yang R, et al. Increasing the activity and selectivity of Co-based FTS catalysts supported by carbon materials for direct synthesis of clean fuels by the addition of chromium. *J Catal* 2019;370:251–64. <https://doi.org/10.1016/j.jcat.2018.12.022>.
- [4] Li Z, Liu F, Ding Y, Wang F, You H, Jin C. Preparation and properties of Cu-Ni bimetallic oxide catalyst supported on activated carbon for microwave assisted catalytic wet hydrogen peroxide oxidation for biologically pretreated coal chemical industry wastewater treatment. *Chemosphere* 2019;214:17–24. <https://doi.org/10.1016/j.chemosphere.2018.09.098>.
- [5] Borodziński A, Bonarowska M. Relation between crystallite size and dispersion on supported metal catalysts. *Langmuir* 1997;13:5613–20. <https://doi.org/10.1021/la962103u>.
- [6] Cao Y, Sui Z, Zhu Y, Zhou X, Chen D. Selective Hydrogenation of Acetylene over Pd-In/Al<sub>2</sub>O<sub>3</sub> Catalyst: Promotional Effect of Indium and Composition-Dependent Performance. *ACS Catal* 2017;7:7835–46. <https://doi.org/10.1021/acscatal.7b01745>.

## CHAPTER 5: Cu/ZrO<sub>2</sub> based heterogeneous catalysts screening

---

**Extracted from the article:** *Furanic biofuels production from biomass using Cu-based heterogeneous catalysts*

**Authors:** Nerea Viar, Jesus M. Requies, Ion Agirre, Aitziber Iriondo, Pedro L. Arias

**Journal, volume and pages:** Energy 172, 531-544

**Date of publication:** January 2019





## Table of contents

5.1 EXPERIMENTAL. ....	123
5.1.1 Catalyst preparation. ....	123
5.1.2 Catalyst characterization. ....	124
5.1.3 Activity test. ....	124
5.2 RESULTS AND DISCUSSION. ....	124
5.2.1 Optimal operating conditions. ....	124
5.2.2 Cu loading. ....	125
5.2.2.1 Characterization for CuZr catalysts. ....	125
5.2.2.2 Activity results for CuZr catalysts. ....	128
5.2.3 CeO <sub>2</sub> loading to ZrO <sub>2</sub> support. ....	129
5.2.3.1 Characterization for CuCeZr catalysts. ....	130
5.2.3.2 Activity results for CuCeZr catalysts. ....	133
5.2.4 Ru addition as active phase. ....	134
5.2.4.1 Characterization for RuCuZr catalysts. ....	134
5.2.4.2 Activity results for RuCuZr catalysts. ....	136
5.2.5 Ni addition on the active phase. ....	138
5.2.5.1 Characterization results for NiCuZr. ....	138
5.2.5.2 Activity results for NiCuZr. ....	142



The hydrogenolysis of HMF to produce DMF and/or DMTHF has been widely studied in discontinuous systems operating in liquid phase, as it has been extensively described in the state of art (see Chapter 2). However, the need of continuous systems, which are preferable to be used on an industrial scale and provide higher efficiencies and lower production costs, encouraged the development of this PhD thesis. The lack of investigations in continuous systems required an initial catalyst screening. Copper was selected as principal active phase and zirconium as support, based on previous investigations [1]. Therefore, in this chapter CuZr based catalysts were modified with noble and non-noble metals to determine the most promising combination.

## 5.1 Experimental.

### 5.1.1 Catalyst preparation.

Copper based CuZr catalysts with different metal loadings were prepared by wetness impregnation method following the procedure detailed in section 4.1.1 of Chapter 4. Additionally, the support was modified impregnating ceria employinh the same method, obtaining CeO<sub>2</sub>-ZrO<sub>2</sub>. Then, Cu was loaded to the new support by wetness impregnation, synthetizing CuCeZr catalysts.

Moreover, noble (Ru) and non-noble (Ni) active metals were loaded to CuZr catalyst. The ruthenium was synthetized by sequential impregnation. This implies a previous impregnation of Cu onto the support, followed by drying and calcination steps. Then, Ru was loaded to the monometallic CuZr catalyst following the same procedure, obtaining Ru-CuZr. Conversely, nickel was co-impregnated with copper, involving the impregnation of both metals in the same step. The synthetized catalyst was denoted as NiCuZr catalyst.

### 5.1.2 Catalyst characterization.

The physicochemical properties of the samples were analysed by N<sub>2</sub>-physisorption, Inductively Coupled Plasma Optical Emission Spectroscopy (ICP-OES), Temperature Programmed Desorption with ammonia (NH<sub>3</sub>-TPD), Temperature Programmed Reduction with hydrogen (H<sub>2</sub>-TPR), X-ray Diffraction (XRD) and X-ray Photoelectron Spectroscopy (XPS).

Detailed information about the abovementioned characterization techniques is described in section 4.3. of Chapter 4. The support was firstly treated under air at 250 °C for 2 h to be evaluated at the same conditions as the synthesized catalysts. Moreover, for those techniques at which it was not possible to reduce the catalyst *in situ*, the catalyst was previously reduced at 275 °C for 2 h at a flow of pure H<sub>2</sub>.

### 5.1.3 Activity test.

The activity tests were carried out in a continuous fixed-bed reactor, following the procedure detailed in section 4.2. of Chapter 4.

## 5.2 Results and discussion.

### 5.2.1 Optimal operating conditions.

An initial catalytic screening was carried out in order to set the most optimal operating conditions, varying the temperature, H<sub>2</sub> pressure and the need or not of the previous reduction of the catalyst. The obtained results are summarized in Table 5.1.

Consequently, the subsequent activity experiments were carried out at the following operating conditions: T = 275 °C, P = 15 bar of H<sub>2</sub>, no pretreatment (reduction) of the catalysts and a WHSV (g<sub>HMF</sub>/g<sub>cat</sub>·h) of 0.15 h<sup>-1</sup>. It seems that the catalyst was completely reduced before the beginning of the reaction, while working up to the reaction operating conditions. Thus, there was no need of a previous reduction.

**Table 5.1.** Activity results after 6 hours-on-stream at different operating conditions at WHSV = 0.15 h<sup>-1</sup>.

Catalyst	Reaction conditions			DMF (%)	DMTHF (%)
	Temperature (°C)	Pressure (bar)	Pre-reduction		
1Ru15CuZr	<b>200</b>	15	Yes	9.1	2.5
1Ru15CuZr	<b>250</b>	15	Yes	21.4	1.8
1Ru15CuZr	<b>275</b>	15	Yes	25.2	1.6
30CuZr	275	<b>15</b>	Yes	25.9	0.0
30CuZr	275	<b>20</b>	Yes	25.9	0.0
1Ru30CuZr	275	15	<b>Yes</b>	21.3	1.2
1Ru30CuZr	275	15	<b>No</b>	21.7	3.6
30CuZr	275	15	<b>Yes</b>	25.9	0.0
30CuZr	275	15	<b>No</b>	26.3	0.0

### 5.2.2 Cu loading.

Monometallic catalysts with different mass percentage (15, 30 and 45 wt %) of Cu in ZrO<sub>2</sub> were synthesized to investigate the effect of the metal content on the catalyst's activity.

#### 5.2.2.1 Characterization for CuZr catalysts.

The textural properties of the synthesized catalysts were analysed by N<sub>2</sub>-physisorption and the obtained results are summarized in Table 5.2. The bare support exhibited high BET surface area (137.6 m<sup>2</sup>/g). The addition of Cu onto the ZrO<sub>2</sub> mesoporous support caused a decrease in the specific surface area of the catalysts, possibly due to the presence of CuO species blocking the pores, decreasing the total surface area [2]. In the case of 15CuZr catalyst, some pores were obstructed, reducing the total surface area and pore volume, but increasing the average pore diameter. In 45CuZr catalyst, all the textural properties were decreased, implying large particles of Cu and low dispersion of the metal. In Table 5.2 the real metallic content of the catalysts can be observed, which was lower than the nominal one.

**Table 5.2.** Textural, chemical and acidic properties for the CuZr catalysts.

Catalyst	BET <sup>a</sup> (m <sup>2</sup> /g)	Pore volume <sup>a</sup> (cm <sup>3</sup> /g)	Average pore diameter <sup>a</sup> (nm)	Cu <sup>b</sup> (%)	Desorbed NH <sub>3</sub> <sup>c</sup> (mmol/g <sub>cat</sub> )
ZrO <sub>2</sub>	137.6	0.27	7.2	-	0.39
15CuZr	35.1	0.09	10.7	13.0	0.18
30CuZr	81.8	0.27	13.1	17.0	0.21
45CuZr	52.0	0.04	4.2	28.4	0.10

Determined by <sup>a</sup> N<sub>2</sub>-physisorption, <sup>b</sup> ICP-OES and <sup>c</sup> NH<sub>3</sub>-TPD.

The acidity of the catalysts was studied by NH<sub>3</sub>-TPD and the obtained results are summarized in Table 5.2. The calcined ZrO<sub>2</sub> support exhibited low acidity (0.39 mmol NH<sub>3</sub>/g<sub>cat</sub>). However, the amount of desorbed NH<sub>3</sub> was modified when Cu

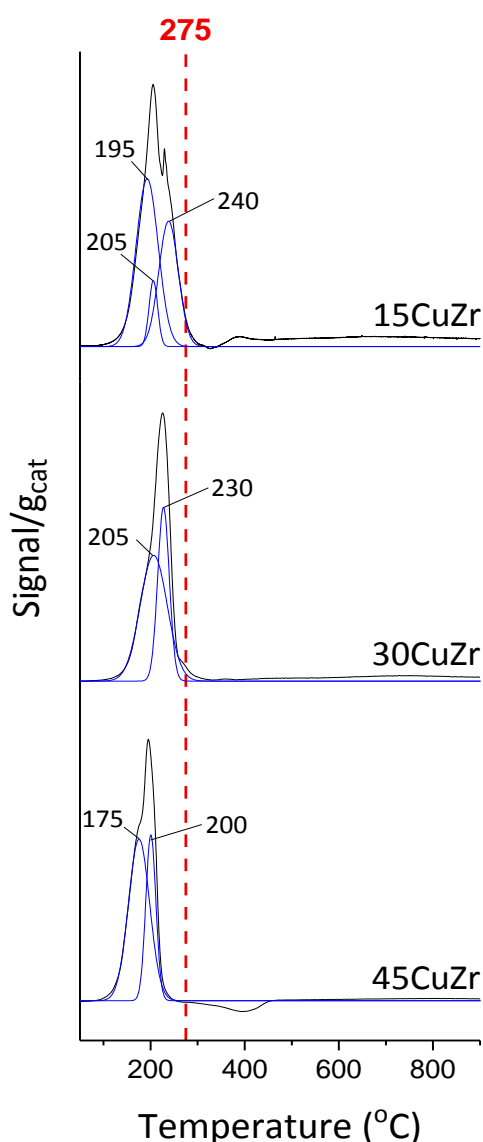


**Figure 5.1.** H<sub>2</sub>-TPR profiles for the CuZr catalysts.

was impregnated. 15CuZr and 30CuZr catalysts showed similar acidity, which was lower than the bare support. Probably, the incorporated Cu particles were partially covering some acidic sites of the support [3]. This effect was more notable when 45CuZr was analysed, possibly implying larger particles covering more acidic sites, which resulted in lower dispersion of Cu. This is in good agreement with the results obtained in textural properties.

The reducibility of the catalysts was examined by H<sub>2</sub>-TPR and the results are described in Figure 5.1. The reaction temperature (275 °C) is outlined in the plot. The calcined CuZr catalysts showed a broad reduction peak within the temperature range 130-300 °C. It has been reported that particles strongly interacting with the support exhibited higher reduction temperatures than particles interacting

weakly with the support. It should be highlighted that the reduction peaks shifted to lower temperatures when Cu amount was increased from 15 to 45 %. This fact suggested that the reducibility of the catalysts improved, and the metal-support interaction was weakened, resulting in a lower metal dispersion in the case of 45CuZr catalyst [4]. This is in good agreement with the obtained results in N<sub>2</sub>-physisorption and acidity characterization.

X-ray diffraction patterns of fresh reduced 15CuZr and 45CuZr catalysts are shown in Figure 5.2. Additionally, the crystallite size of Cu<sup>0</sup> species are specified in the plot, which were calculated by the Scherrer equation. Both catalysts exhibited typical peaks associated to amorphous tetragonal ZrO<sub>2</sub> ( $2\theta = 30.5^\circ$ ) [5,6] and metallic Cu ( $2\theta = 43.4^\circ$ ,  $50.6^\circ$  and  $74^\circ$ ) [7,8]. It can be observed that the crystallite size of 45CuZr catalyst was much larger than 15CuZr catalyst, implying a lower dispersion of Cu [9], which is in accordance with the previous characterization results.

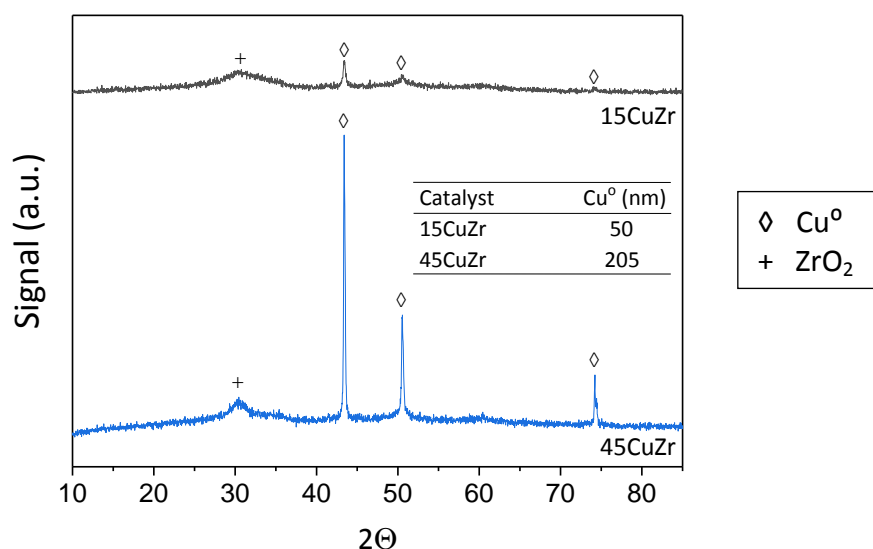


**Figure 5.2.** XRD patterns for the CuZr catalysts.

The obtained XPS results are summarized in Table 5.3. Cu<sup>0</sup>/(Cu<sup>0</sup>+Cu<sup>1+</sup>+Cu<sup>2+</sup>) ratio was calculate to identify the oxidation state of copper before and after the reaction. For this ratio calculation, different energy bands were employed. Cu2p binding energy shows a value of 934 eV for Cu<sup>2+</sup>. However, in this region it is not possible to distinguish between Cu<sup>0</sup> and Cu<sup>1+</sup>, because both of them exhibit the same binding

energy of 932 eV [10]. Therefore, *CuLMM* region was then analysed, where  $\text{Cu}^0$  and  $\text{Cu}^{1+}$  species present a peak at 335 eV and 337.5 eV [10,11], respectively.

**Table 5.3.** XPS results for the CuZr catalysts.

Catalyst	Cu/Zr		$\text{Cu}^0/(\text{Cu}^0+\text{Cu}^{1+}+\text{Cu}^{2+})$		C/Zr	
	Fresh reduced	Used	Fresh reduced	Used	Fresh reduced	Used
<b>15CuZr</b>	0.4	0.3	0.6	0.6	1.1	9.6
<b>30CuZr</b>	0.5	0.3	0.3	0.4	1.7	17.8
<b>45CuZr</b>	1.4	0.2	0.2	0.3	5.4	144.8

As it can be observed, the Cu/Zr surface atomic ratio of fresh reduced catalysts increased when higher Cu loadings were incorporated. After the activity test, a decrease of this ratio could be observed in all the catalysts, which is an indication of some sintering of the active metal or coke deposition taking place. This reduction was especially significant in the case of 45CuZr catalyst. The coke deposition was evidenced by the increase of C/Zr ratio after the reaction, remarkably for 45CuZr catalyst. Even if 15CuZr catalyst showed the lowest Cu/Zr ratio, the observed metallic content ( $\text{Cu}^0/\text{total Cu}$ ) was elevated, implying high metallic Cu content on the surface. In general, the metallic to total Cu ratio suffered a slight increase after the reaction, implying the reduction of a certain amount of Cu, which is reasonable in a  $\text{H}_2$  atmosphere.

#### 5.2.2.2 Activity results for CuZr catalysts.

The catalytic results of CuZr catalysts with different metal loadings are plotted in Figure 5.3. It can be observed that 15CuZr and 30CuZr catalysts exhibited similar behaviour, reaching a maximum yield of around 25 % after 6 h on stream. However, higher loading of Cu (45 %) implied lower dispersion of metallic species and higher coke deposition, involving the deactivation of the catalyst after 3 h on stream. Even if the acidity is an important factor in the reaction, all the Cu monometallic catalysts exhibited equivalent acidity.



The similar selectivity results obtained for 15CuZr and 30CuZr catalysts suggest that the total amount of Cu in the catalytic system not a key factor. It seems that the Cu dispersion and metallic Cu species in the catalyst surface are playing a key role in the DMF production. Taking into account the obtained results, 15 wt % of Cu loading will be considered for further studies.

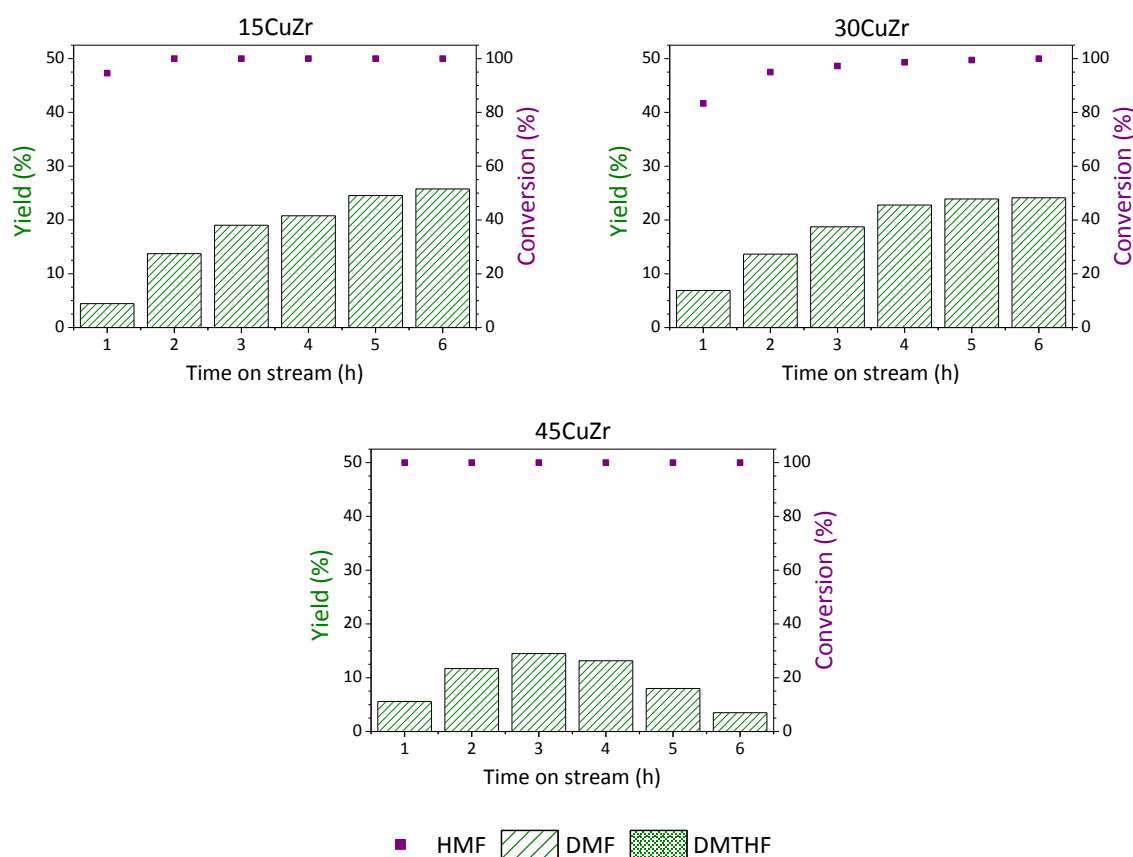


**Figure 5.3.** Activity results for the CuZr based catalysts.

### 5.2.3 CeO<sub>2</sub> loading to ZrO<sub>2</sub> support.

The aim of in this section is to study the variation of the support characteristics by loading different amounts of CeO<sub>2</sub>. It has been previously reported that CeO<sub>2</sub> can vary the acidity of ZrO<sub>2</sub> and enhance the oxygen storage capacity, which results in a higher ability to deliver oxygen to the solid (adsorbed) carbon, implying a removal of the surface solid carbon [12,13]. Thus, the support was varied by impregnating cerium

nitrate in a first step and after drying and calcining the modified support, 15 wt % of Cu was loaded, obtaining Cu/CeO<sub>2</sub>-ZrO<sub>2</sub> catalysts. The loaded ceria was 5 and 20 wt %.

### 5.2.3.1 Characterization for CuCeZr catalysts.

According to N<sub>2</sub> adsorption-desorption results shown in Table 5.4, the calcined ZrO<sub>2</sub> exhibited higher BET surface area than CeO<sub>2</sub>. The presence of ceria on ZrO<sub>2</sub> slightly reduced the surface area and pore volume due to the deposition of CeO<sub>2</sub> on the pores of the support. Nevertheless, the increment of ceria in the catalyst from 5 to 20 wt % did not alter the surface area and pore volume (taking into account that the equipment experimental error is  $\pm 3$  m<sup>2</sup>/g). However, the presence of higher amount of ceria decreased the pore diameter. Probably, the incorporation of more CeO<sub>2</sub> favoured the formation of larger ceria particles.

The addition of Cu onto CeZr support caused a decrease in the specific surface area, possibly due to the support's pore blockage by CuO particles, as explained in CuZr characterization results. This reduction was not significant in the case of 15Cu20CeZr catalyst. It seems that the presence of high ceria loadings modified the way in which Cu was incorporated on the catalytic surface.

**Table 5.4.** Textural, chemical and acidic properties for the CuCeZr catalysts.

Catalyst	BET <sup>a</sup> (m <sup>2</sup> /g)	Pore volume <sup>a</sup> (cm <sup>3</sup> /g)	Average pore diameter <sup>a</sup> (nm)	Cu <sup>b</sup> (%)	Ce <sup>b</sup> (%)	Desorbed NH <sub>3</sub> <sup>c</sup> (mmol/g <sub>cat</sub> )
ZrO <sub>2</sub>	137.6	0.27	7.2	-	-	0.39
CeO <sub>2</sub>	77.2	0.22	11.4	-	-	0.45
5CeZr	112.3	0.23	7.9	-	0.4	0.68
20CeZr	114.1	0.21	3.7	-	2.4	0.53
15CuZr	35.1	0.09	10.7	13.0	-	0.18
15Cu/5CeZr	40.8	0.07	7.2	12.6	0.6	0.32
15Cu/20CeZr	110.3	0.20	7.2	10.3	2.5	0.39

Determined by <sup>a</sup> N<sub>2</sub>-physisoption, <sup>b</sup> ICP-OES and <sup>c</sup> NH<sub>3</sub>-TPD.

The real metal content of the catalysts was determined by ICP-OES and the results are presented in Table 5.4. The real amount of ceria incorporated on the CeZr supports

was significantly inferior to the nominal one. This can be the explanation of the slight difference between the BET surface areas of ceria doped and non-doped zirconia supports. Probably, the surface of zirconium is hardly reactive with the cerium, i.e., the ZrO<sub>2</sub>-CeO<sub>2</sub> interaction is weak, and therefore the CeO<sub>2</sub> did not incorporate on ZrO<sub>2</sub> surface efficiently. These differences were also noticeable in the corresponding ceria-doped supported catalysts. Moreover, the Cu content decreased with the rise of the Ce loading.

The acidity of the supports and catalysts was examined by NH<sub>3</sub>-TPD. CeO<sub>2</sub> bare support showed higher acidity than ZrO<sub>2</sub>. Thus, the incorporation of ceria into ZrO<sub>2</sub> increased the number of acid sites. However, an increase of CeO<sub>2</sub> loading decreased the acidity.

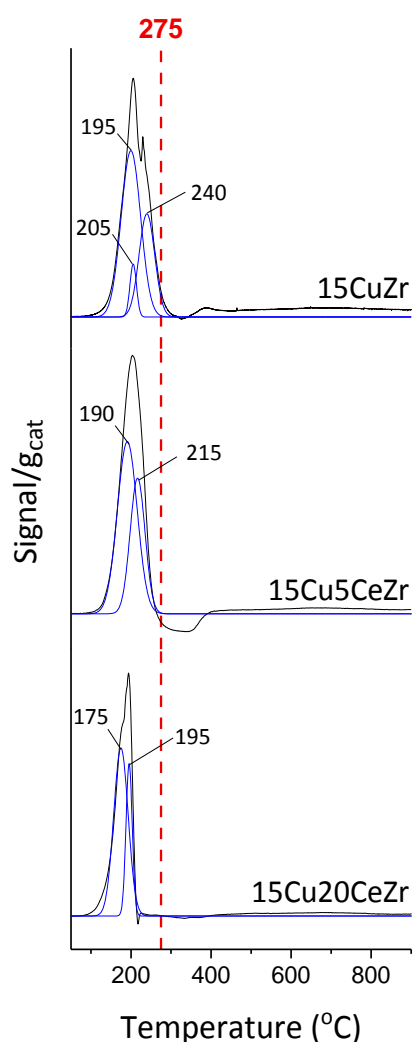


**Figure 5.4.** H<sub>2</sub>-TPR profiles for the CuCeZr catalysts.

According to literature [14], this phenomenon could be probably related to the formation of Zr—O—Ce bonds generated by the interaction between ZrO<sub>2</sub> and CeO<sub>2</sub>. The addition of Cu implied lower acidity than the corresponding supports and higher than the corresponding non-doped Ce catalysts counterparts.

Temperature programmed reduction analyses were carried out in order to evaluate the reducibility of the calcined catalysts and the obtained results are summarized in Figure 5.4. The incorporation of ceria on the support implied a slight decrease in the reduction temperature. This shift to lower temperatures was more noticeable with higher ceria loading [15]. It seems that the presence of ceria declines the metal-support interaction, favouring its reducibility at the expense of a possible decrease of metal dispersion.

The XRD patterns of fresh reduced 15CuZr and 15Cu5CeZr catalysts are shown in Figure 5.5. Peaks associated to CeO<sub>2</sub> [16,17] were not registered, possibly due to the low loading and high dispersion, which generated small crystals that could not be detected by XRD. It is also important to remark that the average crystallite size of Cu<sup>0</sup> increased when CeO<sub>2</sub> was used as ZrO<sub>2</sub> modifier. This agglomeration phenomenon could be related to the reduction of metal-support interaction caused by CeO<sub>2</sub> addition, as H<sub>2</sub>-TPR results suggested.

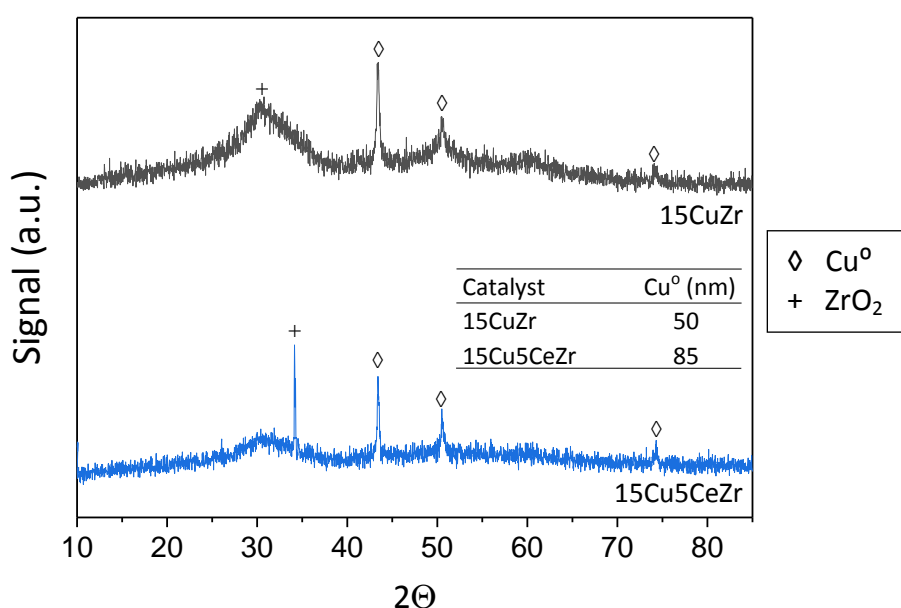


Figure 5.5. XRD patterns for the CuCeZr catalysts.

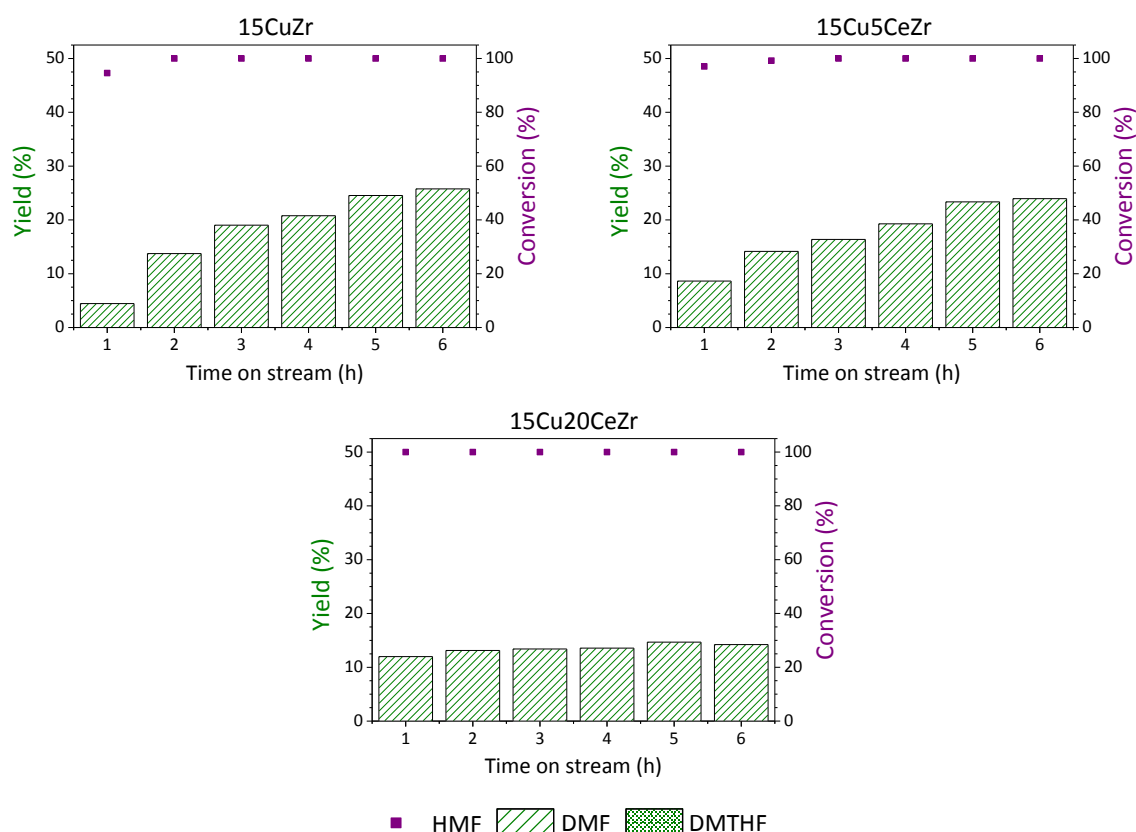
The surface atomic ratios and Cu species ratio obtained by XPS results are presented in Table 5.5. The CeO<sub>2</sub> incorporation did not strongly alter the Cu/Zr ratio of the catalysts. However, it seems that higher Cu<sup>0</sup> surface content was achieved in absence of ceria.

Table 5.5. XPS results for the CuCeZr catalysts.

Catalyst	Cu/Zr		Cu <sup>0</sup> / (Cu <sup>0</sup> +Cu <sup>1+</sup> +Cu <sup>2+</sup> )		Ce/Zr		C/Zr	
	Fresh reduced	Used	Fresh reduced	Used	Fresh reduced	Used	Fresh reduced	Used
15CuZr	0.4	0.3	0.6	0.6	-	-	1.1	9.6
15Cu5CeZr	0.5	0.2	0.3	0.3	< 0.005	< 0.005	4.0	16.5
15Cu20CeZr	0.3	0.3	0.4	0.4	< 0.005	< 0.005	1.7	4.5

The metallic content remained stable after the reaction. All the samples exhibited an increase in the C/Zr ratio, presumably due to coke formation. It is important to remark that high CeO<sub>2</sub> content limited the coke production [18]. Lastly, not noticeable content of Ce was observed in the catalytic surface, which is in good agreement with ICP-OES and XRD results, where the cerium content was very low.

### 5.2.3.2 Activity results for CuCeZr catalysts.



**Figure 5.6.** Activity results for the CuCeZr catalysts.

The activity results of CeO<sub>2</sub>-ZrO<sub>2</sub> based catalysts are summarized in Figure 5.6. It can be observed that the addition of ceria did not enhance the production of desired products. It is important to remark that the real Ce amount was lower than the nominal one. The good behaviour registered for the 15CuZr catalyst, could be due to two reasons: i) a better metal dispersion (see Figure 5.5), favoured by stronger metal-support interaction observed by H<sub>2</sub>-TPR, and ii) its low acidity, which reduced the C—C cleavage, avoiding ring opening products. The expected effect of cerium did

not improve the DMF yield. Therefore, bare  $\text{ZrO}_2$  was selected as support for the following sections.

### 5.2.4 Ru addition as active phase.

Ruthenium is a widely used noble metal for heterogeneous catalytic hydrogenation [19] and particularly for HMF hydrogenolysis [20]. In order to improve the catalytic activity of the most stable catalyst, 15CuZr, Ru was added in a second impregnation, obtaining Ru-Cu/ $\text{ZrO}_2$  catalyst. To examine the effect of Ru in the reaction, 1RuZr catalyst was also synthesized and tested.

#### 5.2.4.1 Characterization for RuCuZr catalysts.

The obtained results by  $\text{N}_2$ -physisorption are summarized in Table 5.6. As expected, the incorporation of metals decreased the surface area, probably due to the partial blocking of the pores [21]. 15CuZr catalyst exhibited much lower surface area and pore volume than 1RuZr catalyst, owing to the higher Cu metal loading [22]. However, monometallic Ru catalyst exhibited higher pore volume than the support, probably due to the obstruction of smaller pores, increasing the total pore volume. Lastly, adding Ru to monometallic 15CuZr catalyst implied a reduction on the surface area and pore volume, but the average pore diameter was enlarged. The pores with narrow diameter were possibly covered by metallic particles, increasing the average pore diameter.

**Table 5.6.** Textural, chemical and acidic properties for the RuCuZr catalysts

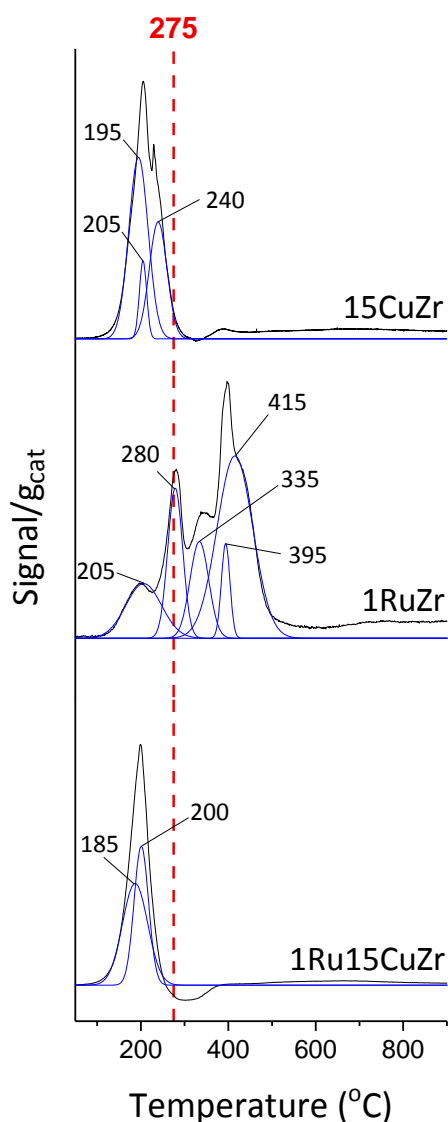
Catalyst	BET <sup>a</sup> ( $\text{m}^2/\text{g}$ )	Pore volume <sup>a</sup> ( $\text{cm}^3/\text{g}$ )	Average pore diameter <sup>a</sup> (nm)	Cu <sup>b</sup> (%)	Ru <sup>b</sup> (%)	Desorbed $\text{NH}_3$ <sup>c</sup> ( $\text{mmol}/\text{g}_{\text{cat}}$ )
<b>ZrO<sub>2</sub></b>	137.6	0.27	7.2	-	-	0.39
<b>15CuZr</b>	35.1	0.09	10.7	13.0	-	0.18
<b>1RuZr</b>	89.3	0.40	18.0	-	0.06	1.24
<b>1Ru15CuZr</b>	22.0	0.07	12.1	10.9	0.26	0.20

Determined by <sup>a</sup>  $\text{N}_2$ -physisorption, <sup>b</sup> ICP-OES and <sup>c</sup>  $\text{NH}_3$ -TPD.

The real metallic content was analysed by ICP-OES and the results are summarized in Table 5.6. The real ruthenium content was much lower than the nominal one, particularly in monometallic 1RuZr catalyst. It seems that copper enhanced the ruthenium deposition on the catalyst, implying higher Ru content in the bimetallic catalyst.

The number of acidic sites was significantly increased when Ru was loaded to the support. Dasireddy et al. [23] suggested that high acidity could be associated with high dispersion of the metal species. However, the acid strength remained almost constant

when a low amount of Ru was added to the CuZr catalysts.



H<sub>2</sub>-TPR profiles of monometallic and bimetallic RuCuZr catalysts are plotted in Figure 5.7. Regarding 1RuZr catalyst, it showed a H<sub>2</sub>-TPR pattern with a broad reduction peak detected within the temperature range of 100-560 °C. The deconvolution of the aforementioned peak suggests a contribution of five peaks centred at 205, 280, 335, 395 and 415 °C. According to the literature [24], the peak centred at 205 °C could be ascribed to the reduction of bulk RuO<sub>2</sub> to Ru<sup>0</sup> [25], while the peaks registered at temperatures above 230 °C might be associated to the reduction of oxidized Ru species strongly interacting with the support. These reduction temperatures suggest that the low amount of Ru incorporated species were highly dispersed. This last fact corroborates the similar conclusion reached while interpreting the NH<sub>3</sub>-TPD results.

**Figure 5.7.** H<sub>2</sub>-TPR profiles for the RuCuZr catalysts.

The H<sub>2</sub>-TPR profile of bimetallic 1Ru15CuZr catalyst is similar to the obtained one for its monometallic counterpart (15CuZr). A reduction temperature decrease of around 20-40 °C was the most important difference observed in the H<sub>2</sub>-TPR profile of bimetallic catalyst [26]. This behaviour indicated that the presence of Ru in the catalyst improved the reducibility of the Cu species.

The surface composition and oxidation state of different catalysts were examined by XPS and the results are presented in Table 5.7. The addition of Ru involved higher Cu/Zr ratio at the beginning of the reaction, apparently improving the dispersion of copper. However, the Cu<sup>0</sup> content of the fresh reduced catalyst was not enriched. After the reaction, the Cu/Zr ratio of the bimetallic catalyst decreased considerably. Contrary to what it was expected, Ru did not avoid the coke deposition on the catalyst, furthermore, it enhanced the C/Zr ratio after the reaction. Coke was probably covering Cu particles, implying the reduction of Cu/Zr ratio. Moreover, sintering of copper could be also a reason of the decrease of this ratio. Lastly, the ruthenium surface exposition was higher in the bimetallic RuCuZr catalyst, which is in good agreement with the ICP-OES results.

**Table 5.7.** XPS results for the RuCuZr catalysts.

Catalyst	Cu/Zr		Cu <sup>0</sup> / (Cu <sup>0</sup> +Cu <sup>1+</sup> +Cu <sup>2+</sup> )		Ru/Zr		C/Zr	
	Fresh reduced	Used	Fresh reduced	Used	Fresh reduced	Used	Fresh reduced	Used
<b>15CuZr</b>	0.4	0.3	0.6	0.6	-	-	1.1	9.6
<b>1RuZr</b>	-	-	-	-	0.08	0.85	1.2	14.6
<b>1Ru15CuZr</b>	1.3	0.2	0.3	0.4	0.4	1.5	7.1	22.6

#### 5.2.4.2 Activity results for RuCuZr catalysts.

The activity results of RuCuZr catalysts are summarized in Figure 5.8. 1RuZr catalyst presented a total conversion of HMF but very low or negligible DMF or DMTHF yields. This means that the presence of Ru implied another reaction path than the HMF hydrogenolysis. The monometallic Ru catalyst probably broke preferentially the C—C bond instead of the C—O bond, which resulted in degradation products [25]. The 1RuZr catalyst was the catalyst with the highest acidity. This characteristic favours the



C—C bond cleavage of the HMF molecule and therefore, the presence of acid sites could cause the degradation or loss of one of the radicals present in the HMF molecule. This strong acidity could also explain the total HMF conversion and the negligible DMF and DMTHF yields.

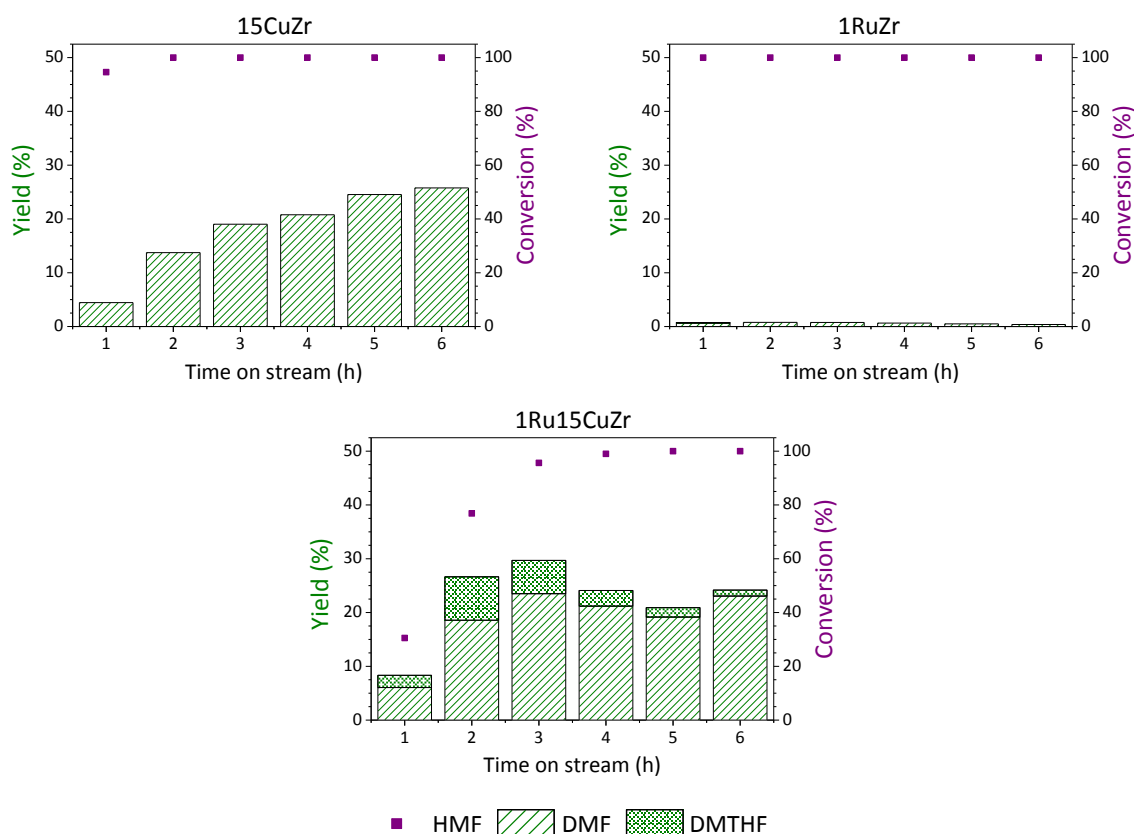


**Figure 5.8.** Activity results for the RuCuZr based catalysts.

The impregnation of Ru in CuZr catalyst implied the production of DMTHF, probably due to the valuable hydrogenation capacity of ruthenium [19]. This noble metal was able to hydrogenate the furanic ring, producing DMTHF from DMF. However, a decrease of the total yield after 3-4 h time on stream could be detected. It seems that the ruthenium is capable of slightly improving the catalytic production of desired products at the beginning of the reaction, probably due to the better dispersion of Cu observed in XPS results and better reducibility of this catalyst. Nonetheless, it suffered from high deactivation problems, observed in the low Cu/Zr ratio and high C/Zr ratio after reaction. Probably, the presence of Ru weakened the Cu-Zr interaction (see H<sub>2</sub>-TPR results), favouring the Cu sintering observed in XPS. Moreover, the coke deposition was also an important cause of deactivation. On this basis, the addition of

Ru did not improve the catalytic activity of the catalyst. Therefore, monometallic 15CuZr catalyst was selected for further studies.

### 5.2.5 Ni addition on the active phase.

Pandhare et al. [27] investigated a bimetallic nickel and copper catalyst supported on alumina in the hydrogenolysis of glycerol. They concluded that the interaction of the metals enhanced the hydrogenolysis of C—O bond and limited the cleavage of C—C, avoiding non desired products. Consequently, 15Ni15CuZr bimetallic catalyst was prepared by coimpregnation method, meaning that both metals were impregnated in the same step. Monometallic 15NiZr catalyst was also synthesized to understand the effect of this metal on the hydrogenolysis of HMF.

#### 5.2.5.1 Characterization results for NiCuZr.

Textural, chemical and acidic properties of CuNi based support and catalysts are summarized in Table 5.8. 15NiZr catalyst showed smaller surface area than 15CuZr catalyst, which can be attributed to the pores blockage by the metallic Ni clusters present on the surface. This can be associated with the low dispersion of the metal [27]. Meanwhile, in the case of the Cu monometallic catalyst, the metal species were more dispersed in the support. In the case of 15Ni15CuZr catalyst, the surface area and pore volume were decreased compared to monometallic 15CuZr catalyst, probably due to the higher metal loading of the bimetallic catalyst.

**Table 5.8.** Textural, chemical and acidic properties for the NiCuZr catalysts.

Catalyst	BET <sup>a</sup> (m <sup>2</sup> /g)	Pore volume <sup>a</sup> (cm <sup>3</sup> /g)	Average pore diameter <sup>a</sup> (nm)	Cu <sup>b</sup> (%)	Ni <sup>b</sup> (%)	Desorbed NH <sub>3</sub> <sup>c</sup> (mmol/g <sub>cat</sub> )
ZrO <sub>2</sub>	137.6	0.27	7.2	-	-	0.39
15CuZr	35.1	0.09	10.7	13.0	-	0.18
15NiZr	5.0	0.03	25.3	-	10.8	1.09
15Ni15CuZr	18.1	0.03	7.7	12.4	13.2	0.35

Determined by <sup>a</sup> N<sub>2</sub>-physisoption, <sup>b</sup> ICP-OES and <sup>c</sup> NH<sub>3</sub>-TPD.

Regarding the metal loading of the catalysts, the experimental value was found to be lower than the nominal content. This difference was higher in the case of 15NiZr catalyst, implying the better impregnation of Cu than Ni on ZrO<sub>2</sub> in the case of monometallic catalysts. In the case of bimetallic catalyst, Cu content was almost identical to the content on monometallic catalyst, but Ni content was increased. It seems that copper improved the impregnation of nickel.

The acidic properties were studied by NH<sub>3</sub>-TPD (see Table 5.8). The acidity was decreased when Cu was loaded onto the support. The incorporated Cu particles could be partially covering acid sites on the support, thus decreasing the catalyst's total

acidity [28,29]. However, the addition of Ni considerably increased this acidity. It seems that the high acidity was related to the presence of Lewis acid sites associated with the presence of Ni<sup>2+</sup> [30]. The acidity calculated for the bimetallic catalyst was slightly lower than that of the support, probably due to a combination of the reasons explained above for monometallic catalysts.

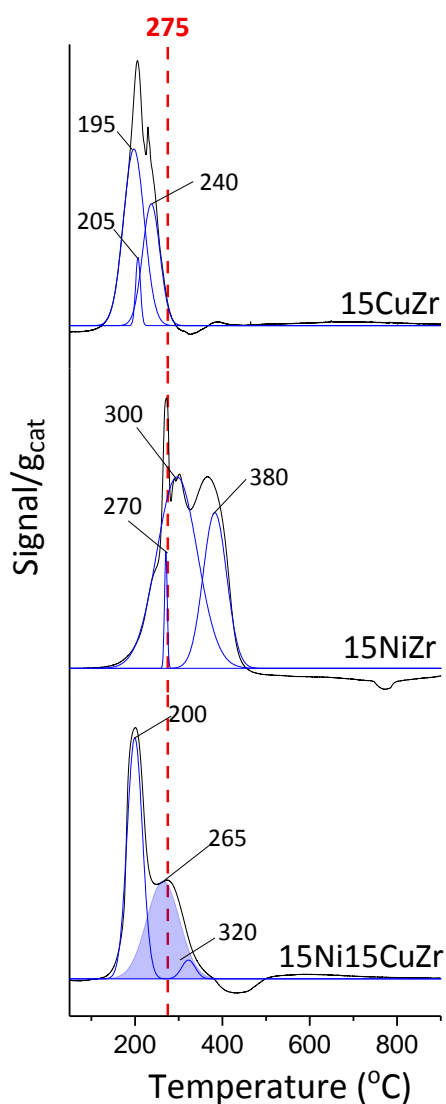


**Figure 5.9.** H<sub>2</sub>-TPR profiles for the NiCuZr catalysts.

The H<sub>2</sub>-TPR profiles and their deconvolution for the monometallic and bimetallic catalysts are summarized in Figure 5.9. The monometallic Cu and Ni catalysts recorded three different peaks. 15NiZr catalyst registered reduction peaks at 270, 300 and 380 °C, involving the need of higher temperatures for the complete reduction of nickel. This implied the formation of Ni<sup>2+</sup> species at lower temperatures, which is in good agreement with the acidity results, where high acidity was related to the presence

of  $\text{Ni}^{2+}$ . This species could be acting as Lewis acid sites. Reports in literature indicate that highly dispersed particles and those particles interacting weakly with the support recorded lower reduction temperatures. In contrast, bulk NiO or CuO and particles interacting strongly with the support registered higher reduction temperatures.

Similarly, the  $\text{H}_2$ -TPR profile of bimetallic catalyst can also be deconvoluted into three reduction peaks. When compared to the monometallic 15NiZr catalyst, all the peaks were shifted to lower temperatures. This observation seems to indicate that Cu facilitated the reducibility of Ni [31–33]. According to the literature [34], the first peak (200 °C) is related to the reduction of the  $\text{Cu}^{2+}$  species, and the last peak (320 °C) is related to  $\text{Ni}^{2+}$  reduction, while the intermediate peak (265 °C, in blue) could be associated with the reduction of Ni-Cu species. These results evidenced an interaction between Ni and Cu.

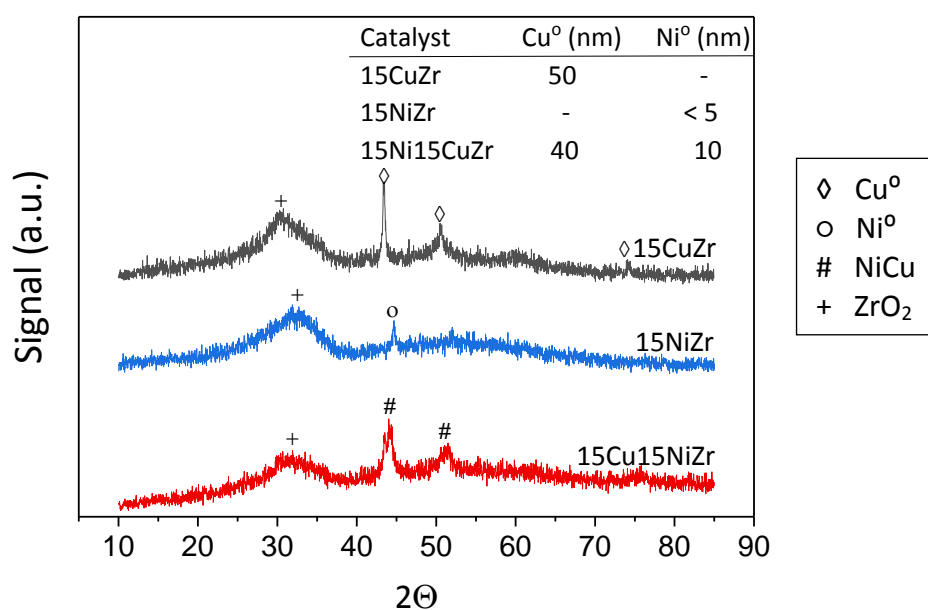


**Figure 5.10.** XRD patterns for the NiCuZr catalysts.

The obtained X-ray diffraction patterns are plotted in Figure 5.10. The monometallic Cu catalyst registered defined peaks associated with metallic Cu crystallites with a size of 50 nm. Conversely, a barely noticeable peak could be discerned in the XRD pattern for the fresh reduced 15NiZr catalyst, which could be ascribed to an amorphous structure. In the case of 15Ni15CuZr catalyst, a double-peak was registered at two different positions at around  $2\theta = 44^\circ$  and  $51^\circ$ . The most intense peak could be deconvoluted

into two peaks, at  $2\theta = 43.7^\circ$  and  $44.1^\circ$ , which are reflection angles between the registered diffraction peaks of pure Cu<sup>0</sup> ( $2\theta = 43.4^\circ$ ) and Ni<sup>0</sup> ( $2\theta = 44.7^\circ$ ), which involved an interaction between both metals [7], as observed in H<sub>2</sub>-TPR results. It can be noticed that the crystallite size of the phase richer in Cu was decreased to 40 nm, comparing with 15CuZr catalyst. Presumably, Ni enhanced the dispersion of Cu, reducing its crystallite size in the bimetallic catalyst.

**Table 5.9.** XPS results for the NiCuZr catalysts.

Catalyst	Cu/Zr		Cu <sup>0</sup> / (Cu <sup>0</sup> +Cu <sup>1+</sup> +Cu <sup>2+</sup> )		Ni/Zr		Ni <sup>0</sup> / (Ni <sup>0</sup> +Ni <sup>2+</sup> )		C/Zr	
	Fresh reduc	Used	Fresh reduc	Used	Fresh reduc	Used	Fresh reduc	Used	Fresh reduc	Used
<b>15CuZr</b>	0.4	0.3	0.6	0.6	-	-	-	-	1.1	9.6
<b>15NiZr</b>	-	-	-	-	0.2	0.1	0.2	0.3	5.0	20.7
<b>15Ni15CuZr</b>	1.6	0.5	0.3	0.5	1.4	1.3	0.3	0.2	7.2	6.7

The oxidation state of the species formed after the catalyst preparation and their atomic ratios were studied by XPS for fresh reduced and used catalysts. The results are summarized in Table 5.9. The monometallic Cu catalyst recorded a higher metal-to-Zr ratio than 15NiZr catalyst, suggesting that a higher amount of surface metal was available in the 15CuZr catalyst, probably implying a better dispersion of Cu on ZrO<sub>2</sub>, as deduced in textural properties results. Moreover, the 15CuZr catalyst recorded a slight decrease in the Cu/Zr ratio after being used in the reaction, presumably owing to the coke deposition on the active sites and/or metal sintering. Coke formation was confirmed by the C/Zr ratio, which was increased after the reaction for all the prepared catalysts. In the case of monometallic Ni catalyst, the decrease in the metal-to-support ratio (probably caused by sintering of Ni particles) and the increase in the C/Zr ratio after hydrogenolysis were more notable. It is important to note the low Ni<sup>0</sup> content in the fresh reduced 15NiZr catalyst, which was consistent with the H<sub>2</sub>-TPR results, where high reduction temperature was observed. Coke deposition can also be associated with the high acidity [35] ascribed to the presence of Ni<sup>2+</sup> Lewis acid sites.

The bimetallic catalyst showed higher metal-to-support ratio of Ni and Cu, comparing to the respective monometallic catalysts. It seems that the interaction of both metals

favoured their exposition on the catalyst's support. Lastly, the C/Zr ratio of the used bimetallic catalyst was high, implying coke deposition on the active sites.

### 5.2.5.2 Activity results for NiCuZr.

The activity results obtained for NiCuZr based catalysts are summarized in Figure 5.11. 15CuZr catalyst underwent a complete HMF conversion, whereas the monometallic Ni catalyst recorded a conversion over 90 %. The monometallic Cu catalyst reached a DMF yield of approximately 30 % and was found to be stable after 6 h on stream. In contrast, 15NiZr catalyst achieved a maximum yield of 20 % after 4 h time on stream but decreased after this time. In both cases no DMTHF was detected. The better performance of 15CuZr catalyst could be related to its greater BET area and its better reducibility providing a higher HMF conversion and DMF yield. Moreover, the higher acidity of 15NiZr catalyst could be favouring C—C cleavage [36], producing ring-opening products. The deactivation of this catalyst could be caused by coke

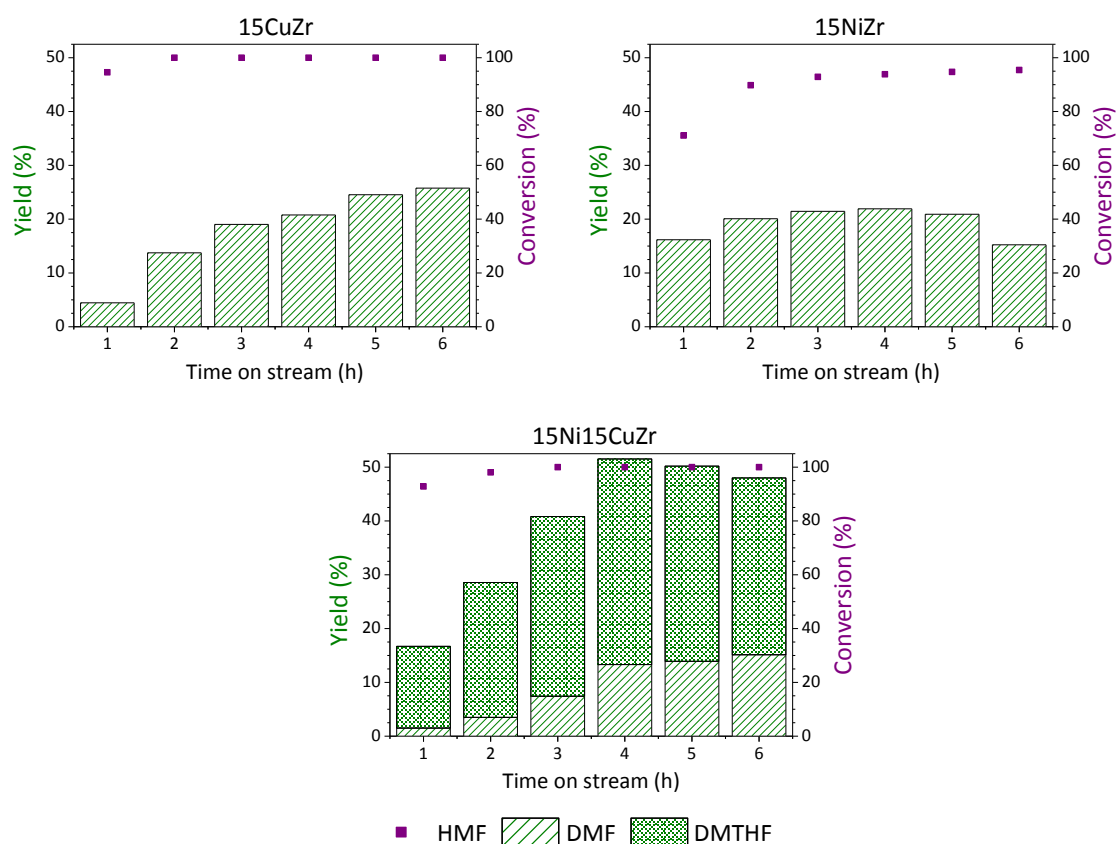


**Figure 5.11.** Activity results for NiCuZr catalysts.

deposition on the active sites and/or by possible particle sintering (determined by XPS).

The activity results of bimetallic catalyst revealed a high yield of over-hydrogenated DMTHF product. The maximum yield was achieved after 4 h of reaction, with a total yield of DMF and DMTHF over 50 %. The good performance of this catalyst can be attributed to the interaction between Cu and Ni metals, as observed in the XRD and H<sub>2</sub>-TPR results. This is in accordance with the literature [3], where Ni-Cu phases were exhibited as extremely active for hydrogenolysis reactions.

In view of the obtained results, a deeper understanding of NiCuZr catalysts will be carried out in the following chapter, considering that the interaction between Ni and Cu could be probably enhancing the production of desired products.

**References**

- [1] Iriondo A, Mendiguren A, Güemez MB, Requies J, Cambra JF. 2,5-DMF production through hydrogenation of real and synthetic 5-HMF over transition metal catalysts supported on carriers with different nature. *Catal Today* 2017;279:286–95. <https://doi.org/10.1016/j.cattod.2016.02.019>.
- [2] Jampa S, Jamieson AM, Chaisuwan T, Luengnaruemitchai A, Wongkasemjit S. Achievement of hydrogen production from autothermal steam reforming of methanol over Cu-loaded mesoporous CeO<sub>2</sub> and Cu-loaded mesoporous CeO<sub>2</sub>–ZrO<sub>2</sub> catalysts. *Int J Hydrogen Energy* 2017;42:15073–84. <https://doi.org/10.1016/j.ijhydene.2017.05.022>.
- [3] Freitas IC, Manfro RL, Souza MMVM. Hydrogenolysis of glycerol to propylene glycol in continuous system without hydrogen addition over Cu-Ni catalysts. *Appl Catal B Environ* 2018;220:31–41. <https://doi.org/10.1016/j.apcatb.2017.08.030>.
- [4] Aguila G, Valenzuela A, Guerrero S, Araya P. WGS activity of a novel Cu-ZrO<sub>2</sub> catalyst prepared by a reflux method. Comparison with a conventional impregnation method. *Catal Commun* 2013;39:82–5. <https://doi.org/10.1016/j.catcom.2013.05.007>.
- [5] Witoon T, Chalorngtham J, Dumrongbunditkul P, Chareonpanich M, Limtrakul J. CO<sub>2</sub> hydrogenation to methanol over Cu/ZrO<sub>2</sub> catalysts: Effects of zirconia phases. *Chem Eng J* 2016;293:327–36. <https://doi.org/10.1016/j.cej.2016.02.069>.
- [6] Patankar SC, Yadav GD. Cascade Engineered Synthesis of γ-Valerolactone, 1,4-Pentanediol, and 2-Methyltetrahydrofuran from Levulinic Acid Using Pd-Cu/ZrO<sub>2</sub> Catalyst in Water as Solvent. *ACS Sustain Chem Eng* 2015;3:2619–30. <https://doi.org/10.1021/acssuschemeng.5b00763>.
- [7] Obregon I, Gandarias I, Miletic N, Ocio A, Arias PL. One-Pot 2-Methyltetrahydrofuran Production from Levulinic Acid in Green Solvents Using



- Ni-Cu/Al<sub>2</sub>O<sub>3</sub> Catalysts. ChemSusChem 2015;8:3483–8.  
<https://doi.org/10.1002/cssc.201500671>.
- [8] Freitas IC, Damyanova S, Oliveira DC, Marques CMP, Bueno JMC. Effect of Cu content on the surface and catalytic properties of Cu/ZrO<sub>2</sub> catalyst for ethanol dehydrogenation. J Mol Catal A Chem 2014;381:26–37.  
<https://doi.org/10.1016/j.molcata.2013.09.038>.
- [9] Chen C, Ruan C, Zhan Y, Lin X, Zheng Q, Wei K. The significant role of oxygen vacancy in Cu/ZrO<sub>2</sub> catalyst for enhancing water-gas-shift performance. Int J Hydrogen Energy 2014;39:317–24.  
<https://doi.org/10.1016/j.ijhydene.2013.10.074>.
- [10] Tajima S, Tsuchiya S, Matsumori M, Nakatsuka S, Ichiki T. Reduction of Copper Oxide Films by an Atmospheric-Pressure Inductively Coupled Plasma Microjet. Trans Mater Res Soc Japan 2010;35 [3]:621–5.
- [11] Zhao S, Yue H, Zhao Y, Wang B, Geng Y, Lv J, et al. Chemoselective synthesis of ethanol via hydrogenation of dimethyl oxalate on Cu/SiO<sub>2</sub>: Enhanced stability with boron dopant. J Catal 2013;297:142–50.  
<https://doi.org/10.1016/j.jcat.2012.10.004>.
- [12] Wolfbeisser A, Sophiphun O, Bernardi J, Wittayakun J, Föttinger K, Rupprechter G. Methane dry reforming over ceria-zirconia supported Ni catalysts. Catal Today 2016;277:234–45. <https://doi.org/10.1016/j.cattod.2016.04.025>.
- [13] Momayez F, Towfighi Darian J, Teimouri Sendesi SM. Synthesis of zirconium and cerium over HZSM-5 catalysts for light olefins production from naphtha. J Anal Appl Pyrolysis 2015;112:135–40. <https://doi.org/10.1016/j.jaap.2015.02.006>.
- [14] Khaodee W, Tangchupong N, Jongsomjit B, Praserttham P, Assabumrungrat S. A study on isosynthesis via CO hydrogenation over ZrO<sub>2</sub>-CeO<sub>2</sub> mixed oxide catalysts. Catal Commun 2009;10:494–501.  
<https://doi.org/10.1016/j.catcom.2008.10.017>.

- [15] Chen Y, Liu D, Yang L, Meng M, Zhang J, Zheng L, et al. Ternary composite oxide catalysts CuO/Co<sub>3</sub>O<sub>4</sub>-CeO<sub>2</sub> with wide temperature-window for the preferential oxidation of CO in H<sub>2</sub>-rich stream. *Chem Eng J* 2013;234:88–98. <https://doi.org/10.1016/j.cej.2013.08.063>.
- [16] Iriondo A, Barrio VL, Cambra JF, Arias PL, Guemez MB, Sanchez-Sanchez MC, et al. Glycerol steam reforming over Ni catalysts supported on ceria and ceria-promoted alumina. *Int J Hydrogen Energy* 2010;35:11622–33. <https://doi.org/10.1016/j.ijhydene.2010.05.105>.
- [17] Gutiérrez-Ortiz JI, De Rivas B, López-Fonseca R, González-Velasco JR. Characterization of the catalytic properties of ceria-zirconia mixed oxides by temperature-programmed techniques. *J Therm Anal Calorim* 2005;80:225–8. <https://doi.org/10.1007/s10973-005-0640-7>.
- [18] Bizkarra K, Barrio VL, Yartu A, Requies J, Arias PL, Cambra JF. Hydrogen production from n-butanol over alumina and modified alumina nickel catalysts. *Int J Hydrogen Energy* 2015;40:5272–80. <https://doi.org/10.1016/j.ijhydene.2015.01.055>.
- [19] Nerozzi F. Heterogeneous Catalytic Hydrogenation. *Platin Met Rev* 2012;56:236–41. <https://doi.org/10.1595/147106712X654187>.
- [20] Hu L, Tang X, Xu J, Wu Z, Lin L, Liu S. Selective transformation of 5-hydroxymethylfurfural into the liquid fuel 2,5-dimethylfuran over carbon-supported ruthenium. *Ind Eng Chem Res* 2014;53:3056–64. <https://doi.org/10.1021/ie404441a>.
- [21] Zhang W, Duan S, Zhang Y. Enhanced selectivity in the conversion of acrolein to 3-picolone over bimetallic catalyst 4.6%Cu–1.0%Ru/HZSM-5 (38) with hydrogen as carrier gas. *React Kinet Mech Catal* 2019;127:391–411. <https://doi.org/10.1007/s11144-019-01558-0>.
- [22] Wu Z, Mao Y, Wang X, Zhang M. Preparation of a Cu–Ru/carbon nanotube catalyst for hydrogenolysis of glycerol to 1,2-propanediol via hydrogen spillover.

- Green Chem 2011;13:1311–6. <https://doi.org/10.1039/c0gc00809e>.
- [23] Dasireddy VDBC, Likoza B. CO<sub>x</sub>-free hydrogen generation via decomposition of ammonia over copper and zinc-based catalysts. *Fuel* 2017;196:325–35. <https://doi.org/10.1016/j.fuel.2017.01.117>.
- [24] Li D, Li R, Lu M, Lin X, Zhan Y, Jiang L. Carbon dioxide reforming of methane over Ru catalysts supported on Mg-Al oxides: A highly dispersed and stable Ru/Mg(Al)O catalyst. *Appl Catal B Environ* 2017;200:566–77. <https://doi.org/10.1016/j.apcatb.2016.07.050>.
- [25] Soares AVH, Salazar JB, Falcone DD, Vasconcellos FA, Davis RJ, Passos FB. A study of glycerol hydrogenolysis over Ru-Cu/Al<sub>2</sub>O<sub>3</sub> and Ru-Cu/ZrO<sub>2</sub> catalysts. *J Mol Catal A Chem* 2016;415:27–36. <https://doi.org/10.1016/j.molcata.2016.01.027>.
- [26] Xia S, Zheng L, Nie R, Chen P, Lou H, Hou Z. Trivalent metal ions M<sup>3+</sup> in M<sub>0.02</sub>Cu<sub>0.4</sub>Mg<sub>5.6</sub>Al<sub>1.98</sub>(OH)<sub>16</sub>CO<sub>3</sub> layered double hydroxide as catalyst precursors for the hydrogenolysis of glycerol. *Cuihua Xuebao/Chinese J Catal* 2013;34:986–92. [https://doi.org/10.1016/s1872-2067\(11\)60505-6](https://doi.org/10.1016/s1872-2067(11)60505-6).
- [27] Pandhare NN, Pudi SM, Biswas P, Sinha S. Vapor phase hydrogenolysis of glycerol to 1,2-propanediol over  $\gamma$ -Al<sub>2</sub>O<sub>3</sub> supported copper or nickel monometallic and copper-nickel bimetallic catalysts. *J Taiwan Inst Chem Eng* 2016;61:90–6. <https://doi.org/10.1016/j.jtice.2015.12.028>.
- [28] Fu Z, Wang Z, Lin W, Song W, Li S. High efficient conversion of furfural to 2-methylfuran over Ni-Cu/Al<sub>2</sub>O<sub>3</sub> catalyst with formic acid as a hydrogen donor. *Appl Catal A Gen* 2017;547:248–55. <https://doi.org/10.1016/j.apcata.2017.09.011>.
- [29] Yang Z, Liu Y, Liu D, Meng X, Liu C. Hydroisomerization of n-octane over bimetallic Ni-Cu/SAPO-11 catalysts. *Appl Catal A Gen* 2017;543:274–82. <https://doi.org/10.1016/j.apcata.2017.06.028>.

- [30] Li JW, Li T, Ma HF, Sun QW, Ying WY, Fang DY. Effect of nickel on phosphorus modified HZSM-5 in catalytic cracking of butene and pentene. *Fuel Process Technol* 2017;159:31–7. <https://doi.org/10.1016/j.fuproc.2016.06.034>.
- [31] Yoshida R, Sun D, Yamada Y, Sato S, Hutchings GJ. Vapor-phase hydrogenation of levulinic acid to  $\gamma$ -valerolactone over Cu-Ni bimetallic catalysts. *Catal Commun* 2017;97:79–82. <https://doi.org/10.1016/j.catcom.2017.04.018>.
- [32] Cai F, Pan D, Ibrahim JJ, Zhang J, Xiao G. Hydrogenolysis of glycerol over supported bimetallic Ni/Cu catalysts with and without external hydrogen addition in a fixed-bed flow reactor. *Appl Catal A Gen* 2018;564:172–82. <https://doi.org/10.1016/j.apcata.2018.07.029>.
- [33] López P, Mondragón-Galicia G, Espinosa-Pesqueira ME, Mendoza-Anaya D, Fernández ME, Gómez-Cortés A, et al. Hydrogen production from oxidative steam reforming of methanol: Effect of the Cu and Ni impregnation on ZrO<sub>2</sub> and their molecular simulation studies. *Int J Hydrogen Energy* 2012;37:9018–27. <https://doi.org/10.1016/j.ijhydene.2012.02.105>.
- [34] Khzouz M, Gkanas EI, Du S, Wood J. Catalytic performance of Ni-Cu/Al<sub>2</sub>O<sub>3</sub> for effective syngas production by methanol steam reforming. *Fuel* 2018;232:672–83. <https://doi.org/10.1016/j.fuel.2018.06.025>.
- [35] Jiao Y, Zhang H, Li S, Guo C, Yao P, Wang J. Impact of acidity in ZrO<sub>2</sub>-TiO<sub>2</sub>-Al<sub>2</sub>O<sub>3</sub> composite oxides on the catalytic activity and coking behaviors during n-decane cracking. *Fuel* 2018;233:724–31. <https://doi.org/10.1016/j.fuel.2018.06.011>.
- [36] El Younssi I, Rhadfi T, Atlamsani A, Quisefit JP, Herbst F, Draoui K. K-10 montmorillonite: An efficient and reusable catalyst for the aerobic CC bond cleavage of  $\alpha$ -substituted ketones. *J Mol Catal A Chem* 2012;363–364:437–45. <https://doi.org/10.1016/j.molcata.2012.07.022>.

## CHAPTER 6: The role of Ni and Cu interaction on the bimetallic Ni-Cu/ZrO<sub>2</sub> catalytic system

---

**Extracted from the article:** *Ni-Cu bimetallic catalytic system for producing 5-hydroxymethylfurfural derived value-added biofuels*

**Authors:** Nerea Viar, Jesus M. Requies, Ion Agirre, Aitziber Iriondo, Miryam Gil-Calvo, Pedro L. Arias

**Journal, volume and pages:** ACS Sustainable Chemistry and Engineering 8, 11183-11193

**Date of publication:** July 2020



## Table of contents

6.1 EXPERIMENTAL .....	153
6.1.1 Catalyst preparation .....	153
6.1.2 Catalyst characterization .....	153
6.1.3 Activity test .....	154
6.2 RESULTS AND DISCUSSION .....	154
6.2.1 Catalyst characterization results .....	154
6.2.1.1 Chemical and textural properties .....	154
6.2.1.2 Reducibility .....	155
6.2.1.3 Acidic properties .....	158
6.2.1.4 XRD characterization of catalysts .....	160
6.2.1.5 Morphological characteristics .....	163
6.2.1.6 Surface properties .....	165
6.2.2 Activity results.....	167
6.2.2.1 Monometallic catalysts.....	167
6.2.2.2 Bimetallic catalysts impregnated in one step.....	168
6.2.2.3 Bimetallic catalysts impregnated in two steps .....	169
6.2.2.4 Study of the evolution of the catalytic system over the reaction .....	171





In the previous chapter a screening of different catalyst was tested. The effect of different supports and active metals was investigated. It was concluded that Ni-Cu bimetallic catalyst supported on ZrO<sub>2</sub> was the most promising catalyst for the hydrogenolysis of HMF to produce desired DMF and DMTHF. In view of these results, this chapter offers a deep analysis of bimetallic NiCu/ZrO<sub>2</sub> catalysts, studying the effect of metal loading and impregnation method.

## 6.1 Experimental

### 6.1.1 Catalyst preparation

Monometallic Ni and Cu catalysts supported on ZrO<sub>2</sub> were synthesized by wetness impregnation method following the procedure detailed in section 4.1.1 of Chapter 4. Moreover, bimetallic catalysts with different metal loadings were prepared by co-impregnation (one-step impregnation) and by sequential steps impregnation (two-steps impregnation), detailed in section 4.1.1 of Chapter 4.

### 6.1.2 Catalyst characterization

The physicochemical properties of the samples were analysed by N<sub>2</sub> physisorption, Inductively Coupled Plasma Optical Emission Spectroscopy (ICP-OES), Temperature Programmed Reduction with hydrogen (H<sub>2</sub>-TPR), Temperature Programmed Desorption with ammonia (NH<sub>3</sub>-TPD), X-ray Diffraction (XRD), Scanning Transmission Electron Microscopy (STEM) and X-ray Photoelectron Spectroscopy (XPS).

Detailed information about the abovementioned characterization techniques are described in section 4.3. of Chapter 4.

### 6.1.3 Activity test

The activity tests were carried out in a continuous fixed-bed reactor following the procedure detailed in section 4.2. of Chapter 4.

## 6.2 Results and discussion

### 6.2.1 Catalyst characterization results

The characterization results obtained by different techniques are described in this section. The supports were firstly thermally treated under air at 250 °C for 2 h to be evaluated at the same conditions as the synthesized catalysts. Moreover, for those techniques at which it was not possible to reduce the catalyst *in situ*, the catalyst was previously reduced at 275 °C for 2 h at a flow of pure H<sub>2</sub>.

#### 6.2.1.1 Chemical and textural properties

**Table 6.1.** Chemical and textural properties for the calcined support and catalysts.

Group	Catalyst	BET (m <sup>2</sup> /g)	Pore volume <sup>a</sup> (nm)	Average pore diameter <sup>a</sup> (nm)	Cu (%)	Ni (%)
<b>Support</b>	ZrO <sub>2</sub>	137.6	0.27	7.2	-	-
<b>Monometallic</b>	15CuZr	35.1	0.10	10.7	13	-
	15NiZr	5.0	0.03	25.3	-	11
<b>Bimetallic (one-step Impregnation)</b>	7Ni7CuZr	5.5	0.05	32.1	5	6
	15Ni7CuZr	18.3	0.03	7.4	4.1	10
	15Ni15CuZr	18.1	0.03	7.7	12	13
	30Ni15CuZr	77.0	0.04	3.8	8	19
<b>Bimetallic (two-steps Impregnation)</b>	15Cu-15NiZr	18.5	0.13	29.6	11	8
	15Ni-15CuZr	12.3	0.03	10.0	8	11
	15Cu-30NiZr	30.0	0.02	4.2	18	22
	30Ni-15CuZr	18	0.02	5.2	12	30

Determined by <sup>a</sup> N<sub>2</sub>-physiosorption and <sup>b</sup> ICP-OES.

Table 6.1 summarizes the textural properties and metal loading for the prepared catalysts determined from the N<sub>2</sub> adsorption-desorption and ICP-OES characterization techniques, respectively.

The calcined ZrO<sub>2</sub> support showed the highest BET surface area and pore volume. These values decreased when Ni and/or Cu were impregnated because the porous structure of the support was blocked by metal deposition [1–3]. Comparing the monometallic catalysts, the 15NiZr catalyst showed a smaller surface area than the 15CuZr, which can be attributed to the blocking of the pores by the metallic Ni clusters present on the surface. In turn, this can be associated with the low dispersion of the metal [3]. Meanwhile, in the case of the Cu monometallic catalyst, the metal species can be more dispersed in the support. In the case of bimetallic catalysts, the alternative method of impregnating first with Ni and then Cu provided a higher surface area, suggesting a better dispersion for the metals.

Regarding the metal loading of the catalysts, the experimental value was found to be lower than the nominal content in most cases, and this difference became greater as the metal loading was increased. For bimetallic catalysts prepared by one-step impregnation, the incorporation of higher Ni loading (keeping the nominal Cu loading constant) meant lower Cu loadings. In the case of bimetallic catalysts impregnated in two steps, the second metal was better impregnated than the first, leading to a higher Cu loading when Ni was impregnated first, and a higher Ni loading when Cu was impregnated first. In these catalysts, in contrast to one-step impregnated catalysts, impregnating higher Ni loadings (keeping the nominal Cu loading constant) provided higher Cu loadings. Finally, it should be noted that the average pore diameter was higher than that in the support in some cases, especially for the 7Ni7CuZr and 15Cu-15NiZr catalysts. This suggests that the smaller pores were filled by the incorporated metals, involving an increase in the average pore diameter [4].

#### 6.2.1.2 Reducibility

The H<sub>2</sub>-TPR profiles and their deconvolution for the monometallic and bimetallic catalysts are summarized in Figure 6.1 and Figure 6.2, respectively. The monometallic

15CuZr catalyst recorded three different peaks at temperatures of 195 °C, 205 °C and 240 °C. Similarly, monometallic 15NiZr registered different peaks at higher temperatures (270 °C, 300 °C and 380 °C). Reports in the literature indicate that highly dispersed particles and those particles interacting weakly with the support record lower reduction temperatures. In contrast, bulk NiO and CuO and particles interact strongly with the support, recording high reduction temperatures [5–7].

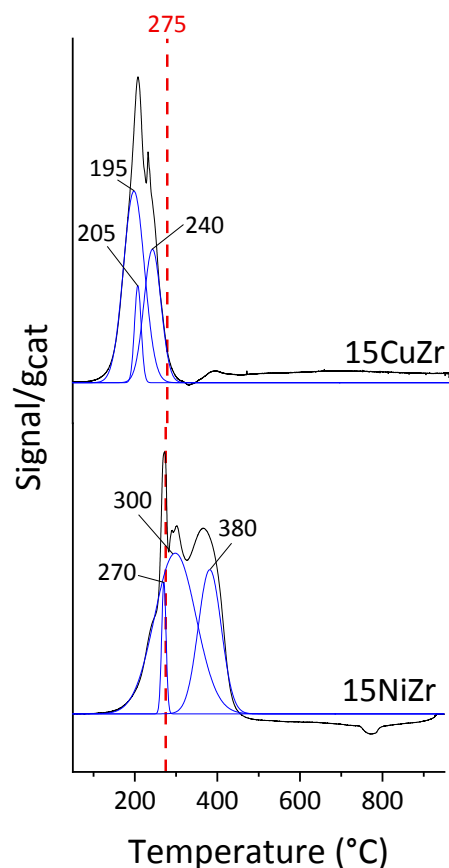


**Figure 6.1.** H<sub>2</sub>-TPR profiles for the monometallic catalysts.

The H<sub>2</sub>-TPR profiles for the bimetallic catalysts can also be deconvoluted into three reduction peaks (see Figure 6.2). When compared to the monometallic 15NiZr catalyst, all of the peaks are shifted to lower temperatures. This observation seems to indicate that Cu facilitates the reducibility of Ni [8–10]. According to the literature [2], the first peak is related to the reduction of the Cu<sup>2+</sup> species, and the last peak to Ni<sup>2+</sup> reduction, while the intermediate peak (in blue) could be associated with the reduction of Ni-Cu species. Table 6.2 presents a summary of the peak temperature and contribution obtained from the deconvolution.

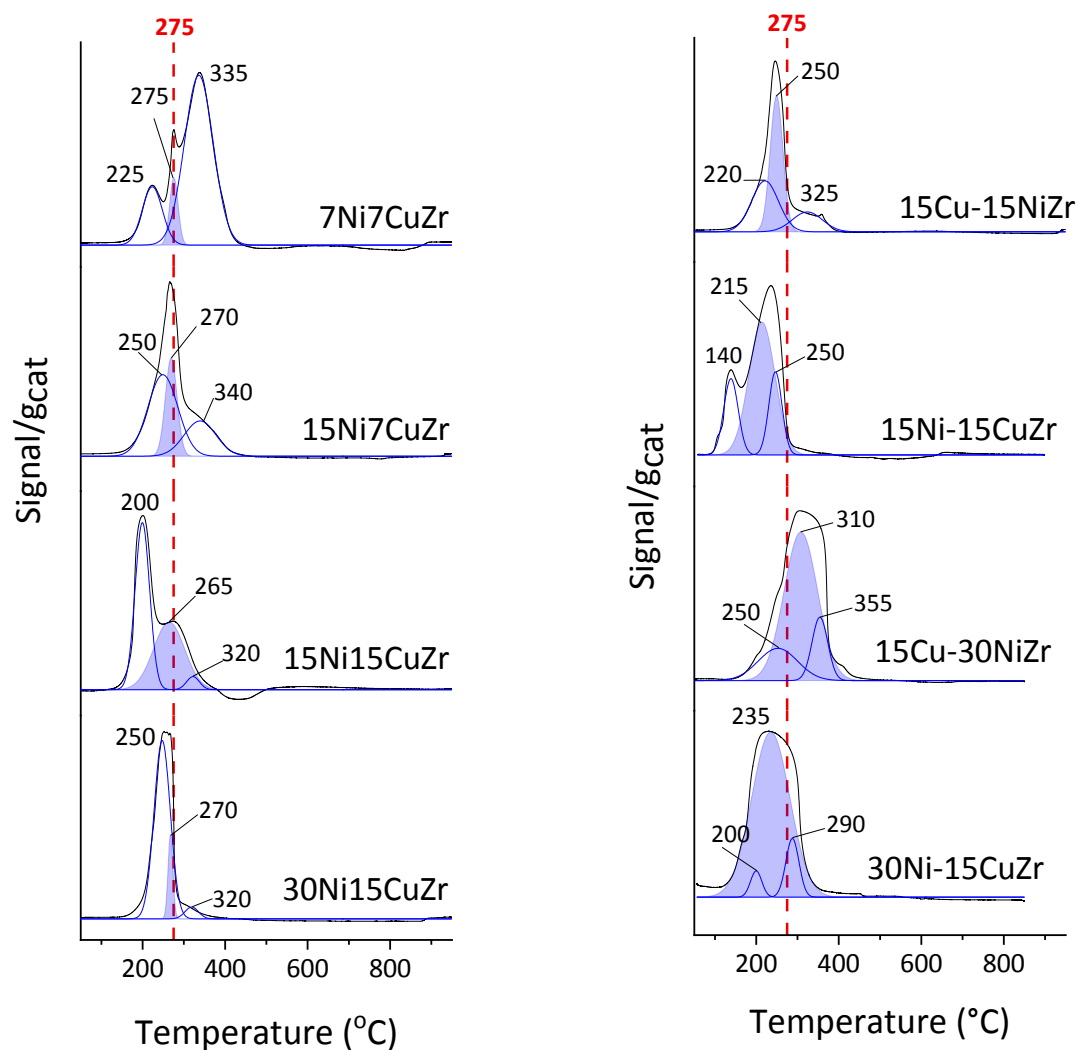


**Figure 6.2.** H<sub>2</sub>-TPR profiles for the bimetallic catalysts.

Based on the results presented in Figure 6.2 and Table 6.2, the bimetallic catalysts impregnated in one step generally recorded a lower contribution for Ni-Cu reduction compared to samples prepared by the two-steps method. This suggests that impregnating metals in sequential steps can promote higher interaction between Ni and Cu species. Furthermore, in the case of the one-step impregnation of bimetallic catalysts, it seems that an increase in metal loading leads to a better reducibility for the catalyst (see Figure 6.2). The 7Ni7CuZr catalyst recorded the highest temperature peak at 335 °C, while, for the 30Ni15CuZr catalyst, this temperature peak decreased to 250 °C. The difference in the reduction temperature can be attributed to a weaker metal support interaction in the latter catalyst, leading to lower reduction temperatures when metal loading is increased [7,11].

Interesting results were found when analysing the H<sub>2</sub>-TPR profiles for those catalysts impregnated in two steps; the reduction temperature differs depending on the impregnation sequence for the metals. Specifically, a better reducibility was observed when Ni was impregnated in a second step (highest temperature peak: 215 °C for the 15Ni-15CuZr catalyst, and 235 °C for the 30Ni-15CuZr catalyst) (see Figure 6.2), while a higher reduction temperature was detected when Ni was impregnated first (250 °C for the 15Cu-15NiZr catalyst and 310 °C for the 15Cu-30NiZr catalyst). According to the literature [12], the metal impregnated in the first step records a stronger interaction with the support. When impregnating Ni first, there is a higher interaction between Ni and ZrO<sub>2</sub>, resulting in a higher reduction temperature. Moreover, impregnating Ni in the second step meant a higher contribution, and, therefore, higher interaction between both metals. Finally, higher Ni loading also involved higher interaction between Ni and Cu.

**Table 6.2.** Deconvolution of H<sub>2</sub>-TPR profiles (maximum temperature of the reduction peaks and contribution in area %).

Group	Catalyst	Cu		Ni-Cu		Ni	
		T (°C)	Area (%)	T (°C)	Area (%)	T (°C)	Area (%)
<b>Bimetallic (one-step Impregnation)</b>	<b>7Ni7CuZr</b>	225	18	275	9	335	74
	<b>15Ni7CuZr</b>	250	52	270	24	340	24
	<b>15Ni15CuZr</b>	200	52	265	45	320	4
	<b>30Ni15CuZr</b>	250	84	270	12	320	5
<b>Bimetallic (two-steps Impregnation)</b>	<b>15Cu-15NiZr</b>	220	37	250	47	325	16
	<b>15Ni-15CuZr</b>	140	19	215	61	250	19
	<b>15Cu-30NiZr</b>	250	17	310	69	355	14
	<b>30Ni-15CuZr</b>	200	4	235	86	290	10

### 6.2.1.3 Acidic properties

The acidic properties were studied by NH<sub>3</sub>-TPD. Some authors have reported that high acidity favors C–C bond cleavage, leading to the formation of degradation and/or ring-opening products [13,14]. This phenomenon needs to be avoided in this reaction.

Table 6.3 shows that the ZrO<sub>2</sub> support had low acidity, with a value of 0.39 mmol NH<sub>3</sub>/g<sub>cat</sub>. In the case of monometallic catalysts, acidity decreased when Cu was loaded onto the support. The incorporated Cu particles could be partially covering acid sites on the support, thus decreasing the catalyst's total acidity [15,16]. However, the addition of Ni considerably increased this acidity. It seems that the high acidity detected for the monometallic 15NiZr catalyst was related to the presence of Lewis acid sites associated with the presence of Ni<sup>2+</sup> [17]. This is in good agreement with the H<sub>2</sub>-TPR results, where higher temperatures are needed to reduce this catalyst, involving the formation of Ni<sup>2+</sup> species with stronger interaction with the support that can also act as Lewis acid sites.

**Table 6.3.** Amount of NH<sub>3</sub> desorbed in NH<sub>3</sub>-TPD.

Group	Catalyst	mmol NH <sub>3</sub> /g <sub>cat</sub>
<b>Support</b>	ZrO <sub>2</sub>	0.39
<b>Monometallic</b>	15CuZr	0.18
	15NiZr	1.09
<b>Bimetallic (one-step Impregnation)</b>	7Ni7CuZr	1.12
	15Ni7CuZr	0.41
	15Ni15CuZr	0.35
	30Ni15CuZr	0.38
<b>Bimetallic (two-steps Impregnation)</b>	15Cu-15NiZr	0.38
	15Ni-15CuZr	0.11
	15Cu-30NiZr	0.16
	30Ni-15CuZr	0.17

The acidity calculated for the bimetallic catalysts was similar to or lower than that of the support, except for the 7Ni7CuZr catalyst. In this last case, a similar effect to that found for the monometallic Ni catalyst may be taking place. The harder reducibility of this sample, as observed from the H<sub>2</sub>-TPR profiles, can be explained by the formation of Ni<sup>2+</sup> species that strongly interact with the support and act as Lewis acid sites [18]. This fact is also in good agreement with the XPS results, where the Ni<sup>0</sup>/(Ni<sup>0</sup>+Ni<sup>2+</sup>) for the fresh-reduced catalyst is low when compared to the other bimetallic catalysts. The remaining bimetallic catalyst prepared in a single step recorded comparable or slightly

lower acidity values compared to the support. In the case of the bimetallic catalyst impregnated in two steps, the acidity was found to be even lower, except for the 15Cu-15NiZr catalyst. The double calcination of these latter catalysts can obviously favor a decrease in the number of acid sites.

#### 6.2.1.4 XRD characterization of catalysts

The XRD patterns for the fresh-reduced and used catalysts are shown in Figure 6.3 and Figure 6.4. The reflections detected in these diffraction patterns correspond to  $\text{Cu}^0$  ( $2\theta = 43.4^\circ$ ,  $50.5^\circ$  and  $74.2^\circ$ ) and  $\text{Ni}^0$  ( $2\theta = 44.7^\circ$ ,  $52.1^\circ$  and  $76.3^\circ$ ). Diffraction peaks ascribed to carbon were detected in the used catalysts ( $2\theta = 35.8^\circ$ , and  $60.1^\circ$ ), which may be related to coke formation under reaction conditions [15,19–21]. A high peak at  $2\theta = 35.9^\circ$  was observed in some used catalysts. This peak was attributed to CSi, which was used to fix the catalytic bed. Moreover, the average Ni and Cu crystallite sizes for these catalysts were calculated by the Scherrer equation, and these data are summarized in Table 6.4. Concerning monometallic catalysts (see Figure 6.3) the fresh-reduced 15CuZr catalyst registered defined peaks associated with metallic Cu crystallites with a size of 50 nm. After the reaction, they were transformed into small crystallites that could hardly be detected by XRD. A barely noticeable peak can be discerned in the XRD pattern for the freshly reduced 15NiZr catalyst, which can be ascribed to an amorphous structure. Moreover, peaks related to carbon deposition were observed in the used catalyst.

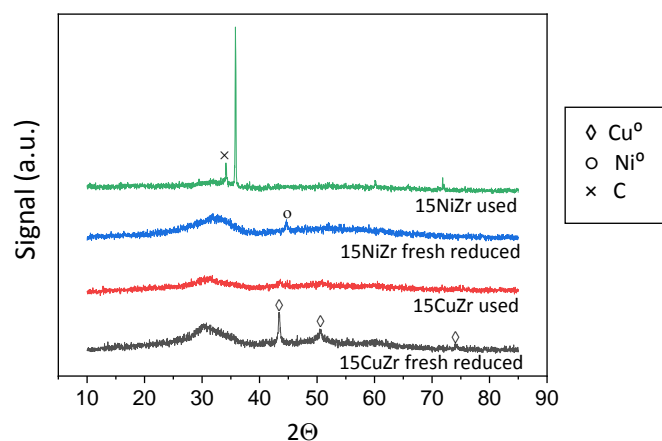
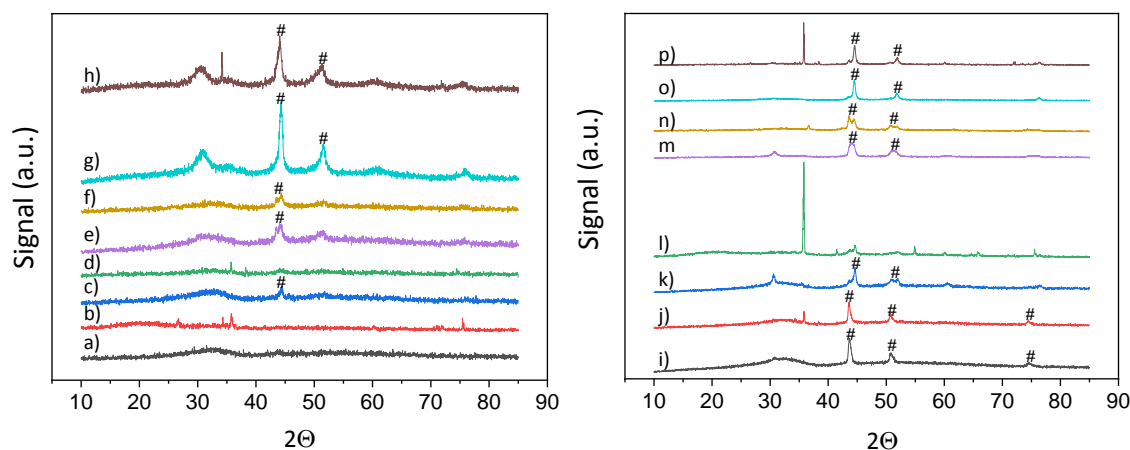


**Figure 6.3.** XRD patterns for the monometallic catalysts



**Table 6.4.** Crystallite size of different catalysts.

Group	Catalyst	Cu (nm)		Ni (nm)	
		Fresh reduced	Used	Fresh reduced	Used
Monometallic	15CuZr	50	< 5	-	-
	15NiZr	-	-	< 5	< 5
Bimetallic (one-step Impregnation)	7Ni7CuZr	< 5	< 5	< 5	< 5
	15Ni7CuZr	< 5	< 5	20	< 5
	15Ni15CuZr	40	35	10	15
	30Ni15CuZr	< 5	< 5	15	10
Bimetallic (two-steps Impregnation)	15Cu-15NiZr	30	40	15	20
	15Ni-15CuZr	10	< 5	15	< 5
	15Cu-30NiZr	20	25	15	15
	30Ni-15CuZr	15	30	30	35



a) 7Ni7CuZr FR; b) 7Ni7CuZr U; c) 15Ni7CuZr FR; d) 15Ni7CuZr U; e) 15Ni15CuZr FR; f) 15Ni15CuZr U; g) 30Ni15CuZr FR; h) 30Ni15CuZr U; i) 15Cu-15NiZr FR; j) 15Cu-15NiZr U; k) 15Ni-15CuZr FR; l) 15Ni-15CuZr U; m) 15Cu-30NiZr FR; n) 15Cu-30NiZr U; o) 30Ni-15CuZr FR; p) 30Ni-15CuZr U. FR: Fresh reduced; U: used; #NiCu

**Figure 6.4.** XRD patterns for the bimetallic catalysts

The reduced and used bimetallic 7Ni7CuZr catalyst impregnated in one step did not record any peaks related to Ni<sup>0</sup> or Cu<sup>0</sup>. This means that this catalyst was composed mainly of small crystallites before the reaction, and that these crystallites did not recrystallize during the reaction. Similarly, the 15Ni7CuZr catalyst showed a small peak ( $2\theta = 44.7^\circ$ ) that may be related to metallic Ni crystallites with an average size of 20 nm. After the reaction, Ni crystallites were not detectable by XRD (crystallite size < 5 nm). The interaction between Ni and Cu crystallites could not be observed in any of these cases.

In contrast, the 15Ni15CuZr catalyst registered a double-peak in both the fresh-reduced and used catalysts at two different positions  $2\theta = 43 - 44^\circ$  and at  $2\theta = 51^\circ$ , which may be related to Ni-Cu crystallites. A comparison of crystallite size before and after the reaction showed that the size of the Cu-enriched crystallites decreased, while the size of those enriched in Ni increased. This finding suggests that a rearrangement of the crystallites occurred during the reaction, leading to smaller Cu-enriched crystallites and larger Ni-enriched crystallites. Finally, the crystallites observed in the 30Ni15CuZr catalyst were enriched in Ni, decreasing in size from 15 nm to 10 nm after hydrogenolysis reaction. Cu crystallites were not detectable.

The bimetallic 15Cu-15NiZr and 15Ni-15CuZr catalysts impregnated in two steps recorded highly intensive signals ascribed to a Ni-Cu combination. The crystallite size increased slightly in the case of 15Cu-15NiZr, probably due to the sintering of the metallic sites. When adding a higher Ni loading, i.e., 15Cu-30NiZr, the catalyst recorded a similar crystallite size before and after the reaction. This means that the crystallite structure was kept stable during the reaction. In contrast, the crystallites in the 30Ni-15CuZr catalyst grew, probably because of a sintering effect.

To understand the difference in the crystal composition between pure Ni and Cu and bimetallic Ni-Cu, an enlarged graph for the fresh catalysts is reported in Figure 6.5. The monometallic Cu and Ni registered a diffraction peak at  $2\theta = 43.4^\circ$  and  $2\theta =$

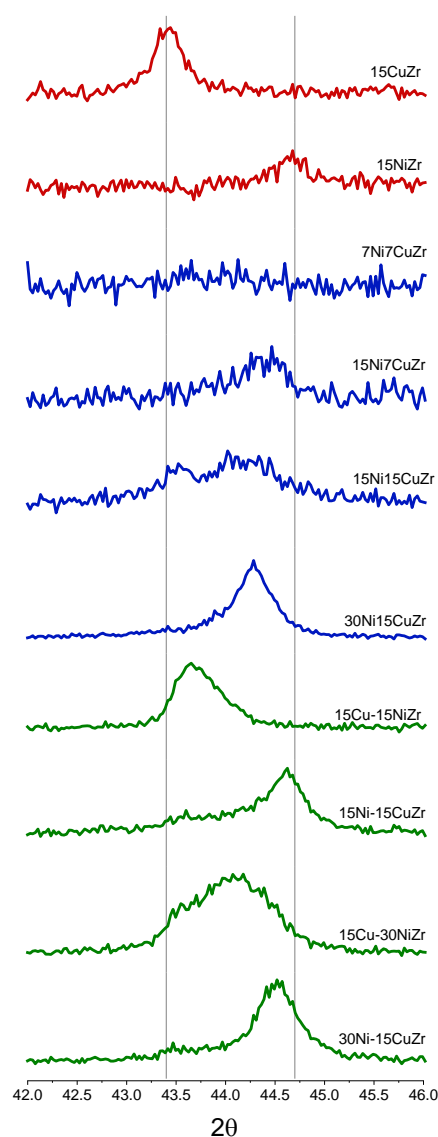


**Figure 6.5.** XRD enlarged graph ( $2\theta = 42.0 - 46.0$ ) for the monometallic and bimetallic catalysts.

44.7°, respectively. The bimetallic catalysts recorded a reflection angle between these two limits, meaning that the crystallites were formed by both Ni and Cu metals. In the case of bimetallic catalysts impregnated in two steps, adding Cu in a first step produced crystallites enriched in Ni. Moreover, impregnating Ni in a first step provided Cu-enriched crystals. This is consistent with the Ni and Cu loadings measured by ICP-OES.

### 6.2.1.5 Morphological characteristics

**Table 6.5.** Mean particle size for the bimetallic catalysts.

<b>Group</b>	<b>Catalyst</b>	<b>Mean particle size (nm)</b>
<b>Bimetallic (one-step Impregnation)</b>	<b>15Ni15CuZr</b>	55.5
	<b>30Ni15CuZr</b>	48.6
	<b>15Cu-15NiZr</b>	44.7
<b>Bimetallic (two-steps Impregnation)</b>	<b>15Ni-15CuZr</b>	22.9
	<b>15Cu-30NiZr</b>	26.9
	<b>30Ni-15CuZr</b>	20.9

The elemental maps for the most interesting bimetallic catalysts were obtained by Scanning Transmission Electron Microscopy, which was used to calculate the average size of the metallic particles. The maps for the fresh-reduced catalysts and the value of the average particle size are shown in the Supporting information (Figure 6.6) and Table 6.5, respectively. The elemental maps reflected the interaction between Ni and Cu ascribed to bimetallic particles. Moreover, an optimal dispersion of these particles in the support was observed. Regarding the mean particle size, the bimetallic catalysts impregnated in one step recorded a higher particle size than the catalysts impregnated in two steps, and, in this sense, lower particle sizes generally lead to a higher dispersion of active sites. However, the 15Cu-15NiZr catalyst did not follow this tendency; in spite of being synthesized in two steps, it showed similar particle sizes compared to those catalysts prepared in a single impregnation step.

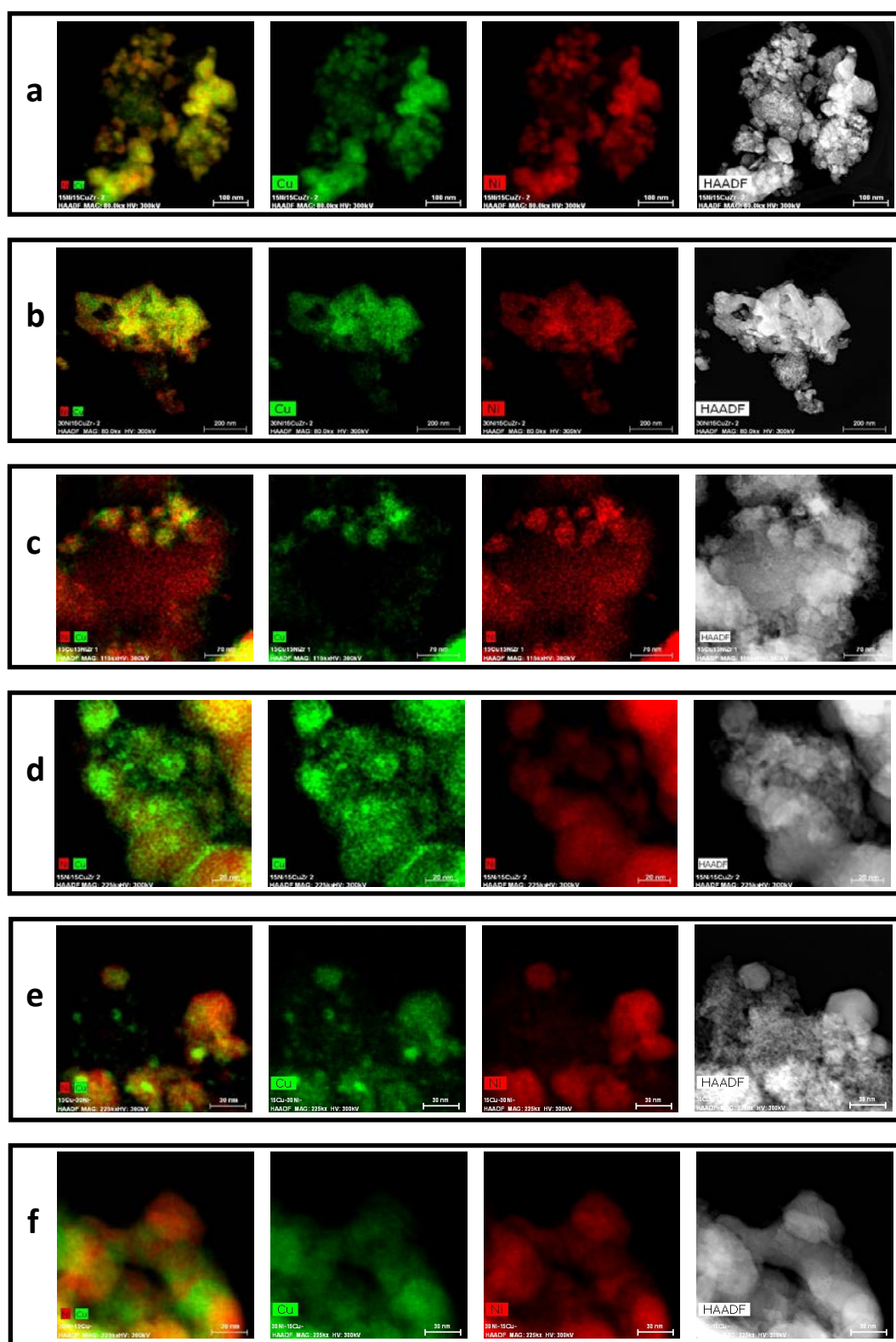


**Figure 6.6.** STEM images for the bimetallic catalysts: a) 15Ni15CuZr; b) 30Ni15CuZr; c) 15Cu-15NiZr; d) 15Ni-15CuZr; e) 15Cu-30NiZr; f) 30Ni-15CuZr.

## 6.2.1.6 Surface properties

The oxidation state of the species formed after catalyst preparation and their atomic ratios were studied by XPS for fresh-reduced and used catalysts. The results are summarized in Table 6.6. The ratios between the metallic Cu and Ni and the sum of their ions were calculated to understand whether the species underwent oxidation or reduction during the reaction. The Ni<sup>0</sup>/Zr ratio was also calculated due to the importance of surface metallic Ni content in the product distribution.

**Table 6.6.** XPS results for the monometallic and bimetallic catalysts.

Group	Catalyst		Cu/Zr	$\frac{Cu^0}{Cu^{total}}$	Ni/Zr	$\frac{Ni^0}{Ni^{total}}$	$\frac{Ni^0}{Zr}$	C/Zr
Monometallic	15CuZr	FR	0.37	0.62	-	-	-	1.12
		U <sup>a</sup>	0.25	0.56	-	-	-	10.80
	15NiZr	FR	-	-	0.15	0.17	0.03	4.96
		U <sup>a</sup>	-	-	0.07	0.24	0.02	35.68
Bimetallic (one-step Impregnation)	7Ni7CuZr	FR	0.22	0.28	0.04	0.27	0.01	6.63
		U <sup>a</sup>						Only C
	15Ni7CuZr	FR	0.27	0.27	0.58	0.44	0.26	63.09
		U <sup>a</sup>	0.62	0.43	0.35	0.30	0.11	260.7
	15Ni15CuZr	FR	1.59	0.25	1.35	0.32	0.42	7.20
		U <sup>b</sup>	0.28	0.66	1.32	0.24	0.32	20.67
	30Ni15CuZr	FR	0.51	0.31	0.44	0.44	0.19	4.19
		U <sup>b</sup>	0.43	0.52	0.23	0.29	0.07	78.92
Bimetallic (two-steps Impregnation)	15Cu-15NiZr	FR	0.43	0.57	0.05	0.36	0.02	38.39
		U <sup>c</sup>	2.56	0.59	0.48	0.35	0.17	126.2
	15Ni-15CuZr	FR	0.57	0.30	0.54	0.42	0.23	4.28
		U <sup>c</sup>	0.77	0.52	0.79	0.48	0.38	51.48
	15Cu-30NiZr	FR	1.26	0.48	1.35	0.53	0.71	11.44
		U <sup>c</sup>	0.61	0.59	1.32	0.28	0.37	18.97
	30Ni-15CuZr	FR	1.46	0.52	1.46	0.54	0.79	5.15
		U <sup>c</sup>	1.20	0.73	1.26	0.29	0.36	49.04

FR: fresh reduced; U: used. <sup>a</sup> Used catalyst operating conditions: T = 275 °C; P<sub>H<sub>2</sub></sub> = 15 bar; time on stream: 10 h. <sup>b</sup> Used catalyst operating conditions: T = 275 °C; P<sub>H<sub>2</sub></sub> = 15 bar; time on stream: 24 h. <sup>c</sup> Used catalyst operating conditions: T = 275 °C; P<sub>H<sub>2</sub></sub> = 15 bar; time on stream: 25 h.  $Cu^{total} = Cu^0 + Cu^{1+} + Cu^{2+}$ ;  $Ni^{total} = Ni^0 + Ni^{2+}$ .

A comparison of the monometallic catalysts showed that the 15CuZr catalyst recorded a higher metal-to-Zr ratio than the 15NiZr catalyst, suggesting that a higher amount of surface metal was available in the 15CuZr catalyst. Moreover, the monometallic Cu catalyst recorded a slight decrease in the Cu/Zr ratio after being used in the reaction, presumably owing to the coke deposition on the active sites and/or metal sintering. Coke formation was confirmed by the C/Zr ratio, which was observed to increase after the reaction for all the prepared catalysts. In the case of the monometallic Ni catalyst, the decrease in the metal-to-support ratio (probably caused by the sintering of Ni particles) and the increase in the C/Zr ratio after hydrogenolysis were more notable, as well as their observation in the XRD results. It is important to note the low  $\text{Ni}^0/(\text{Ni}^0+\text{Ni}^{2+})$  ratio for the fresh-reduced Ni monometallic catalyst, which was consistent with the  $\text{H}_2$ -TPR results, where a high reduction temperature was observed. Coke deposition can also be associated with the high acidity [22] ascribed to the presence of  $\text{Ni}^{2+}$  Lewis acid sites (as shown by the  $\text{NH}_3$ -TPD results).

The catalysts prepared by one-step impregnation behaved differently depending on the Ni and Cu loading. Both the 7Ni7CuZr catalyst and the 15NiZr catalyst recorded a low  $\text{Ni}^0/(\text{Ni}^0+\text{Ni}^{2+})$  ratio in the fresh-reduced state. This finding closely matches the  $\text{H}_2$ -TPR and  $\text{NH}_3$ -TPD results, whereby these catalysts presented higher reduction temperatures and higher acidities. The used 15NiZr catalyst was completely covered by carbon, according to the high acidity observed in its  $\text{NH}_3$ -TDP. A high carbon deposition was also observed for the 15Ni7CuZr catalyst. In addition, note should be taken of the high  $\text{Ni}^0/\text{Zr}$  ratio of the 15Ni15CuZr catalyst, which decreased after the reaction, indicating that Ni was oxidized during the reaction. In this sense, the butanol or water produced as a byproduct during the hydrogenolysis reaction could oxidize the Ni species to NiO during the reaction, as reported previously [23–25]. The high Cu/Zr ratio detected in the fresh-reduced catalyst fell sharply after the reaction. Finally, the 30Ni15CuZr catalyst recorded lower metal-to-support ratios, and a decrease in these ratios after the reaction, probably because of the inaccessibility of the metallic sites after being partially covered by carbon deposits. Indeed, a high C/Zr ratio was observed for this catalyst after reaction, which was ascribed to a high coke deposition on its surface.

Concerning the bimetallic catalysts synthesized in two steps, the 15Cu-15NiZr catalyst recorded the highest carbon deposition, which was consistent with its higher acidity (see Table 6.3. Moreover, this catalyst recorded low metal-to-support ratios before the reaction, which increased after 25 h on stream; this could be explained by the carbon deposition on the catalyst support, implying that less support was accessible after the reaction. A similar effect was observed for the 15Ni-15CuZr catalyst, where higher metal-to-support ratios were obtained in the used catalysts. Moreover, metals were reduced during the reaction. When impregnating a higher amount of Ni (for the 15Cu-30NiZr and 30Ni-15CuZr catalysts), higher Ni/Zr ratios were obtained, which in turn slightly decreased after the reaction. In the case of the reduced 30Ni-15CuZr catalyst, the metal-to-support ratio was higher than that of the 15Cu-30NiZr catalyst. In both cases,  $\text{Ni}^0/\text{Zr}$  was high at the beginning of the reaction, but Ni was partially oxidized during the reaction, and, therefore, a lower ratio was recorded after the reaction. As explained before, either the solvent or the water produced during the reaction could be the agents responsible for metallic Ni oxidation.

## 6.2.2 Activity results

### 6.2.2.1 Monometallic catalysts

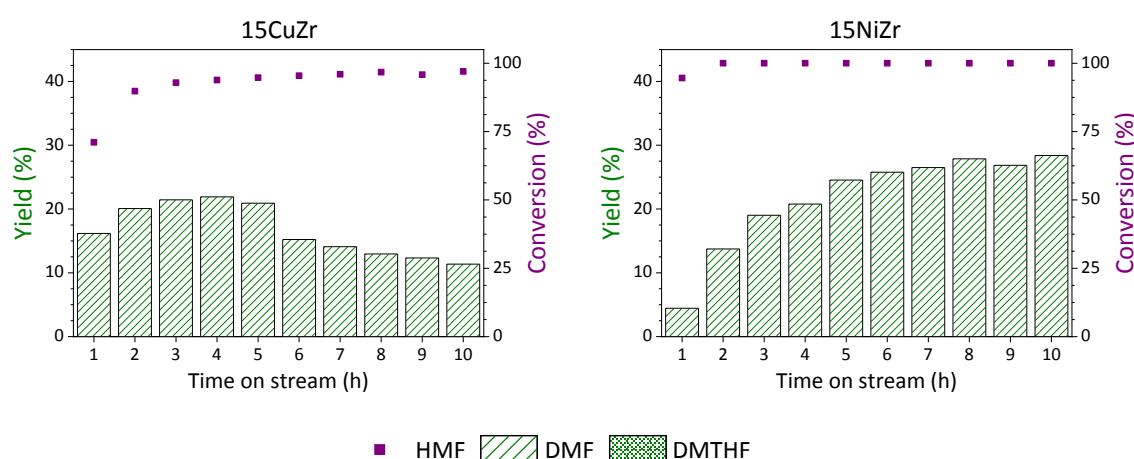


**Figure 6.7.** Conversion and yield for the monometallic catalysts (operating conditions:  $T = 275\text{ }^{\circ}\text{C}$  and  $P_{\text{H}_2} = 15\text{ bar}$ )

The activity results for the monometallic catalysts are summarized in Figure 6.7. The 15CuZr catalyst underwent a complete HMF conversion, whereas the monometallic Ni catalyst recorded a conversion of over 90 %. The 15CuZr catalyst recorded a DMF yield of approximately 30 %, and was found to be stable after 10 h on stream. In contrast, the 15NiZr catalyst reached a maximum yield of 20 % after 4 h time on stream, but decreased to 10 % after 10 h reaction time. In both cases, no DMTHF was detected. The better performance of the 15CuZr catalyst could be related to its greater BET area and its better reducibility providing a higher HMF conversion and DMF yield. Moreover, the higher acidity of the 15NiZr catalyst can favour C–C cleavage, producing ring-opening products [26]. The deactivation of this catalyst could be caused by the coke deposition on the active sites (determined by XPS and XRD characterization techniques) and/or by possible particle sintering (as observed from the data derived from XPS).

#### 6.2.2.2 Bimetallic catalysts impregnated in one step

The activity results for bimetallic catalysts impregnated in one step are summarized in Figure 6.8. For the 7Ni7CuZr and 15Ni7CuZr catalysts, the reaction was stopped after 10 h due to the poor total yield and the observed deactivation after 7 h on stream. In both cases, a small amount of DMTHF was detected in the first reaction hours. The high carbon deposition may cover the active metal sites, and, thus, result in the deactivation of the catalysts. In contrast, impregnating higher amounts of Ni and Cu (15Ni15CuZr and 30Ni15CuZr catalysts) provided higher yields for the desired products during 24 h of reaction time (the figures for the conversion and yields at 23 h are the averages for the overall production during the night). The good performance of these catalysts can be attributed to their higher interaction between Cu and Ni metals, as observed in the XRD results. Therefore, there seems to be a close relationship between the DMTHF and DMF yield obtained and the Ni-Cu interaction formed in each catalyst (Figure 6.10). The high DMTHF production associated with the 15Ni15CuZr catalyst at the beginning of the reaction (40 % yield of DMTHF at 4 h of reaction time) can be linked to the high metallic Ni content on the surface of the catalyst detected by XPS,



which has a high hydrogenation capacity. After the reaction, the catalyst showed some Ni oxidation, which may be responsible for the decrease in the production of DMTHF, which seems to take place through DMF hydrogenation. Finally, the 30Ni15CuZr catalyst recorded a maximum DMF yield of 25 %, which remained almost constant after 24 h of reaction. As regards the aforementioned catalyst, a small production of DMTHF was observed at the beginning of the reaction. This may be due to the smaller amount of metallic Ni observed by XPS and the lower dispersion of the metals due to larger crystallites, compared to the 15Ni15CuZr catalyst.

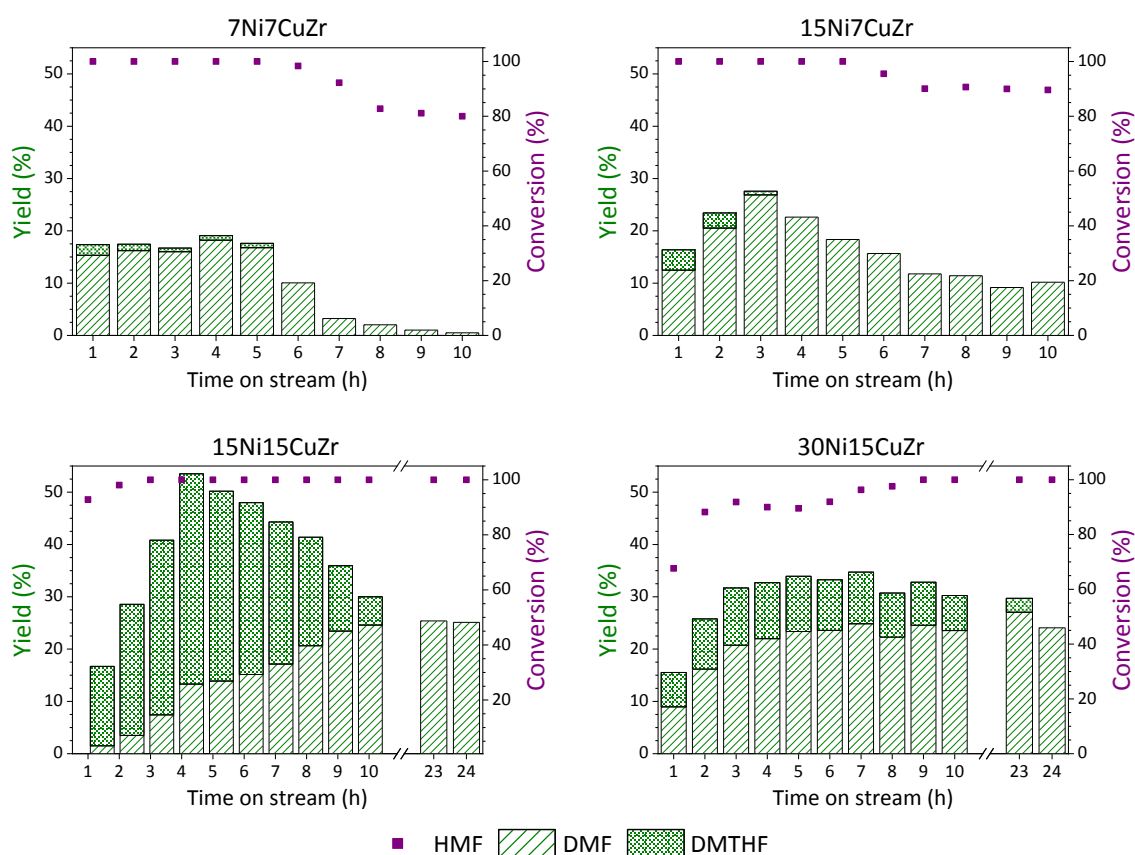


**Figure 6.8.** Conversion and yield for the bimetallic catalysts impregnated in one step (operating conditions:  $T = 275\text{ }^{\circ}\text{C}$  and  $P_{\text{H}_2} = 15\text{ bar}$ )

### 6.2.2.3 Bimetallic catalysts impregnated in two steps

Figure 6.9 shows the activity results for the bimetallic catalysts impregnated in two steps. The high production of DMF and DMTHF is probably related to the interaction of Ni and Cu (Figure 6.10). Moreover, the yields for the desired products are higher than

that found for the bimetallic catalysts impregnated in one step. This can be ascribed to the lower particle size of these catalysts. The 15Cu-15NiZr catalyst reached a maximum DMF yield of 50 % after 8 h of time on stream, which then fell to 10 % after 25 h, probably due to the sintering of metal particles and/or coke deposition on the active sites. Furthermore, this catalyst hardly produced any DMTHF. In contrast, the 15Ni-15CuZr catalyst recorded a lower deactivation after 25 h time on stream; reaching a maximum DMF yield of 70 % after 8 h. The higher yield observed in this catalyst may be related to its smaller bimetallic Ni-Cu particles with higher dispersion. In addition, the higher metal-to-support ratio observed by XPS may enhance the production of the desired products.

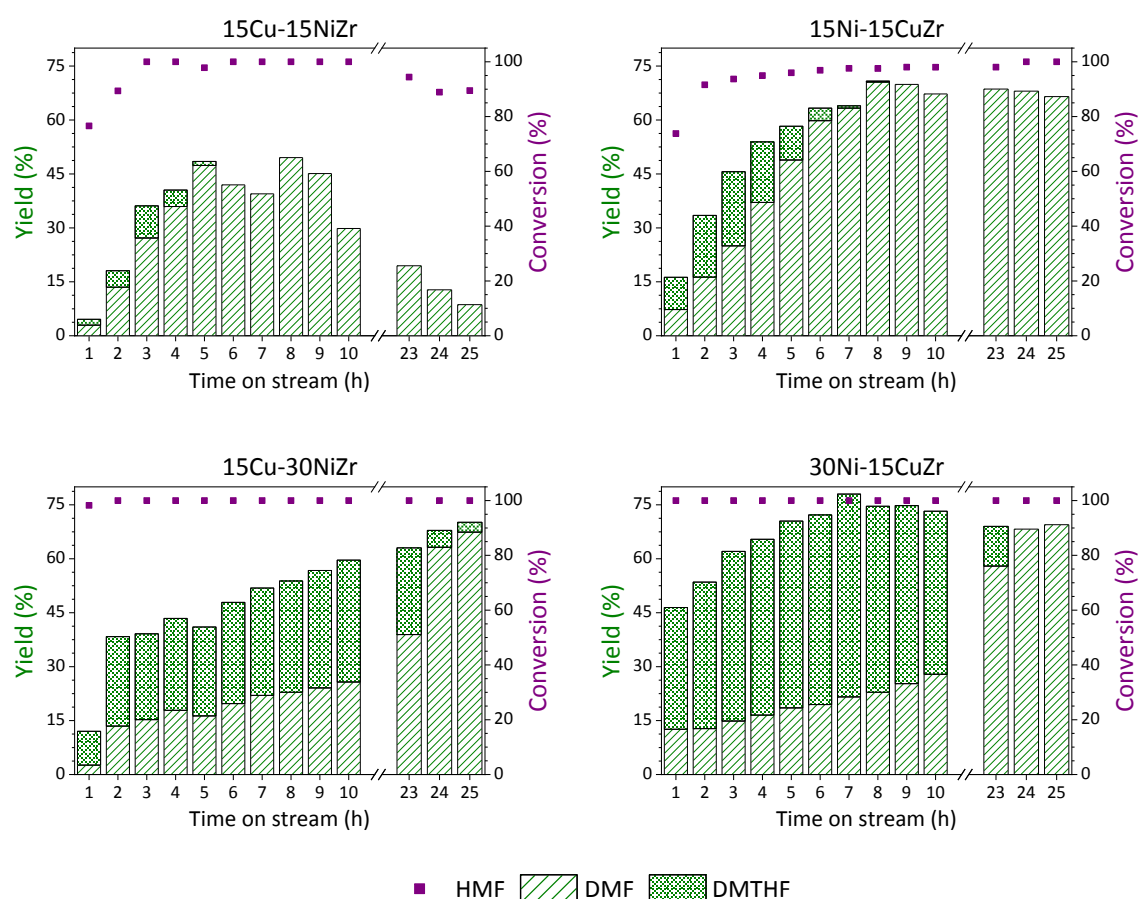


**Figure 6.9.** Conversion and yield for the bimetallic catalysts impregnated in two steps (operating conditions:  $T = 275\text{ }^{\circ}\text{C}$  and  $P_{\text{H}_2} = 15\text{ bar}$ ).

The 15Cu-30NiZr and 30Ni-15CuZr catalysts recorded high yields of DMTHF. The higher metallic Ni surface content observed by XPS produces higher DMTHF due to the

hydrogenating capacity of Ni [27]. Both catalysts showed a similar tendency, achieving high DMTHF yields at the first stage of the reaction, and high DMF yields after 23 h of time on stream. As indicated by the results obtained from XPS (see Table 6.6), Ni was partially oxidized during the reaction, presumably suppressing its DMF hydrogenation capacity and producing DMF instead of DMTHF. However, the 15Cu-30NiZr catalyst recorded a lower DMTHF yield during the reaction. This can be ascribed to the lower Ni/Zr and Cu/Zr ratios observed in XPS; with higher Ni loading implying lower particle size, which resulted in a better dispersion for the catalyst. Additionally, the interaction of Ni-Cu observed in the H<sub>2</sub>-TPR profiles became stronger when the Ni loading was increased. These two considerations can explain the better performance of the catalysts with higher Ni loadings.

As noted, there seems to be a close relationship between the Ni-Cu interactions observed in H<sub>2</sub>-TPR deconvolution profiles and the maximum yield obtained (the sum of DMF and DMTHF production).

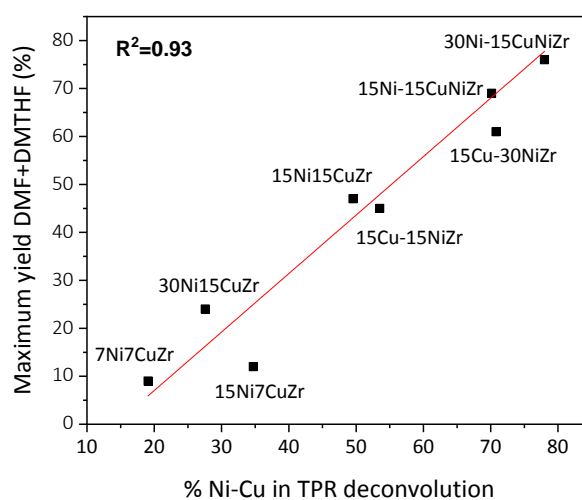


**Figure 6.10.** Relation between % Ni-Cu and maximum yield

#### 6.2.2.4 Study of the evolution of the catalytic system over the reaction

As discussed above, some catalysts produced DMTHF at the beginning of the reaction, probably due to the presence of Ni metal active sites. However, the lower Ni<sup>0</sup>/Ni<sup>2+</sup>

ratio observed in the used catalysts suggests a progressive Ni oxidation process during the reaction, which decreases the hydrogenation capacity. To confirm these results, different activity tests were carried out by using the 15Cu-30NiZr catalyst for different on stream times (see Table 6.7). The used catalyst at these different reaction times was then characterized by XRD and XPS techniques to observe the evolution of the catalyst properties.

**Table 6.7.** XRD results for the 15Cu-30NiZr catalyst tested at different reaction times.

Time on stream (h)	Cu/Zr	Cu <sup>0</sup> / (Cu <sup>0</sup> +Cu <sup>1+</sup> +Cu <sup>2+</sup> )	Ni/Zr	Ni <sup>0</sup> / (Ni <sup>0</sup> +Ni <sup>2+</sup> )	Ni <sup>0</sup> /Zr
<b>Fresh-reduced</b>	1.26	0.48	1.35	0.53	0.71
<b>3 h</b>	1.22	0.50	1.34	0.46	0.62
<b>6 h</b>	1.21	0.49	1.26	0.40	0.50
<b>10 h</b>	0.71	0.49	1.22	0.34	0.41
<b>25 h</b>	0.61	0.59	1.02	0.28	0.37

The XRD results summarized in Table 6.7 show that the Ni and Cu crystallites followed a similar pattern during the first 10 hours of reaction time, showing a slight decrease in the contribution of the Ni crystallites. This suggests that some Ni crystallites lose some crystallinity during the reaction. After 25 h of reaction time, this decline became more significant. In addition, this trend is comparable to the DMTHF yield profile observed during the activity tests. Specifically, a higher DMTHF yield was observed at the beginning of the reaction, where Ni crystallites remained almost stable, and DMTHF production decreased while Ni crystallites became less crystalline.

**Table 6.8.** XPS results for the 15Cu-30NiZr catalyst tested at different reaction times.

Time on stream (h)	Crystallite size (nm)		Contribution (%)	
	Cu	Ni	Cu	Ni
<b>Fresh-reduced</b>	30	10	16	84
<b>3 h</b>	25	10	15	85
<b>6 h</b>	30	10	20	80
<b>10 h</b>	25	10	22	78
<b>25 h</b>	25	15	44	56

Finally, the XPS technique was used to understand the change in the oxidation state of metallic species during the reaction, and the results are summarized in Table 6.8. In general, a difference is found between the Cu and Ni oxidation-reduction trends. Cu was reduced during the reaction due to the H<sub>2</sub> atmosphere inside the reactor. However, Ni underwent an oxidation process during the reaction, which could be observed from the decrease in the Ni<sup>0</sup>/Zr ratio during the reaction, and may be the reason for the observed decrease in DMTHF production. In fact, when the metallic Ni on the surface was oxidized, its hydrogenating capacity was reduced, which means the hydrogenation process for DMF to produce DMTHF was limited.

In general, bimetallic catalysts recorded a better performance and stability than their monometallic counterparts. This is probably due to the presence of the Ni-Cu interaction. In addition, impregnating Ni and Cu metals in sequential steps was found to lead to higher Ni-Cu interaction, smaller particles size and lower acidity. These lower acidity values possibly prevented C—C cleavage and avoided the production of ring-opening products. Moreover, the lower acidity involved less coke deposition, which resulted in lower catalyst deactivation. Another important conclusion is that metallic Ni deposited onto the surface of the catalyst was responsible for DMTHF production. This Ni was partially oxidized during the reaction, leading to a loss in hydrogenating capacity, which limited the hydrogenation step of DMF to DMTHF. Finally, impregnating Ni in a second step involved better reducibility and enhanced dispersion for the metals. Despite the fact that at the begin of the reaction higher Ni loading implied higher production of desired products, after 25 h of reaction, 15Ni-15CuZr and 30Ni-15CuZr catalysts reached similar DMF yield (around 70 %). For this reason, and trying to avoid the use of excess of metal, 15Ni-15CuZr catalyst will be considered for further investigations.

**References**

- [1] Li X, Xiang M, Wu D. Hydrogenolysis of glycerol over bimetallic Cu–Ni catalysts supported on hierarchically porous SAPO-11 zeolite. *Catal Commun* 2019;119:170–5. <https://doi.org/10.1016/j.catcom.2018.11.004>.
- [2] Khzouz M, Gkanas EI, Du S, Wood J. Catalytic performance of Ni-Cu/Al<sub>2</sub>O<sub>3</sub> for effective syngas production by methanol steam reforming. *Fuel* 2018;232:672–83. <https://doi.org/10.1016/j.fuel.2018.06.025>.
- [3] Pongsombate A, Imyen T, Dittanet P, Embley B, Kongkachuichay P. Direct synthesis of dimethyl carbonate from CO<sub>2</sub> and methanol by supported bimetallic Cu–Ni/ZIF-8 MOF catalysts. *J Taiwan Inst Chem Eng* 2017;80:16–24. <https://doi.org/10.1016/j.jtice.2017.07.019>.
- [4] Requies JM, Frias M, Cuezva M, Iriondo A, Agirre I, Viar N. Hydrogenolysis of 5-Hydroxymethylfurfural To Produce 2,5-Dimethylfuran over ZrO<sub>2</sub> Supported Cu and RuCu Catalysts. *Ind Eng Chem Res* 2018;57:11535–46. <https://doi.org/10.1021/acs.iecr.8b01234>.
- [5] Jia X, Zhang X, Rui N, Hu X, Liu C jun. Structural effect of Ni/ZrO<sub>2</sub> catalyst on CO<sub>2</sub> methanation with enhanced activity. *Appl Catal B Environ* 2019;244:159–69. <https://doi.org/10.1016/j.apcatb.2018.11.024>.
- [6] Pérez-Hernández R, Gutiérrez-Martínez A, Espinosa-Pesqueira ME, Estanislao ML, Palacios J. Effect of the bimetallic Ni/Cu loading on the ZrO<sub>2</sub> support for H<sub>2</sub> production in the autothermal steam reforming of methanol. *Catal Today* 2015;250:166–72. <https://doi.org/10.1016/j.cattod.2014.08.009>.
- [7] Pastor-Pérez L, Gu S, Sepúlveda-Escribano A, Reina TR. Bimetallic Cu–Ni catalysts for the WGS reaction – Cooperative or uncooperative effect? *Int J Hydrogen Energy* 2019;4. <https://doi.org/10.1016/j.ijhydene.2018.12.127>.
- [8] Cai F, Pan D, Ibrahim JJ, Zhang J, Xiao G. Hydrogenolysis of glycerol over supported bimetallic Ni/Cu catalysts with and without external hydrogen

- addition in a fixed-bed flow reactor. *Appl Catal A Gen* 2018;564:172–82. <https://doi.org/10.1016/j.apcata.2018.07.029>.
- [9] Yoshida R, Sun D, Yamada Y, Sato S, Hutchings GJ. Vapor-phase hydrogenation of levulinic acid to  $\Gamma$ -valerolactone over Cu-Ni bimetallic catalysts. *Catal Commun* 2017;97:79–82. <https://doi.org/10.1016/j.catcom.2017.04.018>.
- [10] López P, Mondragón-Galicia G, Espinosa-Pesqueira ME, Mendoza-Anaya D, Fernández ME, Gómez-Cortés A, et al. Hydrogen production from oxidative steam reforming of methanol: Effect of the Cu and Ni impregnation on ZrO<sub>2</sub> and their molecular simulation studies. *Int J Hydrogen Energy* 2012;37:9018–27. <https://doi.org/10.1016/j.ijhydene.2012.02.105>.
- [11] Torres D, Pinilla JL, Suelves I. Screening of Ni-Cu bimetallic catalysts for hydrogen and carbon nano filaments production via catalytic decomposition of methane. *Appl Catal A, Gen* 2018;559:10–9. <https://doi.org/10.1016/j.apcata.2018.04.011>.
- [12] Yang Z, Liu Y, Li Y, Zeng L, Liu Z, Liu X, et al. Effect of preparation method on the bimetallic NiCu/SAPO-11 catalysts for the hydroisomerization of n-octane. *J Energy Chem* 2019;28:23–30. <https://doi.org/10.1016/j.jechem.2017.10.003>.
- [13] Iriondo A, Mendiguren A, Güemez MB, Requies J, Cambra JF. 2,5-DMF production through hydrogenation of real and synthetic 5-HMF over transition metal catalysts supported on carriers with different nature. *Catal Today* 2017;279:286–95. <https://doi.org/10.1016/j.cattod.2016.02.019>.
- [14] Alamillo R, Tucker M, Chia M, Pagán-torres Y, Dumesic J. Green Chemistry using heterogeneous catalysts † 2012;14. <https://doi.org/10.1039/c2gc35039d>.
- [15] Yang Z, Liu Y, Liu D, Meng X, Liu C. Hydroisomerization of n-octane over bimetallic Ni-Cu/SAPO-11 catalysts. *Appl Catal A Gen* 2017;543:274–82. <https://doi.org/10.1016/j.apcata.2017.06.028>.
- [16] Fu Z, Wang Z, Lin W, Song W, Li S. High efficient conversion of furfural to 2-methylfuran over Ni-Cu/Al<sub>2</sub>O<sub>3</sub> catalyst with formic acid as a hydrogen donor.

- Appl Catal A, Gen 2017;547:248–55.  
<https://doi.org/10.1016/j.apcata.2017.09.011>.
- [17] Li JW, Li T, Ma HF, Sun QW, Ying WY, Fang DY. Effect of nickel on phosphorus modified HZSM-5 in catalytic cracking of butene and pentene. *Fuel Process Technol* 2017;159:31–7. <https://doi.org/10.1016/j.fuproc.2016.06.034>.
- [18] Ye RP, Gong W, Sun Z, Sheng Q, Shi X, Wang T, et al. Enhanced stability of Ni/SiO<sub>2</sub> catalyst for CO<sub>2</sub> methanation: Derived from nickel phyllosilicate with strong metal-support interactions. *Energy* 2019;188:116059. <https://doi.org/10.1016/j.energy.2019.116059>.
- [19] Srivastava S, Jadeja GC, Parikh J. Synergism studies on alumina-supported copper-nickel catalysts towards furfural and 5-hydroxymethylfurfural hydrogenation. *J Mol Catal A Chem* 2017;426:244–56. <https://doi.org/10.1016/j.molcata.2016.11.023>.
- [20] Freitas IC, Manfro RL, Souza MMVM. Applied Catalysis B: Environmental Hydrogenolysis of glycerol to propylene glycol in continuous system without hydrogen addition over Cu-Ni catalysts. *Applied Catal B, Environ* 2018;220:31–41. <https://doi.org/10.1016/j.apcatb.2017.08.030>.
- [21] Kleebusch E, Patzig C, Höche T, Rüssel C. agent - Crystallization and microstructure studied by XRD and ( S ) TEM-EDX 2018;44:19818–24. <https://doi.org/10.1016/j.ceramint.2018.07.239>.
- [22] Jiao Y, Zhang H, Li S, Guo C, Yao P, Wang J. Impact of acidity in ZrO<sub>2</sub>-TiO<sub>2</sub>-Al<sub>2</sub>O<sub>3</sub> composite oxides on the catalytic activity and coking behaviors during n-decane cracking. *Fuel* 2018;233:724–31. <https://doi.org/10.1016/j.fuel.2018.06.011>.
- [23] Goyal R, Sarkar B, Bag A, Siddiqui N, Dumbre D, Lucas N, et al. Studies of synergy between metal – support interfaces and selective hydrogenation of HMF to DMF in water. *J Catal* 2016;340:248–60. <https://doi.org/10.1016/j.jcat.2016.05.012>.



- [24] Ballesteros-Plata D, Infantes-Molina A, Rodríguez-Cuadrado M, Rodríguez-Aguado E, Braos-García P, Rodríguez-Castellón E. Incorporation of molybdenum into Pd and Pt catalysts supported on commercial silica for hydrodeoxygenation reaction of dibenzofuran. *Appl Catal A Gen* 2017;547:86–95. <https://doi.org/10.1016/j.apcata.2017.08.034>.
- [25] Chimentão RJ, Miranda BC, Ruiz D, Gispert-Guirado F, Medina F, Llorca J, et al. Catalytic performance of zinc-supported copper and nickel catalysts in the glycerol hydrogenolysis. *J Energy Chem* 2020;42:185–94. <https://doi.org/10.1016/j.jechem.2019.07.003>.
- [26] El Younsi I, Rhadfi T, Atlamsani A, Quisefit JP, Herbst F, Draoui K. K-10 montmorillonite: An efficient and reusable catalyst for the aerobic CC bond cleavage of  $\alpha$ -substituted ketones. *J Mol Catal A Chem* 2012;363–364:437–45. <https://doi.org/10.1016/j.molcata.2012.07.022>.
- [27] Huang YB, Chen MY, Yan L, Guo QX, Fu Y. Nickel-tungsten carbide catalysts for the production of 2,5-dimethylfuran from biomass-derived molecules. *ChemSusChem* 2014;7:1068–72. <https://doi.org/10.1002/cssc.201301356>.



**CHAPTER 7: Biomass-derived carbon as catalyst support in  
bimetallic Ni-Cu catalysts**

---



## Table of contents

7.1 EXPERIMENTAL .....	183
7.1.1 Catalyst preparation .....	183
7.1.2 Catalyst characterization .....	183
7.1.3 Activity test .....	184
7.2 RESULTS AND DISCUSSION .....	184
7.2.1 Catalyst characterization results .....	184
7.2.1.1 Elemental analysis (CHN) .....	184
7.2.1.2 Chemical and textural properties .....	185
7.2.1.3 Acidic properties .....	186
7.2.1.4 XRD characterization of the catalysts .....	188
7.2.1.5 Morphological characteristics .....	190
7.2.1.6 Surface properties .....	192
7.2.2 Activity results .....	195
7.2.2.1 Monometallic catalysts .....	195
7.2.2.2 Bimetallic catalysts .....	197



In the previous chapter the interaction between Ni and Cu in bimetallic Ni-Cu/ZrO<sub>2</sub> catalysts was investigated. Based on the results observed, carbon supports will be examined in the following chapter. Commercial carbon and biomass-derived carbon will be employed as catalytic support for monometallic Ni and Cu and bimetallic Ni-Cu catalysts.

## 7.1 Experimental

### 7.1.1 Catalyst preparation

Four different supports were prepared. The first two supports were synthesized as explained in Chapter 4 (section 4.1.2.): *Carbon support preparation*, obtaining commercial carbon (CC) and biomass-derived carbon (BC). These supports were employed to synthesize monometallic and bimetallic catalysts. The prepared catalysts were labelled as Ni/CC, Ni/BC, Cu/CC, Cu/BC, Ni-Cu/CC and Ni-Cu/BC.

Additionally, another two supports were synthesized as explained in Chapter 4 (section 4.1.2.): *Carbon support preparation with acidic pretreatment*. The obtained supports were denominated as treated commercial carbon (TCC) and treated biomass-derived carbon (TBC). Due to stability problems detected on monometallic catalysts, these supports with acidic treatment were only employed as supports for the bimetallic catalysts. The obtained catalysts were designated as Ni-Cu/TCC and Ni-Cu/TBC.

### 7.1.2 Catalyst characterization

The physicochemical properties of the samples were analysed by elemental analysis (CHN), Inductively Coupled Plasma Optical Emission Spectroscopy (ICP-OES), N<sub>2</sub>-physisorption, Temperature Programmed Desorption with ammonia (NH<sub>3</sub>-TPD), X-ray Diffraction (XRD), Transmission Electron Microscopy (TEM) and X-ray Photoelectron Spectroscopy (XPS).

Detailed information about the abovementioned characterization techniques are described in section 4.3. of Chapter 4.

### 7.1.3 Activity test

The activity tests were carried out in a continuous fixed-bed reactor following the procedure detailed in section 4.2. of Chapter 4.

## 7.2 Results and discussion

### 7.2.1 Catalyst characterization results

The characterization results obtained by different techniques are described in this section. The supports were firstly thermally treated under an inert atmosphere of N<sub>2</sub> at 500 °C for 2 h to be evaluated at the same conditions as the synthesised catalysts. Moreover, for those techniques at which it was not possible to reduce the catalyst *in situ*, the catalyst was previously reduced at 275 °C for 2 h at a flow of pure H<sub>2</sub>.

#### 7.2.1.1 Elemental analysis (CHN)

**Table 7.1.** Elemental analysis for the carbon supports determined by CHN analyses.

<b>Carbon</b>	<b>C (%)</b>	<b>H (%)</b>	<b>N (%)</b>	<b>O<sup>b</sup> (%)</b>
<b>Commercial carbon<sup>a</sup></b>	80.29	0.85	0.61	18.25
<b>Treated commercial carbon<sup>a</sup></b>	69.83	2.00	0.98	27.19
<b>Biomass-derived carbon<sup>a</sup></b>	77.67	2.61	0.38	19.34
<b>Treated biomass-derived carbon<sup>a</sup></b>	67.76	1.41	0.94	29.89

<sup>a</sup> Bare carbons (without kaolin). <sup>b</sup> Calculated by difference.

The elemental composition of the different bare carbon materials (without the addition of kaolin) obtained from the CHN analyses are summarized in Table 7.1. Oxygen was determined by difference. Commercial and biomass-derived carbon showed similar composition, with a slight difference in H content. In contrast, the



treated commercial and biomass-derived carbon exhibited higher oxygen content, compared to the untreated supports, implying the oxidation of the material [1], probably due to the fact that  $\text{HNO}_3$  is a good oxidation agent. This effect has been previously reported in literature [2].

### 7.2.1.2 Chemical and textural properties

The textural properties determined by  $\text{N}_2$ -physisorption of different supports and catalysts are summarized in Table 7.2 and Table 7.3, respectively.

**Table 7.2.** Textural properties for the thermally treated supports (obtained from  $\text{N}_2$ -physisorption).

<b>Support</b>	<b>BET</b> ( $\text{m}^2/\text{g}$ )	<b>Pore volume</b> (nm)	<b>Average pore diameter</b> (nm)
<b>Commercial carbon</b> (without kaolin)	991	0.05	1.8
<b>Commercial carbon</b>	767	0.01	1.9
<b>Treated commercial carbon</b> (without kaolin)	964	0.04	2.2
<b>Treated commercial carbon</b>	744	0.09	2.4
<b>Biomass-derived carbon</b> (without kaolin)	977	0.47	3.5
<b>Biomass-derived carbon</b>	715	0.11	2.5
<b>Treated biomass-derived carbon</b> (without kaolin)	912	0.47	3.6
<b>Treated biomass-derived carbon</b>	482	0.29	4.0
<b>Kaolin</b>	18	0.09	21.6

The commercial and biomass-derived carbons (without kaolin) exhibited comparable BET surface areas (higher than  $970 \text{ m}^2/\text{g}$ ). However, biomass-derived carbon showed higher pore volume and pore diameter. In both materials, the acidic treatment did not alter significantly the textural properties. Lastly, the addition of kaolin reduced the total surface area, which may be related to the poor surface area observed for the bare kaolin ( $18 \text{ m}^2/\text{g}$ ).

The monometallic catalysts showed a decrease in the specific surface area (ranged from 240 to 310 m<sup>2</sup>/g) when compared with the supports, most probably as a consequence of a partial blockage of the support's pores by metal deposition [3]. This effect is more remarkable in the case of the bimetallic catalysts (120-190 m<sup>2</sup>/g), associated to the higher metal loading of these catalysts, involving larger obstruction of the porous structure. This was also observed by Andrade et al. [4]. In general, catalysts supported on the biomass-derived carbon showed lower BET surface area. This trend was more noticeable for the monometallic catalysts.

**Table 7.3.** Chemical and textural properties for the monometallic and bimetallic catalysts.

Catalyst	BET <sup>a</sup> (m <sup>2</sup> /g)	Pore volume <sup>a</sup> (nm)	Average pore diameter <sup>a</sup> (nm)	Cu <sup>b</sup> (%)	Ni <sup>b</sup> (%)
Ni / CC	309	0.09	3.1	-	15
Ni / BC	241	0.12	3.6	-	16
Cu / CC	282	0.06	2.7	15	-
Cu / BC	311	0.19	4.1	15	-
Ni-Cu / CC	143	0.05	3.3	21	23
Ni-Cu / TCC	190	0.04	2.8	16	16
Ni-Cu / BC	135	0.08	3.8	22	22
Ni-Cu / TBC	119	0.05	3.4	14	17

Obtained from <sup>a</sup> N<sub>2</sub>-physisorption and <sup>b</sup> ICP-OES.

The real metal contents of the catalysts, studied by ICP-OES (see Table 7.3), were similar to the nominal ones, except for bimetallic catalysts supported in non pretreated carbons. The higher carbon concentration of these supports, determined in CHN analysis, could favour the metal deposition. The catalysts were thermally treated, firstly after the deposition of Cu and then after the deposition of Ni. These two thermal treatments implied some thermal decomposition of part of the carbon, resulting in higher metal loading than the nominal one.

### 7.2.1.3 Acidic properties

The surface acidity of the bare supports and catalysts was investigated by the NH<sub>3</sub>-TPD characterization technique. The results are summarized in Figure 7.1.

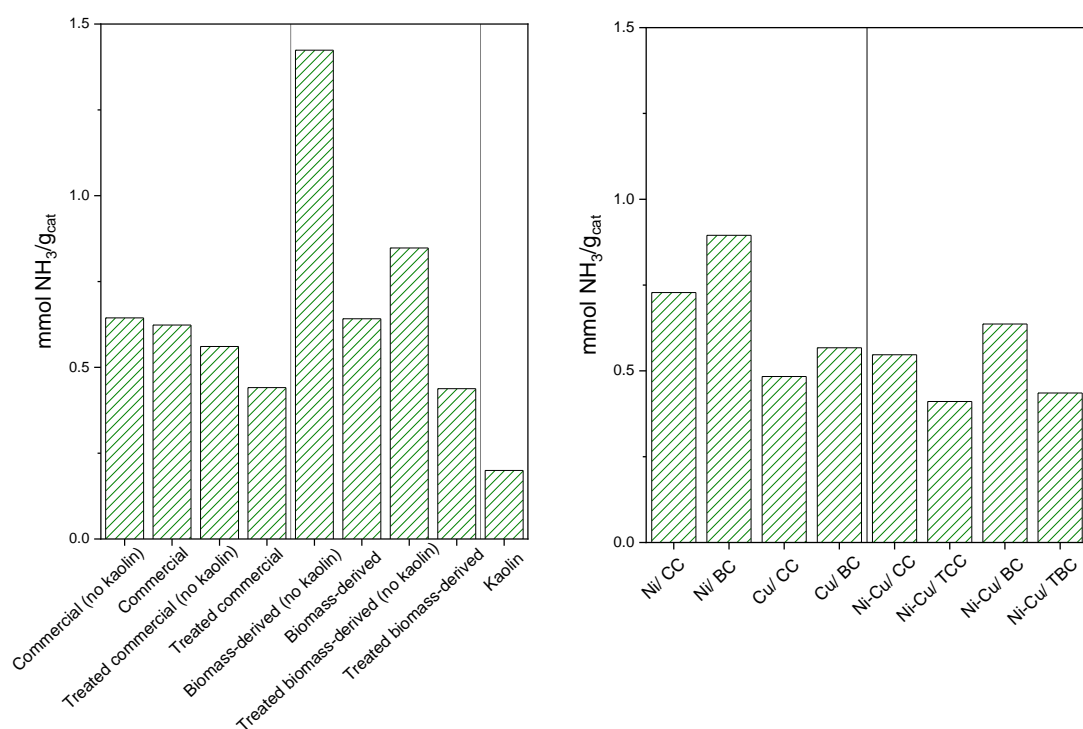


**Figure 7.1.** Amoun of NH<sub>3</sub> desorbed in NH<sub>3</sub>-TPD for the different thermally treated supports and catalysts.

The commercial carbon without kaolin exhibited a lower acidity compared to the biomass-derived carbon in absence of kaolin. The addition of kaolin decreased significantly the acidity of the biomass-derived carbon [5], probably due to the fact that bare kaolin presented a low acidity. Moreover, the treatment decreased the acidity of both commercial and biomass-derived carbons. It is important to remark that even if the difference in the acidity of pure commercial (0.64 mmol NH<sub>3</sub>/g<sub>cat</sub>) and biomass-derived carbon (1.42 mmol NH<sub>3</sub>/g<sub>cat</sub>) is significant, after the impregnation of kaolin the acidity is almost identical in both carbons (0.62 and 0.64, respectively). A similar effect was observed with the treated carbons, where the addition of kaolin involved final similar acidities, around 0.44 mmol NH<sub>3</sub>/g<sub>cat</sub>.

The impregnation of Ni in the supports enhanced the acidity of the monometallic catalysts. It has been extensively reported that the non-reduced Ni<sup>+2</sup> species act as Lewis acid sites, increasing the total acidity of the catalyst [6,7]. The higher acidity of the catalyst supported on biomass-derived carbon is in good agreement with the results observed in XPS (explained below) where a larger content of Ni<sup>+2</sup> was observed on the catalyst surface, involving an increase in the acidity. By contrast, the monometallic copper catalysts exhibited lower acidities than the supports. Cu particles

could be covering or could have reacted with the acidic sites, reducing the total acidity of these catalysts [4].

The bimetallic catalyst showed similar acidities than the supports. Presumably, even if some acidic sites were covered by metallic species, the presence of nickel cations implied the existence of Lewis acid sites, which compensated the loss of the original supports acid sites [8,9].

#### 7.2.1.4 XRD characterization of the catalysts

The X-ray diffraction patterns of the fresh reduced and used catalysts are depicted in Figure 7.2 for monometallic catalysts and and Figure 7.3 for bimetallic catalysts. Moreover, the average crystallite size of the metallic phases, calculated by Scherrer equation, are summarized in Table 7.4.

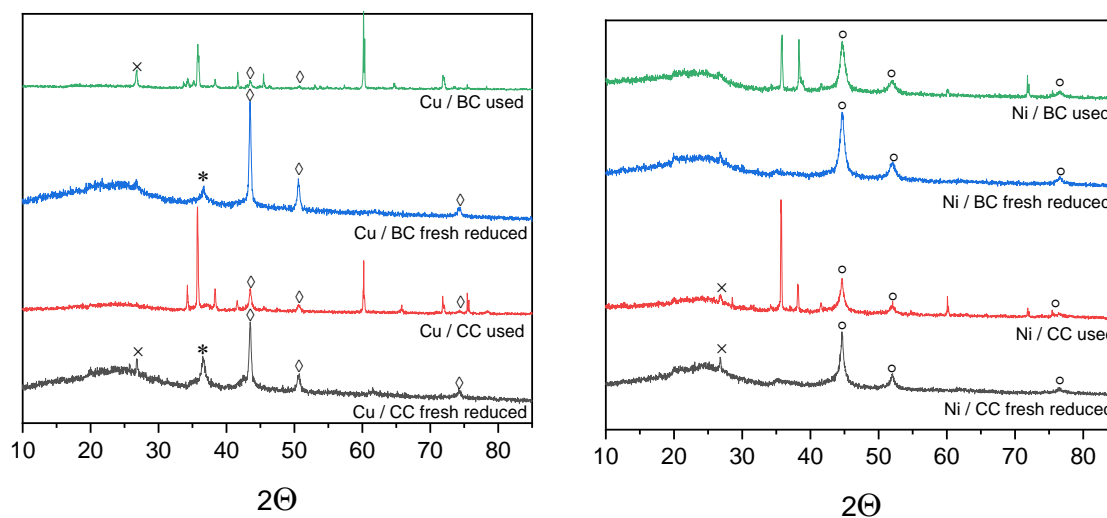


**Figure 7.2.** XRD patterns for the monometallic catalysts ( $\times$  C,  $\ast$   $\text{Cu}_2\text{O}$ ,  $\diamond$   $\text{Cu}^0$ ,  $\circ$   $\text{Ni}^0$ ).

The diffraction patterns of monometallic nickel catalysts displayed diffraction peaks at  $2\theta = 44.5^\circ$ ,  $51.8^\circ$  and  $76.4^\circ$ , ascribed to metallic Ni [10]. Similarly, Cu based catalysts exhibited diffraction peaks at  $2\theta = 43.3^\circ$ ,  $50.4^\circ$  and  $74.1^\circ$ , attributed to metallic Cu [10]. The catalyst supported on commercial carbon exhibited a lower crystallite size, implying a better dispersion of Cu on this support. The nickel based monometallic catalysts presented a lower crystallite size than the Cu based catalysts [11]. After

reaction, all the monometallic catalysts exhibited similar crystallite size to the initial ones, revealing a good stability of the metallic phases in these catalysts.

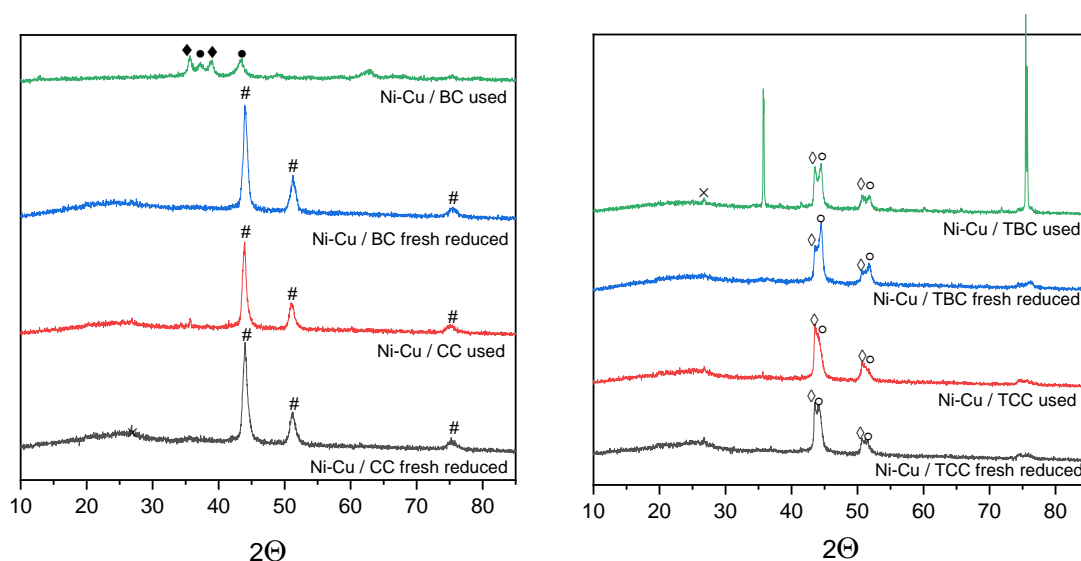


**Figure 7.3.** XRD pattern for the bimetallic catalysts (x C, # NiCu,  $\diamond$  Cu<sup>0</sup>,  $\blacklozenge$  CuO,  $\circ$  Ni<sup>0</sup>,  $\bullet$  NiO).

**Table 7.4.** Crystallite size (nm) for the monometallic and bimetallic catalysts.

Catalyst	Fresh reduced		Used	
	Ni	Cu	Ni	Cu
Ni / CC	20	-	20	-
Ni / BC	15	-	10	-
Cu / CC	-	40	-	35
Cu / BC	-	45	-	45
Ni-Cu / CC	10 <sup>a</sup>		15 <sup>a</sup>	
Ni-Cu / TCC	10	30	10	35
Ni-Cu / BC	15 <sup>a</sup>		5 (NiO)	15 (CuO)
Ni-Cu / TBC	15	20	15	25

<sup>a</sup>Ni-Cu crystallites

The bimetallic catalysts exhibited peaks among the diffraction peaks of Ni and Cu (as can be observed in Figure 7.4), evidencing a possible interaction of the metals. The catalysts supported on the non-treated carbon exhibited a homogeneous peak ascribed to Ni-Cu crystals with small crystallites of 10-15 nm. In the case of the bimetallic catalysts supported on treated carbon, two peaks can be identified,

attributed to an alloy richer in Cu and an alloy richer in Ni. In this samples, the alloy richer in Cu presented larger crystallite size (20-30 nm), that increased during the reaction, which is probably attributable to the sintering effect during the reaction. On the contrary, the alloy richer in Ni exhibited stable crystallites of 10-15 nm. The evidence of two different Ni-Cu alloys in the catalyst has been previously reported [4,12]. It should be remarked that even if there are two peaks, they are located at an intermediate position, implying the formation of Ni-Cu alloy and not crystals of pure Ni and pure Cu.

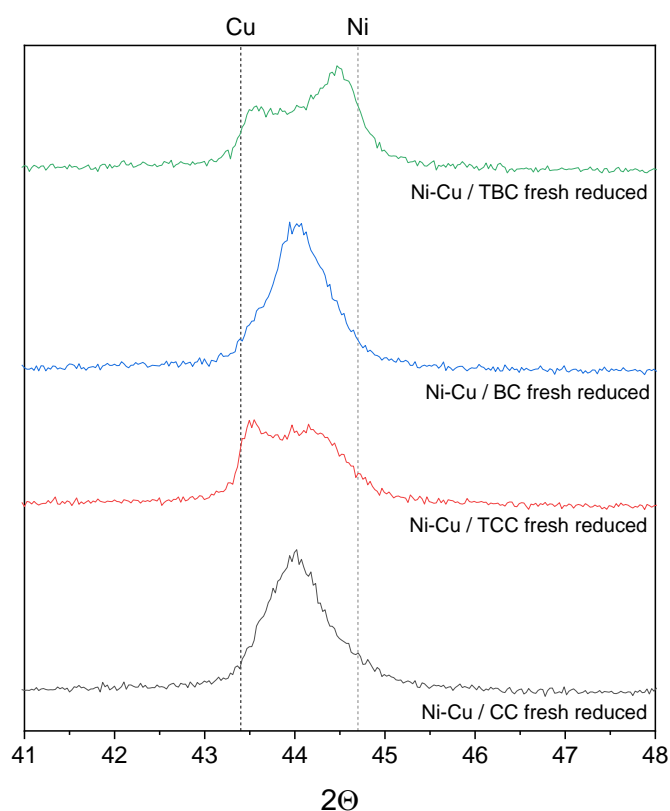


**Figure 7.4.** XRD patterns for the fresh reduced bimetallic catalysts (enlarged graph).

### 7.2.1.5 Morphological characteristics

The morphology, size and dispersion of the metallic particles of the most interesting catalysts were investigated by TEM. The dispersion and mean particle size were calculated according to the procedure described by Borodziński and Bonarowska [13] and are summarized in Table 7.5. Additionally, the corresponding histograms and profiles of the accumulated frequencies are displayed in Figure 7.5.

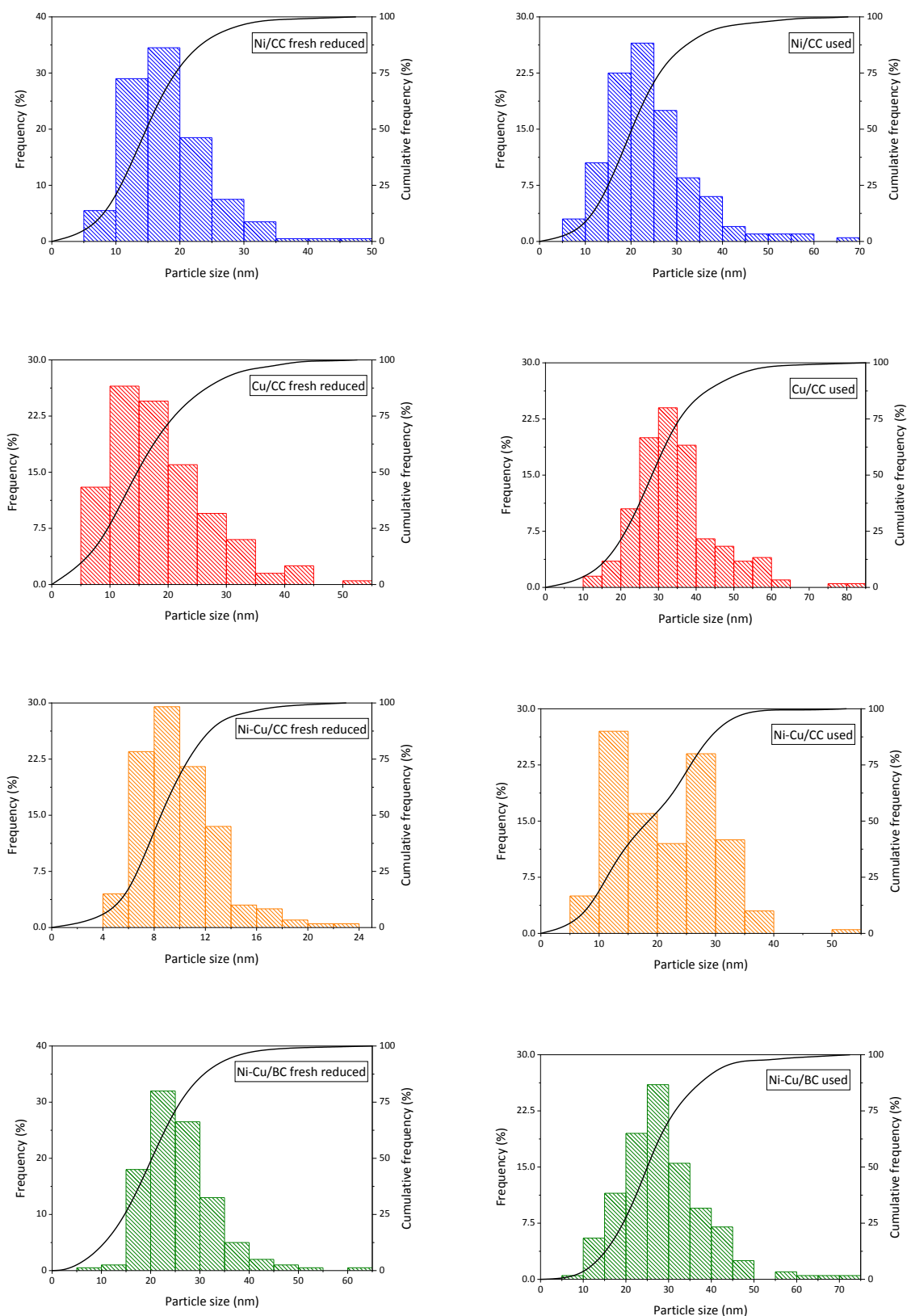


**Figure 7.5.** Particle size distribution (histograms) and cumulative frequency profiles for the fresh reduced and used catalysts.

The monometallic Ni and Cu catalysts exhibited similar dispersion and particle size in the fresh reduced samples. However, the particle size was enlarged during the reaction, decreasing the total dispersion of these catalysts. The increase on the size could be related to the sintering of metallic particles. This effect was more evident in the case of the Cu/CC catalyst.

In the case of the bimetallic catalysts, there is a noticeable difference in the dispersion and particle size of fresh reduced catalyst supported on the commercial and biomass-derived carbon. It seems that commercial carbon is able to disperse more efficiently the particles, increasing the active metal exposition on the surface. Nevertheless, the particle grew along the reaction in the case of the bimetallic catalyst supported on commercial carbon, implying a reduction of the dispersion in this this catalyst.

**Table 7.5.** Dispersion and metallic particle size for the most relevant fresh reduced and used catalysts.

Catalyst		Dispersion (%)	$d_{\text{mean}}$ (nm)
Ni / CC	Fresh reduced	5	23
	Used	4	32
Cu / CC	Fresh reduced	5	26
	Used	3	42
Ni-Cu / CC	Fresh reduced	11	12
	Used	5	27
Ni-Cu / BC	Fresh reduced	4	30
	Used	3	36

#### 7.2.1.6 Surface properties

The elemental composition (see Table 7.6) and oxidation state (see Table 7.7) of the catalysts before (fresh reduced) and after (used) the reaction were examined by the XPS technique. The carbon content increased in all the used catalysts, probably due to coke deposition on the surface during the reaction, which can imply a deactivation of the catalysts.



**Table 7.6.** Elemental composition for the monometallic and bimetallic catalysts.

Catalyst		C	Ni	Cu	Ni/Cu	Others <sup>a</sup>
Ni / CC	Fresh reduced	30.2	27.7	-	-	42.1
	Used	37	21.2	-	-	41.8
Ni / BC	Fresh reduced	28.5	4.5	-	-	67.0
	Used	31.3	4.8	-	-	64.1
Cu / CC	Fresh reduced	31.6	-	18.5	-	49.9
	Used	46.1	-	11.7	42.2	
Cu / BC	Fresh reduced	35.1	-	9.8	-	55.1
	Used	49.7	-	10.1	-	40.2
Ni-Cu / CC	Fresh reduced	13.0	21.4	19.2	1.1	46.4
	Used	18.3	23.4	10.1	2.3	48.2
Ni-Cu / TCC	Fresh reduced	14.4	25.6	10.7	2.4	49.3
	Used	23.4	21.0	11.1	1.9	44.5
Ni-Cu / BC	Fresh reduced	24.1	23.6	8.9	2.7	43.4
	Used	39.5	19.9	7.8	2.6	32.8
Ni-Cu / TBC	Fresh reduced	46.3	10.3	3.1	3.3	40.3
	Used	53.7	8.6	4.0	2.1	33.7

<sup>a</sup>Others: O, Al, Si.

The surface metal content in the monometallic catalysts was higher when the commercial carbon was employed as support. The higher BET surface area observed with the N<sub>2</sub>-physisorption technique and the higher C content in this support detected in the CHN analysis could be favouring the higher deposition of the active phase on the catalyst surface. In the case of the catalysts supported on the commercial carbon, the metallic content decreased after reaction, possibly as a result of coke deposition on the metallic sites, and also probably due to metal particles sintering on the surface, although the average particle size measure by XRD does not change significantly. This is in good agreement with the results obtained by the TEM technique.

The bimetallic catalysts supported on the treated biomass-derived carbon exhibited lower surface metal contents, probably resulting from a decrease of the metallic particles dispersion, involving poorer metal contents on the surface. In general, the metal contents of the bimetallic catalysts declined after the reaction. This was presumably caused by coke deposition and by the sintering. The ratio of Ni/Cu was higher than the bulk ratio obtained in ICP-OES results, suggesting an enrichment of Ni

in the catalysts surface, an effect that has been previously observed [10]. The impregnation of Ni in the second step could favour the higher exposition of this metal on the surface.

**Table 7.7.** Oxidation state of Ni and Cu for the monometallic and bimetallic catalysts.

Catalyst		Ni <sup>0</sup> / (Ni <sup>0</sup> + Ni <sup>2+</sup> )	Cu <sup>0</sup> / (Cu <sup>0</sup> + Cu <sup>1+</sup> + Cu <sup>2+</sup> )
Ni / CC	Fresh reduced	0.84	-
	Used	0.70	-
Ni / BC	Fresh reduced	0.41	-
	Used	0.71	-
Cu / CC	Fresh reduced	-	0.58
	Used	-	0.10
Cu / BC	Fresh reduced	-	0.24
	Used	-	0.56
Ni-Cu / CC	Fresh reduced	0.80	0.27
	Used	0.30	0.51
Ni-Cu / TCC	Fresh reduced	0.69	0.36
	Used	0.47	0.49
Ni-Cu / BC	Fresh reduced	0.19	0.22
	Used	0.22	0.22
Ni-Cu / TBC	Fresh reduced	0.40	0.29
	Used	0.39	0.25

To understand the oxidation state of nickel and copper, the ratio of Ni<sup>0</sup> or Cu<sup>0</sup> to the total metal content was studied. In monometallic catalysts supported on the commercial carbon elevated Ni<sup>0</sup> or Cu<sup>0</sup> contents were observed. They decreased after the reaction, indicating some oxidation of the metallic particles. The water generated as by-product or the solvent (1-butanol) could be favouring this oxidation of the metallic species [14]. On the contrary, the catalysts supported on the biomass-derived carbon exhibited lower Ni<sup>0</sup> or Cu<sup>0</sup> contents, but these contents were increased during the reaction, involving a reduction of the oxide species. This can be assigned to an easier reducibility due to a lower interaction with the support in the H<sub>2</sub>-rich atmosphere.

The bimetallic catalysts supported on the commercial carbon showed high Ni<sup>0</sup> and Cu<sup>0</sup> contents. After reaction, Ni was oxidized and conversely, Cu was reduced. On the

contrary, catalyst supported on biomass-derived carbon presented low metallic contents, which remained almost identical after the reaction. In general, it seems that if there is a high exposition of reduced species in the catalyst surface, some species are oxidized during the reaction.

It is important to highlight that the oxide phases detected in XPS was not observed in the XRD results, except for the bimetallic catalyst supported on biomass-derived carbon. This fact indicates that the oxide species were highly dispersed on the catalyst surface [12,15].

## 7.2.2 Activity results

In all the studied catalysts the achieved HMF conversion was 100 % under the operating conditions of 275 °C and 15 bar of H<sub>2</sub> (WHSV = 0.15 h<sup>-1</sup>). The objective was to study the desired products yields along the time-on-stream.

The acidity is an important property in this reaction. High acidity can promote C—C cleavage encouraging ring opening products [16]. This effect needs to be avoided. However, it has been reported that acidic sites can promote the activation of carbonyl group and favour the hydrogen transfer reaction [17,18]. Therefore, a controlled surface acidity is crucial in this process.

### 7.2.2.1 Monometallic catalysts

The activity results of the monometallic catalysts are summarized in Figure 7.6. Ni based catalysts exhibited high yields of DMTHF at the beginning of the reaction. However, this production was reduced after 5 h of reaction, enhancing the production of DMF. Ni<sup>0</sup> on surface seems to be responsible of the hydrogenation of C=C bond, producing DMTHF. This nickel tends to oxidize during the reaction, possibly losing the hydrogenating capacity. Therefore, at the end of the reaction, the obtained product was DMF. On the contrary, Cu based catalysts were not able to produce DMTHF.

In general, the catalysts impregnated in the commercial carbon were more active in the production of the desired products at the beginning of the reaction. This fact could be explained by the higher metallic content observed on the surface of this catalysts. Moreover, the lower acidity could favour the prevention of C—C cleavage, avoiding ring-opening products and favouring the production DMF and DMTHF.

All the monometallic catalysts exhibited deactivation problems, except the Ni/BC. This effect was more pronounced in the case of Cu based catalysts. Probably, the sintering effect observed in the TEM images (which was more evident in the case of Cu/CC) and coke deposition observed in the XPS results could be responsible of the deactivation of these catalysts.

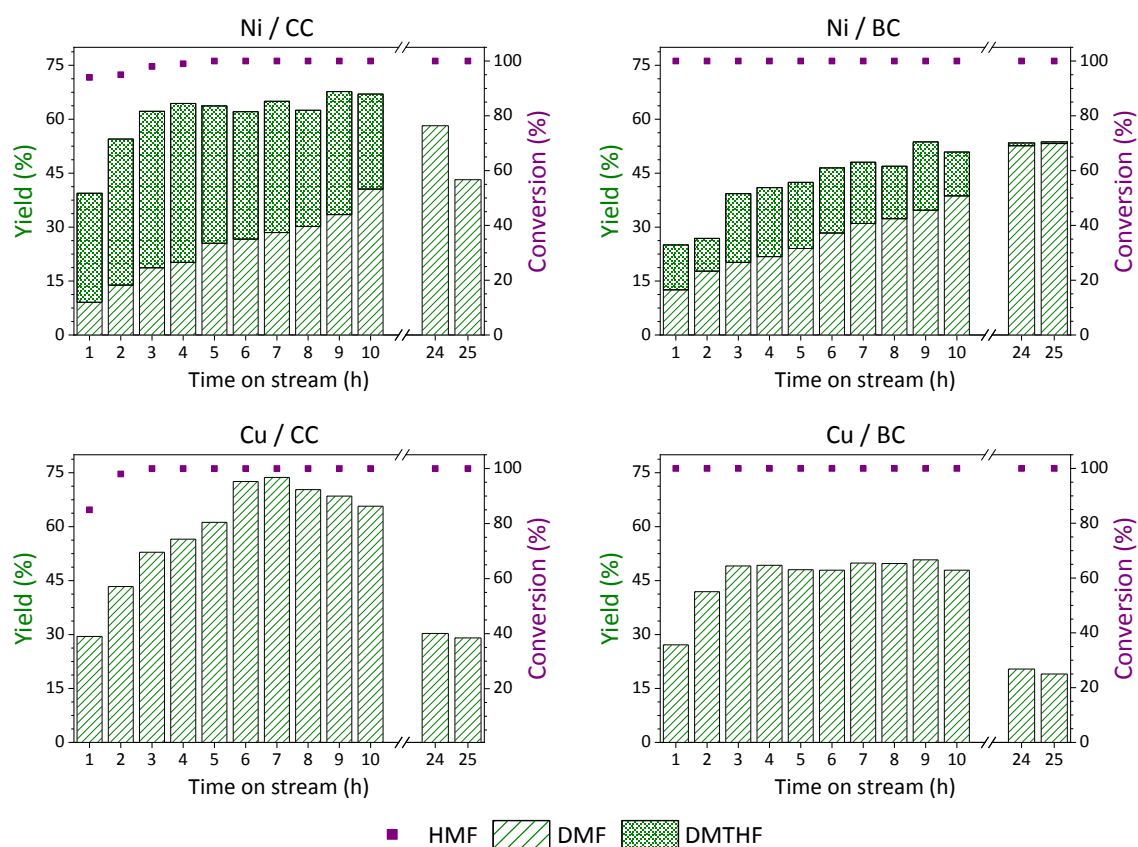


**Figure 7.6.** Conversion and yield for the monometallic catalysts (operating conditions: T = 275 °C and P<sub>H<sub>2</sub></sub> = 15 bar)

## 7.2.2.2 Bimetallic catalysts

The obtained HMF conversion and DMF-DMTHF yields when using bimetallic catalysts are outlined in Figure 7.7. In general, there is no significant difference between catalysts supported on non-treated and treated carbons. This can be considered as a positive aspect, implying an easier synthesis of the catalyst, avoiding the previous treatment of the support. Moreover, bimetallic catalysts exhibited better stability than the corresponding monometallic catalysts, probably due to the interaction between the Ni and Cu metals [14].

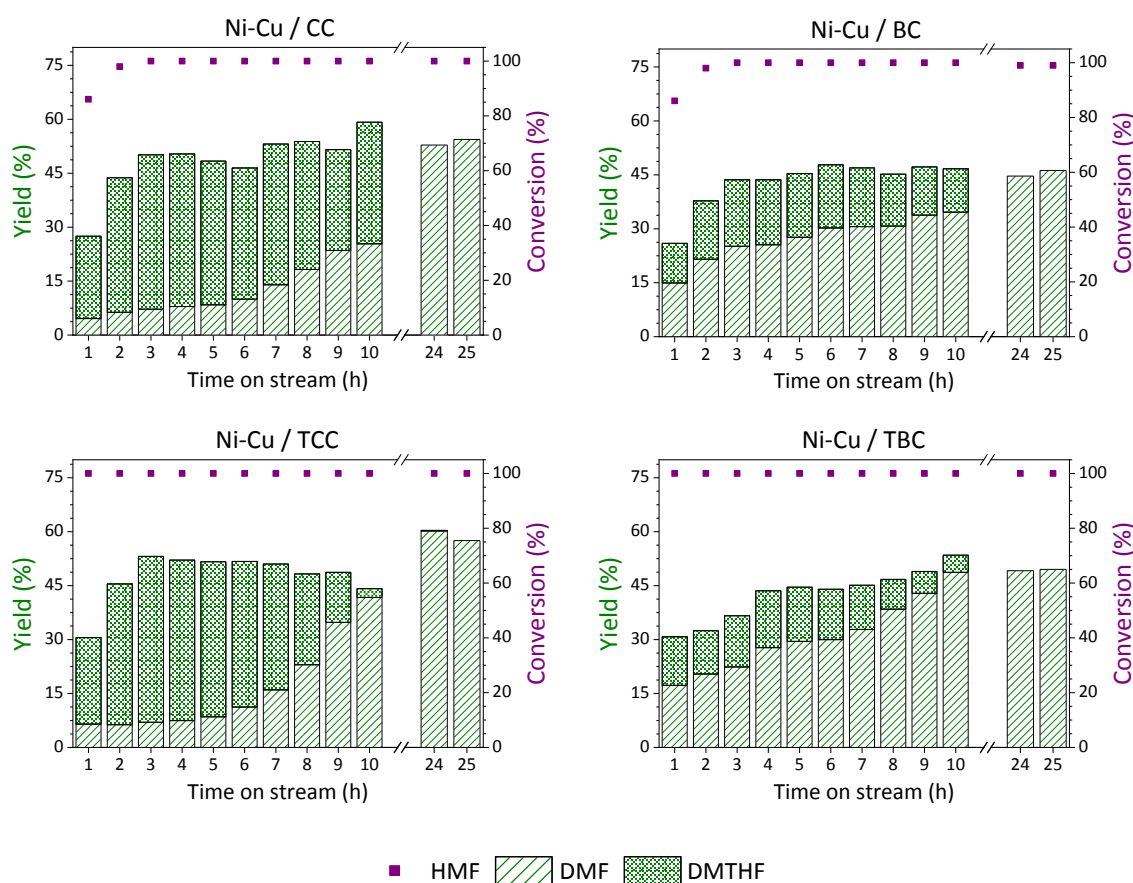


**Figure 7.8.** Conversion and yield for the bimetallic catalysts (operating conditions:  $T = 275\text{ }^{\circ}\text{C}$  and  $P_{\text{H}_2} = 15\text{ bar}$ )

The catalysts supported on commercial carbon exhibited higher production rate of the desired DMF and DMTHF, probably due to their higher metal content observed in the surface of the catalysts by XPS and their higher dispersion calculated from TEM images.

Moreover, a higher DMTHF yield was detected in these catalysts, which may be related to the metallic Ni<sup>0</sup> available on the catalyst surface. Even if at the beginning of the reaction catalysts supported on commercial carbon exhibited better catalytic performance, the results at the end of the reaction time tested (25 h) were similar for all the bimetallic catalysts, exhibiting reasonable stability and achieving a DMF yield around 50 % in all the cases. This is in good agreement with the observed results from the TEM images, where similar particle size and dispersion were detected after the reaction for all the bimetallic catalysts.

The loss of the catalytic production of DMTHF of catalysts supported on commercial carbon during the reaction has been previously reported [14]. This effect was related to the oxidation of Ni<sup>0</sup> during the reaction, missing the hydrogenating capacity of the furan ring, therefore producing DMF. This is in good agreement with the XPS results, where the catalysts supported on commercial carbon exhibited the oxidation of Ni after reaction.

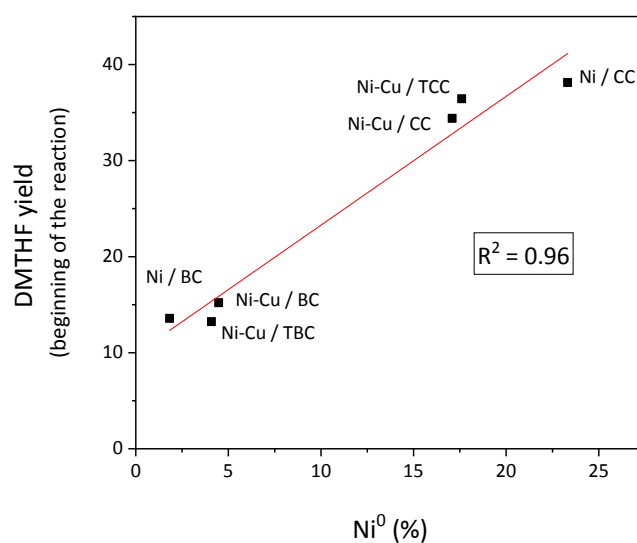


**Figure 7.9.** Relation between DMTHF production at the beginning of the reaction and the metallic Ni content on the catalyst surface.

The relation between the DMTHF production at the beginning of the reaction (average yield of DMTHF during the first 3 h of reaction) and the metallic Ni content on fresh reduced catalyst surface (calculated from the total Ni amount and the Ni<sup>0</sup> ratio) was plotted in Figure 7.8. It can be observed that there is a linear and positive correlation between both parameters. Moreover, it is clear that the catalysts supported on

commercial carbon exhibited an elevated Ni<sup>0</sup> content on the surface, producing higher DMTHF at the beginning of the reaction. The higher metallic Ni<sup>0</sup> content could be related to the interaction between metal and support, enhancing the exposition and the stability of the metal.

Moreover, the metallic Cu on the surface seems to be important in the total production of DMF and DMTHF during the first stage of the reaction. There is a strong correlation between the metallic Cu content on the surface and the total mean production of DMF and DMTHF during the first 10 h of reaction (see Figure 7.9). It seems that metallic content of both Cu and Ni are important for the hydrogenolysis of HMF. Cu<sup>0</sup> involves high hydrogenolysis to desired products, while Ni<sup>0</sup> enhances the hydrogenation of C=C bond, obtaining higher DMTHF yield.

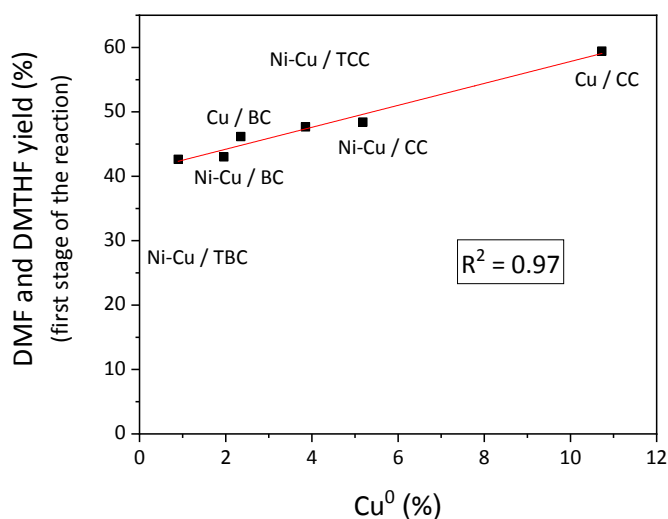


**Figure 7.10.** Relation between DMF and DMTHF mean production at the first stage of the reaction and the metallic Cu content on the catalyst surface.

In general, the reached conversion of HMF in all the tested catalysts was 100 %. The complete conversion permitted the comparison of the total yield of desired products obtained by different catalysts. However, this condition can limit the interpretation of the deactivation of the catalysts.

The bimetallic catalysts, regardless of the support, showed a better balance of the acid sites and the metallic sites (Ni-Cu active species) to end with stable operation. DMF

yield above 50 % was reached after 25 hours-on-stream in all the bimetallic catalysts. For further stability tests, it should be taken into account the coke deposition observed in all the catalyst.

The monometallic nickel catalysts were able to produce DMTHF. Conversely, Cu based catalysts were not able to produce DMTHF. This implied the need of Ni to hydrogenate the C=C bond. In general, monometallic catalysts showed high yields to desired products at the beginning of the reaction. However, they were deactivated (except Ni/BC), probably due to the sintering of metallic active sites. This effect was more severe in the case of copper based catalysts.

The commercial carbon exhibited higher Ni and/or Cu surface content and Ni<sup>0</sup> and/or Cu<sup>0</sup> surface content than the biomass-derived carbon. This involved higher yields of desired products at the beginning of the reaction. However, similar results were obtained with both supports after 25 hours-on-stream.

Lastly, it is important to remark that the metallic content of Cu presented a strong relation with the total production of DMF and DMTHF at the first phase of the reaction. Similarly, metallic Ni is correlated with the hydrogenation capacity of C=C bond of the catalyst.



**References**

- [1] Matos I, Neves PD, Castanheiro JE, Perez-Mayoral E, Martin-Aranda R, Duran-Valle C, et al. Mesoporous carbon as an efficient catalyst for alcoholysis and aminolysis of epoxides. *Appl Catal A Gen* 2012;439–440:24–30. <https://doi.org/10.1016/j.apcata.2012.06.036>.
- [2] Brazil TR, Junior MSO, Baldan MR, Massi M, Rezende MC. Effect of different superficial treatments on structural, morphological and superficial area of Kraft lignin based charcoal. *Vib Spectrosc* 2018;99:130–6. <https://doi.org/10.1016/j.vibspec.2018.08.021>.
- [3] Pastor-Pérez L, Gu S, Sepúlveda-Escribano A, Reina TR. Bimetallic Cu–Ni catalysts for the WGS reaction – Cooperative or uncooperative effect? *Int J Hydrogen Energy* 2019;44:4011–9. <https://doi.org/10.1016/j.ijhydene.2018.12.127>.
- [4] de Andrade TS, Souza MMVM, Manfro RL. Hydrogenolysis of glycerol to 1,2-propanediol without external H<sub>2</sub> addition in alkaline medium using Ni-Cu catalysts supported on Y zeolite. *Renew Energy* 2020;160:919–30. <https://doi.org/10.1016/j.renene.2020.06.060>.
- [5] Du X, Kong X, Chen L. Influence of binder on catalytic performance of Ni/HZSM-5 for hydrodeoxygenation of cyclohexanone. *Catal Commun* 2014;45:109–13. <https://doi.org/10.1016/j.catcom.2013.10.042>.
- [6] Li FX, Wang XF, Zheng Y, Chen JX. Influence of metallic promoters on the performance of Ni/SiO<sub>2</sub> catalyst in the hydrodeoxygenation of anisole. *Ranliao Huaxue Xuebao/Journal Fuel Chem Technol* 2018;46:75–83. [https://doi.org/10.1016/s1872-5813\(18\)30005-7](https://doi.org/10.1016/s1872-5813(18)30005-7).
- [7] Wang X, Chen J. Effects of indium on Ni/SiO<sub>2</sub> catalytic performance in hydrodeoxygenation of anisole as model bio-oil compound: Suppression of benzene ring hydrogenation and C-C bond hydrogenolysis. *Cuihua Xuebao/Chinese J Catal* 2017;38:1818–30. [https://doi.org/10.1016/S1872-2067\(17\)62910-3](https://doi.org/10.1016/S1872-2067(17)62910-3).

- [8] Yang Z, Liu Y, Liu D, Meng X, Liu C. Hydroisomerization of n-octane over bimetallic Ni-Cu/SAPO-11 catalysts. *Appl Catal A Gen* 2017;543:274–82. <https://doi.org/10.1016/j.apcata.2017.06.028>.
- [9] Li X, Xiang M, Wu D. Hydrogenolysis of glycerol over bimetallic Cu–Ni catalysts supported on hierarchically porous SAPO-11 zeolite. *Catal Commun* 2019;119:170–5. <https://doi.org/10.1016/j.catcom.2018.11.004>.
- [10] Liu H, Huang Z, Kang H, Li X, Xia C, Chen J, et al. Efficient bimetallic NiCu-SiO<sub>2</sub> catalysts for selective hydrogenolysis of xylitol to ethylene glycol and propylene glycol. *Appl Catal B Environ* 2018;220:251–63. <https://doi.org/10.1016/j.apcatb.2017.08.022>.
- [11] Gupta D, Kumar R, Pant KK. Hydrotalcite supported bimetallic (Ni-Cu) catalyst: A smart choice for one-pot conversion of biomass-derived platform chemicals to hydrogenated biofuels. *Fuel* 2020;277:118111. <https://doi.org/10.1016/j.fuel.2020.118111>.
- [12] Freitas IC, Manfro RL, Souza MMVM. Hydrogenolysis of glycerol to propylene glycol in continuous system without hydrogen addition over Cu-Ni catalysts. *Appl Catal B Environ* 2018;220:31–41. <https://doi.org/10.1016/j.apcatb.2017.08.030>.
- [13] Borodziński A, Bonarowska M. Relation between crystallite size and dispersion on supported metal catalysts. *Langmuir* 1997;13:5613–20. <https://doi.org/10.1021/la962103u>.
- [14] Viar N, Requies JM, Agirre I, Iriondo A, Gil-Calvo M, Arias PL. Ni-Cu Bimetallic Catalytic System for Producing 5-Hydroxymethylfurfural-Derived Value-Added Biofuels. *ACS Sustain Chem Eng* 2020;8:11183–93. <https://doi.org/10.1021/acssuschemeng.0c02433>.
- [15] Cai F, Pan D, Ibrahim JJ, Zhang J, Xiao G. Hydrogenolysis of glycerol over supported bimetallic Ni/Cu catalysts with and without external hydrogen addition in a fixed-bed flow reactor. *Appl Catal A Gen* 2018;564:172–82.

<https://doi.org/10.1016/j.apcata.2018.07.029>.

- [16] Zhou CH, Deng K, Serio M Di, Xiao S, Tong DS, Li L, et al. Cleaner hydrothermal hydrogenolysis of glycerol to 1,2-propanediol over Cu/oxide catalysts without addition of external hydrogen. *Mol Catal* 2017;432:274–84. <https://doi.org/10.1016/j.mcat.2017.02.008>.
- [17] Zhang J, Chen T, Jiao Y, Wang L, Wang J, Chen Y, et al. Role of acidity in catalytic cracking of n-decane over supported Pt-based catalysts. *Appl Surf Sci* 2020;507:145113. <https://doi.org/10.1016/j.apsusc.2019.145113>.
- [18] Zhu Y, Kong X, Zheng H, Ding G, Zhu Y, Li YW. Efficient synthesis of 2,5-dihydroxymethylfuran and 2,5-dimethylfuran from 5-hydroxymethylfurfural using mineral-derived Cu catalysts as versatile catalysts. *Catal Sci Technol* 2015;5:4208–17. <https://doi.org/10.1039/c5cy00700c>.



## **CHAPTER 8: Conclusions**

---



In the current PhD thesis, an exhaustive study of different catalytic systems for the hydrogenolysis of HMF has been carried out. After a preliminary study of Cu/ZrO<sub>2</sub> based catalyst modification, a deeper study of bimetallic Ni-Cu/ZrO<sub>2</sub> catalysts has been carried out, implying the understanding of the possible interaction of the non-noble active metals. Lastly, the use of biomass-derived carbon was studied as catalyst support.

In this Chapter 8, the most significant conclusions achieved in this PhD dissertation will be summarized.

### **Cu/ZrO<sub>2</sub> based heterogeneous catalysts screening.**

The main objective of this work was to study the effects of different possible modifications of Cu/ZrO<sub>2</sub> based catalyst on the activity of HMF hydrogenolysis towards DMF and DMTHF. The main conclusions achieved can be summarized as follows:

1. 275 °C and 15 bar of H<sub>2</sub> pressure were selected as the most suitable operating conditions. Moreover, there was no need of a previous reduction step of the catalyst before the reaction.
2. Elevated Cu loading (45 wt %) implied lower dispersion of the metallic species, reducing the catalytic activity. 15 wt % of copper was selected as the optimum loading, reaching a maximum DMF yield of 25 % after 6 h on stream.
3. The incorporation of CeO<sub>2</sub> to the support did not have the desired effect: it did not enhance the production of desired products. The reason for this could be that wetness impregnation method did not incorporate ceria on ZrO<sub>2</sub> efficiently.
4. The incorporation of Ru in CuZr implied the production of DMTHF, probably due to the higher hydrogenation capacity of this noble metal. The ruthenium slightly improved the catalytic production of the desired products, reaching a total yield of 30 % of DMF and DMTHF after 3 hours-on-stream. However, it was deactivated, possibly due to Cu sintering and coke deposition. Therefore, the Ru incorporation did not improve the catalytic activity of the catalyst.

5. The use of bimetallic Ni-Cu/ZrO<sub>2</sub> catalyst, prepared in a single co-impregnation step, allowed achieving high yields of the desired products, especially DMTHF. The maximum yield was achieved after 4 hours-on-stream, with a total yield of DMF and DMTHF over 50 %. Cu and Ni interaction observed in the XRD and H<sub>2</sub>-TPR results could be the reason why the hydrogenolysis reaction was favoured.

#### **The role of Ni and Cu interaction on the bimetallic Ni-Cu/ZrO<sub>2</sub> catalytic system.**

This work proved that bimetallic Ni-Cu/ZrO<sub>2</sub> enhanced the hydrogenolysis of HMF to desired DMF and DMTHF, comparing with their monometallic counterparts. Moreover, the relevance of the impregnation method was evidenced, involving the modification of the physicochemical characteristics of the catalysts and thus, the activity results. The main conclusions attained are the following ones:

6. The use of bimetallic catalysts involved higher production of DMF and DMTHF, possibly due to the interaction between Ni and Cu. Ni-Cu could be favouring the higher activity and stability observed in these catalysts.
7. Sequential step impregnation lead to higher Ni-Cu interaction, smaller particle size and lower acidity (possibly preventing C—C cleavage and avoiding ring-opening products). These promising characteristics implied higher production of desired products. Most of the catalysts synthesized by this method showed a yield of DMF above 70 % after 25 hours-on-stream.
8. Metallic Ni deposited onto the surface of the catalyst was responsible for DMTHF production. This Ni was partially oxidized during the reaction, leading to a loss in the hydrogenating capacity, which limited the hydrogenation step of DMF to DMTHF. This effect was noticeable in the case of 30Ni-15CuZr, where the maximum DMTHF production (55 %) was reached after 7 hours-on-stream. However, the yield of this product decreased with time, while increasing the production of DMF. At the end of the reaction time tested (25 h), DMF reached a yield of 70 % with no production of DMTHF.
9. The impregnation of Ni in a second step (sequential impregnation) involved the better reducibility and it enhanced the dispersion for both metals. These



valuable characteristics implied a higher exposition of metallic Ni on the surface, involving, as explained above, higher DMTHF production at the beginning of the reaction.

### **Biomass-derived carbon as catalyst support in bimetallic Ni-Cu catalysts.**

The utilization of carbon obtained from agroforestry residues makes the catalytic system greener. The successful utilization of this non-conventional catalytic support would benefit the use of carbon obtained from agroforestry processes, and it would reduce the cost of the catalytic system. The most relevant conclusions of this chapter are summarized as follows:

10. The bimetallic catalysts, regardless the support, showed a better balance of the acid sites and the metallic sites (Ni-Cu active species) to end with a stable catalytic behaviour. A DMF yield above 50 % was reached after 25 hours-on-stream in all the bimetallic catalysts.
11. Even if the bimetallic catalysts impregnated in commercial carbon exhibited higher yields of the desired products at the beginning of the reaction, similar results were achieved with commercial and biomass-derived carbons at the end of the reaction. This promising result implies the possibility of employing biomass-derived carbon as catalytic support.
12. The acidic treatment and the later neutralization processing did not alter the catalytic activity of the catalysts. This suggests that there is no need of the pretreatment of the carbon support, involving a simpler synthesis of the catalysts.
13. The monometallic catalysts supported on commercial carbon exhibited higher yields to the desired products due to the higher metal content and lower acidity offered by these catalysts. The maximum yield observed in these catalysts was around 70 % after 7 hours-on-stream. However, they exhibited deactivation problems, probably due to the sintering effect and coke deposition on the catalyst surface.

14. Nickel based monometallic catalysts were able to produce the over-hydrogenated product, DMTHF, unlike monometallic Cu catalysts, implying the need of Ni for the hydrogenation of C=C bond.
15. There is a correlation between the metallic Cu content on the catalyst surface and the total DMF and DMTHF production at the first stage of the reaction. Moreover, metallic Ni content on the catalyst surface is correlated with the hydrogenation capacity of C=C bond of the catalyst, involving the production of DMTHF.

In a near future, the results of this work could be complemented with the corresponding kinetic study. This kinetic study, together with a more detailed identification of the unknown by-products, would allow carrying out a preliminary basic engineering study of DMF-DMTHF production. Therefore, a techno-economic comparison with the current oil-based conventional processes could be performed, assessing the viability of the process.

Moreover, instead of using synthetic HMF, this platform molecule produced from real biomass could be tested, making the process more realistic. The use of real biomass will probably cause difficulties on the catalytic system activity and stability, due to the impurities this real biomass presents.

## NEREA VIAR ANTUÑANO

Date of birth: July 26, 1992.

Place of birth: Getxo, Biscay.

Telephone number: +34 94 601 72 97

Email address: [nerea.viar@ehu.eus](mailto:nerea.viar@ehu.eus)

Contact address: Torres Quevedo Plaza, 1. 48013-Bilbao.

Languages: Spanish (Native), Basque (C1) and English (CAE).



### Education and training

*2016 - present*

**PhD student** at the School of Engineering of Bilbao (UPV/EHU) in the SuPrEn research group

*May - October, 2019*

**Six-month-research stay** at the University of Bologna (Italy) in the Industrial Chemistry Department

*2014 - 2016*

**Master's degree in Industrial Engineering** (specialisation in Chemical Engineering) at the School of Engineering of Bilbao (UPV/EHU).

**Five-month-international stay** at the Eindhoven University of Technology (The Netherlands).

*2010 - 2014*

**Degree in Industrial Technology Engineering** at the School of Engineering of Bilbao (UPV/EHU).

**Five-month-international stay** at the Aarhus University (Denmark).

### Publications

- "Hydrogenolysis of 5-hydroxymethylfurfural to produce 2,5-dimethylfuran over ZrO<sub>2</sub> supported Cu and RuCu catalysts", J. M. Requies, M. Frias, M. Cuezva, A. Iriondo, I. Agirre and N. Viar, *Industrial & Engineering Chemistry Research*, 57 (2018) 11535-11546.

- “Furanic biofuels production from biomass using Cu-based heterogeneous catalysts”, N. Viar, J. M. Requies, I. Agirre, A. Iriondo and P. L. Arias, *Energy*, 172 (2019) 531-544.
- “Ni-Cu bimetallic catalytic system for producing 5-hydroxymethylfurfural-derived value-added biofuels”, N. Viar, J. M. Requies, I. Agirre, A. Iriondo, M. Gil-Calvo and P. L. Ariar, *ACS Sustainable Chemistry & Engineering*, 8 (2020) 11183-11193.
- “Value-added bio-chemicals commodities from catalytic conversion of biomass derived furan-compounds”, A. Iriondo, I. Agirre, N. Viar and J. M. Requies, *Catalysts*, 10 (2020) 895.
- “Evaluation of the  $ZrO_2/Al_2O_3$  suste, as catalysts in the catalytic transfer hydrogenation of furfural to obtain furfuryl alcohol”, J. A. Cecilia, C. García-Sancho, C. P. Jiménez-Gómez, N. Viar, R. Moreno-Tost, J. Mérida-Robles, J. M. Requies, P. Maireles-Torres, *Applied Catalysis A*, 609 (2021) 117905.

#### **Contribution to Conferences**

- 10<sup>th</sup> International Conference on Sustainable Energy & Environmental Protection (Bled – Slovenia, 2017).  
Oral presentation, “2,5-DMF production from biomass using heterogeneous catalysts”.  
N. Viar, J. M. Requies, I. Agirre and P. L. Arias.
- 4<sup>th</sup> International Congress on Catalysis for Biorefineries (Lyon – France, 2017).  
Poster presentation, “Ni-Cu bimetallic catalysts for hydrogenolysis of HMF for the production of DMF and DMTHF”.  
N. Viar, J. Requies and P. L. Arias.
- 11<sup>th</sup> International Conference on Sustainable Energy and Environmental Protection (Paisley – United Kingdom, 2018).  
Oral presentation, “Bimetallic catalysts for the hydrogenolysis of HMF to produce DMF and DMTHF”.  
N. Viar, J. Requies, I. Agirre, A. Iriondo and P. L. Arias.

- 4<sup>th</sup> International Symposium on Catalysis for Clean Energy and Sustainable Chemistry (Bilbao – Spain, 2018).  
Poster presentation, “Possible reaction pathway of the hydrogenolysis of HMF to produce DMF and DMTHF”.  
N.Viar, J. M. Requies, I. Agirre, A. Iriondo and P. L. Arias.
- 3<sup>rd</sup> International Congress of Chemical Engineerin (Santander – Spain, 2019).  
Oral presentation, “Ni and Cu interaction for the catalytic production of biofuels”.  
N. Viar, J. M. Requies, I. Agirre and A. Iriondo.
- 5<sup>th</sup> International Congress on Catalysis for Biorefineries (Turku – Finland, 2019).  
Poster presentation, “Catalytic hydrogenolysis of HMF to obtain a new unconventional biofuels: DMF and DMTHF”.  
J. M. Requies, N. Viar, C. Bouzon, A. Iriondo, I. Agirre and P. L. Arias
- 5<sup>th</sup> International Congress on Catalysis for Biorefineries (Turku – Finland, 2019).  
Oral presentation, “Bimetallic Ni-Cu/ZrO<sub>2</sub> catalysts optimization for the production of biofuels”.  
N. Viar, J. M. Requies, I. Agirre, A. Iriondo and P. L. Arias.
- IV Encuentro de Jóvenes Investigadores de la SECAT (Bilbao, 2020).  
Oral presentation, “Residual and commercial carbon support for monometallic catalyst on the production of DMF and DMTHF”.  
N. Viar, J. M. Requies, I. Agirre, A. Iriondo, P. L. Arias.

#### Research project participation

Project Title: *Tecnologías catalíticas avanzadas para la transformación de residuos biomásicos en biocombustibles y productos renovables.*

Supporting Entity: MINECO.

Main researcher: Pedro Luis Arias.

#### Courses

- Aspen Plus: Process Modeling (organized by Aspentech in Bilbao, 2017, 20 h).
- Introduction to Characterization of Adsorbents and Catalysts (organized by Rocasolano Instityte and CSIC, in Jarandilla-Spain, 2017, 20h).

- Fundamentals and Applications of X-ray Photoelectron Spectroscopy (organized by Sgiker in Leioa, 2017, 20 h).
- Fundamentals of Transmission Electron Microscopy in Material Science (organized by Sgiker in Leioa, 2018, 20 h).
- Good laboratory practice: Waste management (organized by the UPV/EHU Sustainability Department online, 2018, 25 h).
- Awareness of first aid in case of chemical splashes (organized by PREVOR in Leioa, 2018, 5 h).
- Swagelok Workshop (organized by Swagelok in Bilbao, 2018, 5 h).